On the Biological Activity of the Natural Product (+)-Avrainvillamide

On the Biological Activity of the Natural Product (+)-Avrainvillamide

A dissertation presented

by

Herschel Mukherjee

to

The Department of Chemistry and Chemical Biology

in partial fulfillment of the requirements

for the degree of

Doctor of Philosophy

in the subject of

Chemistry

Harvard University

Cambridge, Massachusetts

April, 2015

Dissertation Advisor: Herschel Mukherjee

Professor Andrew G. Myers

On the Biological Activity of the Natural Product (+)-Avrainvillamide

ABSTRACT

Nucleophosmin (NPM1) is a multifunctional phosphoprotein localized predominantly within the nucleoli of eukaryotic cells. Mutations within its C-terminal domain are frequently observed in patients with acute myeloid leukemia (AML), are thought to play a key role in the initiation and progression of the disease, and result in aberrant, cytoplasmic localization of the mutant protein. It has previously been demonstrated that the electrophilic antiproliferative natural product (+)-avrainvillamide binds to proteins, including nucleophosmin, by *S*-alkylation of cysteine residues. In this thesis we report that the biological activity of avrainvillamide is mediated by NPM1 and the nuclear export receptor exprtin-1 (Crm1). Using mass spectrometry, we demonstrate that the antiproliferative activity of a series of avrainvillamide analogs correlates with their ability to bind C-terminal NPM1 truncation constructs; it is also observed that the interaction between avrainvillamide and the C-terminal domain of NPM1 is fully reversible under our experimental conditions. We report that avrainvillamide restores nucleolar localization of certain AML-associated mutant forms of NPM1 and provide evidence that this relocalization is mediated by interactions of avrainvillamide with mutant NPM1 and Crm1. Immunofluorescence and mass spectrometric experiments employing a series of different NPM1 constructs suggest that a specific interaction between avrainvillamide and cysteine-275 of certain NPM1 mutants mediates the relocalization of these proteins to the nucleolus. Avrainvillamide is

further shown to inhibit nuclear export of Crm1 cargo proteins, including AML-associated NPM1 mutants; this marks the first evidence that avrainvillamide directly influences the biology of a cellular target other than NPM1. We also observe that avrainvillamide treatment displaces thr^{199}-phosphorylated NPM1 from duplicated centrosomes, leads to an accumulation of supernumerary centrosomes, and causes mitotic defects *in vitro*. Finally, we show that avrainvillamide treatment increases levels of thr^{199}-phosphorylated NPM1 by inhibiting the action of protein phosphatase 1 beta on phosphorylated NPM1, thereby indirectly displacing NPM1 from nucleoli and destabilizing nucleolar and nuclear structure.

Table of Contents

Acknowledgements

While nearing the end of my graduate career leaves me with a definite sense of personal accomplishment, it goes without saying that I would not have achieved nearly as much if not for the constant support of the people around me. First and foremost, I have to thank Andy for his mentorship over the past six years. His meticulous approach to research was a constant source of inspiration and led me to continually challenge myself with my work. I must also thank the other members of my dissertation committee, Prof. Jacobsen, who also served on all of my advisory committees, and Prof. Balskus, who graciously joined my committee on rather short notice. I am also grateful for the support I received from Prof. Betley, who served on my first advisory committee, and Prof. Saghatelian, whose door was always open whenever I needed a chat. I would also like to acknowledge Prof. Brian Stoltz and Prof. Douglas Rees from the California Institute of Technology, who were amazing mentors during my days as an undergraduate, and were instrumental in my decision to pursue higher education in chemistry.

Then there's the host of colleagues who were instrumental in providing hands-on assistance in research, particularly as I transitioned from synthetic chemistry to chemical biology. I owe thanks to the long list of researchers who provided the groundwork for my contributions to the avrainvillamide project, particularly the three I was fortunate to meet in person—Dr. Kok-Ping Chan, Dr. Matthew Meketa, and Mariah Hanley. Beyond the Myers group, I thank to David Sherman and Janine May of the Kahne group, who helped me with basic chemical biology techniques; Dr. Joshua Vaughan and Eileen Sun of the Zhuang group, who provided their expert advice in the realm of fluorescence microscopy; and Dr. Jeremy Wulff and Dr. Sunia Trauger, who provided assistance with mass spectrometry. I would also like to express my gratitude to Dr. Jonathan Mortison, who was a fantastic coworker during my time on the

tetracycline project (which is not reported here), and to Dr. Oleksandr Zhurakovskyi, for his careful proofreading of this dissertation. Lastly, I must acknowledge financial support from the National Science Foundation in the form of a pre-doctoral research fellowship, and from the National Institutes of Health, who provided the funding for the avrainvillamide project.

While I certainly had a strong network of mentors and colleagues to help overcome challenges in the lab, I had an arguably stronger network of family and friends to help restore my sanity when I needed it most. I am indebted to Meredith for ability to act as my best friend, my voice of reason, and my strongest supporter over the past several years. I would also not have accomplished nearly as much throughout my life if not for the support of my parents, Ujjal and Madhuri, my brother, Sanjay, and my grandfather, Gururaj, who perhaps more than anyone else I know has always epitomized a love of learning. I am also grateful for the extended network of family that I have in Massachusetts—Madhav, Sujata, Praveen, Karen, Neil, Roy—that have always been willing to open their doors for me when I've needed it. Lastly, and unfortunately, rather impersonally, I would like to thank everyone who helped remind me that there is more to life than the lab—whether by joining me on the ultimate field, visiting me even though I was rarely able to reciprocate, or contributing to my collection of cards hanging near my desk—your friendship and support has gone a long way towards helping me survive the past six years.

Glossary of Abbreviations

AML	acute myeloid leukemia
bp	base pairs
BSA	bovine serum albumin
CA	calyculin A
CD	circular dichroism
Crm1	exportin-1 (chromosome region maintenance 1 homolog)
dba	dibenzylideneacetone
DMF	N,N-dimethylformamide
DMSO	dimethyl sulfoxide
DNA	deoxyribonucleic acid
DTT	dithiothreitol
eGFP	enhanced green fluorescent protein
eq	molar equivalents
ESI	electrospray ioniziation
ETD	electron transfer dissociation
FBS	fetal bovine serum
FLT3	fms-like tyrosine kinase 3
FT	Fourier transform
g	gravitational force
g	gram
GFP	green fluorescent protein
GI_{50}	concentration for 50% growth inhibition
HEPES	2-[4-(2-hydroxyethyl)piperazin-1-yl]ethanesulfonic acid
hr	hour

HIV	human immunodeficiency virus
IB	immunoblot blocking (buffer)
ICR	ion cyclotron resonance
IFAD	immunofluorescence antibody dilution (buffer)
ITD	internal tandem duplication
K_d	dissociation constant
KHMDS	potassium hexamethyldisilazide
L	liter
LMB	leptomycin B
M	molar
m/z	mass-to-charge ratio
miRNA	micro RNA
min	minute
mol	mole
MOPS	3-morpholinopropane-1-sulfonic acid
MS	mass spectrometry
MW	molecular weight
NES	nuclear export sequence
NLS	nuclear localization sequence
NoLS	nucleolar localization sequence
NPM1	nucleophosmin 1 gene
NPM1	nucleophosmin 1.1 protein
NPM1-C_n	C-terminal n amino acids of NPM1.1 protein
NPM2	nucleoplasmin 2
NPM3	nucleoplasmin 3

NPMc+	cytoplasm-positive NPM1 protein
nt	nucleotide
OA	okadaic acid
p53	tumor protein p53
PA	phosphatase assay (buffer)
PBS	phosphate-buffered saline
PS	phosphatase stop (solution)
rDNA	ribosomal DNA
RNA	ribonucleic acid
TBS	tris-buffered saline
TCEP	tris(2-carboxyethyl)phosphine
THF	tetrahydrofuran
TOF	time-of-flight
Tris	tris(hydroxymethyl)aminomethane
w/v	weight-to-volume
v/v	volume-to-volume

Chapter 1

Introduction to Avrainvillamide and Nucleophosmin

1.1 Structure and Biology of Avrainvillamide and Stephacidin B

The natural product avrainvillamide (**1**, Figure 1.1) was first isolated in 2000 from the marine fungus *Aspergillus sp*. CNC358 and was found to display antiproliferative activity against a range of cultured human cancer cell lines.[1] Stephacidin B (**2**), conceptually a dimer of avrainvillamide, was isolated in 2002 from a different producing organism, *Aspergillus ochraceus* WC76466 and was also noted for its potent antiproliferative activity against several cancer cell lines.[2] Interestingly, stephacidin B was reported to be roughly twice as potent as avrainvillamide in each cell line studied, suggesting that stephacidin B and avrainvillamide may readily interconvert in biologically relevant contexts. Indeed, once avrainvillamide and stephacidin were available through synthesis, it was shown that stephacidin B rapidly retrodimerizes in cell culture to afford avrainvillamide.[3] This interconversion occurs before any biological effects are observed, suggesting that the biological activity of stephacidin B likely arises from its ability to serve as an *in vivo* source of avrainvillamide.

Structurally, avrainvillamide is a highly oxidized, prenylated indole alkaloid. The molecule contains a bridged 2,5-diketopiperazine unit, an aromatic chromene moiety, and a unique 3-alkylidene-3*H*-indole-1-oxide functionality. Initial experiments employing simplified avrainvillamide analog **3**, a more accessible compound containing the α,β-unsaturated nitrone functionality, revealed its ability to reversibly alkylate oxygen- and sulfur-centered nucleophiles

[1] Fenical, W.; Jensen, P. R.; Cheng, X. C. Avrainvillamide, a Cytotoxic Marine Natural Product, and Derivatives Thereof. US006066635A May 23, 2000.

[2] Qian-Cutrone, J.; Huang, S.; Shu, Y. Z.; Vyas, D.; Fairchild, C.; Menendez, A.; Krampitz, K.; Dalterio, R.; Klohr, S. E.; Gao, Q. Stephacidin A and B: Two Structurally Novel, Selective Inhibitors of the Testosterone-dependent Prostate LNCaP Cells. *J. Am. Chem. Soc.* **2002**, *124*, 14556-14557.

[3] Wulff, J. E.; Herzon, S. B.; Siegrist, R.; Myers, A. G. Evidence for the Rapid Conversion of Stephacidin B into the Electrophilic Monomer Avrainvillamide in Cell Culture. *J. Am. Chem. Soc.* **2007**, *129*, 4898-4899.

(Figure 1.2 A),[4] suggesting that avrainvillamide may react with biologically relevant nucleophiles in a similar fashion. Stephacidin B lacks this functional group, further supporting the hypothesis that avrainvillamide, and not stephacidin B, is responsible for the observed biological activity of both compounds.

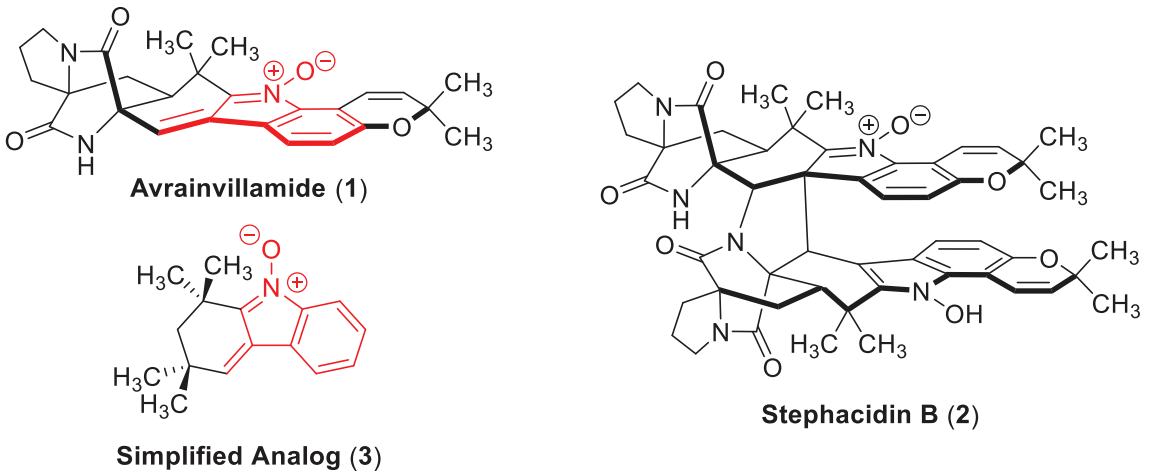

Figure 1.1. Chemical structures of the natural products avrainvillamide (**1**), stephacidin B (**2**), and simplified avrainvillamide analog (**3**). The 3-alkylidene-3*H*-indole-1-oxide functionality is shown in red.

Owing to its complex chemical structure and promising biological activity, avrainvillamide and stephacidin B immediately received the attention of synthetic chemists. Our group reported the first total synthesis of avrainvillamide in 2005,[5] accomplishing the task in 17 steps. This work also demonstrated that avrainvillamide could be converted to stephacidin B under mild conditions (Figure 1.2 B), thereby also marking the first total synthesis of stephacidin B. Several key transformations in this synthetic route are highlighted in Scheme 1.1. Notably, the

[4] Myers, A. G.; Herzon, S. B. Identification of a Novel Michael Acceptor Group for the Reversible Addition of Oxygen- and Sulfur-Based Nucleophiles. Synthesis and Reactivity of the 3-Alkylidene-3H-indole 1-Oxide Function of Avrainvillamide. *J. Am. Chem. Soc.* **2003**, *125*, 12080-12081.

[5] Herzon, S. B.; Myers, A. G. Enantioselective Synthesis of Stephacidin B. *J. Am. Chem. Soc.* **2005**, *127*, 5342-5344.

single stereocenter in intermediate **4**, established by an early-stage Corey-Bakshi-Shibata reduction, dictates the stereochemical outcome of each subsequent reaction. This intermediate is

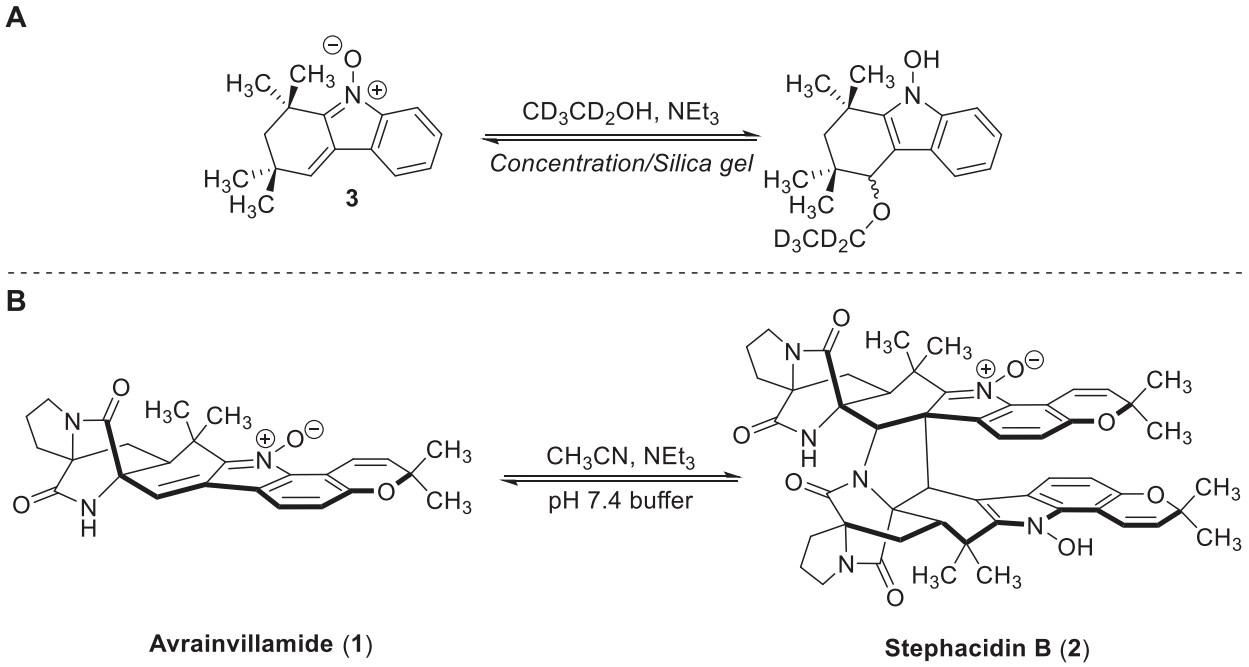

Figure 1.2. (**A**) Reversible 1,5 addition of nucleophiles to the 3-alkylidene-3*H*-indole-1-oxide functionality of **3**. (**B**) Interconversion between avrainvillamide and stephacidin B.

converted in two steps to enone **5**, which is alkylated by the unusual electrophile **6** in one of the key carbon-carbon bond-forming reactions of the route. The resulting enone **7** is elaborated in several steps, including a diastereoselective Strecker-type addition of hydrogen cyanide to an enamine and the platinum-catalyzed reduction of a nitrile to the corresponding primary amide, to provide amide **8**. When **8** is heated in the presence of a free-radical initiator, a series of bond-forming reactions occurs, affording compound **9**, thereby completing the synthesis of the 2,5-diketopiperazine structure found in avrainvillamide. Three synthetic steps are required to convert **9** to key coupling partner **10**. The α-iodoenone **10** is then coupled with *ortho*-nitrostannane **11** (R = CH_3) to yield penultimate intermediate **12**; a final zinc-mediated reductive cyclization affords

avrainvillamide. Notably, this synthetic route, with minor modifications,[6] has been scaled up to yield more than 100 mg of (+)-avrainvillamide and avrainvillamide analogs for evaluation in biological assays.

Scheme 1.1. Abbreviated synthesis of avrainvillamide.

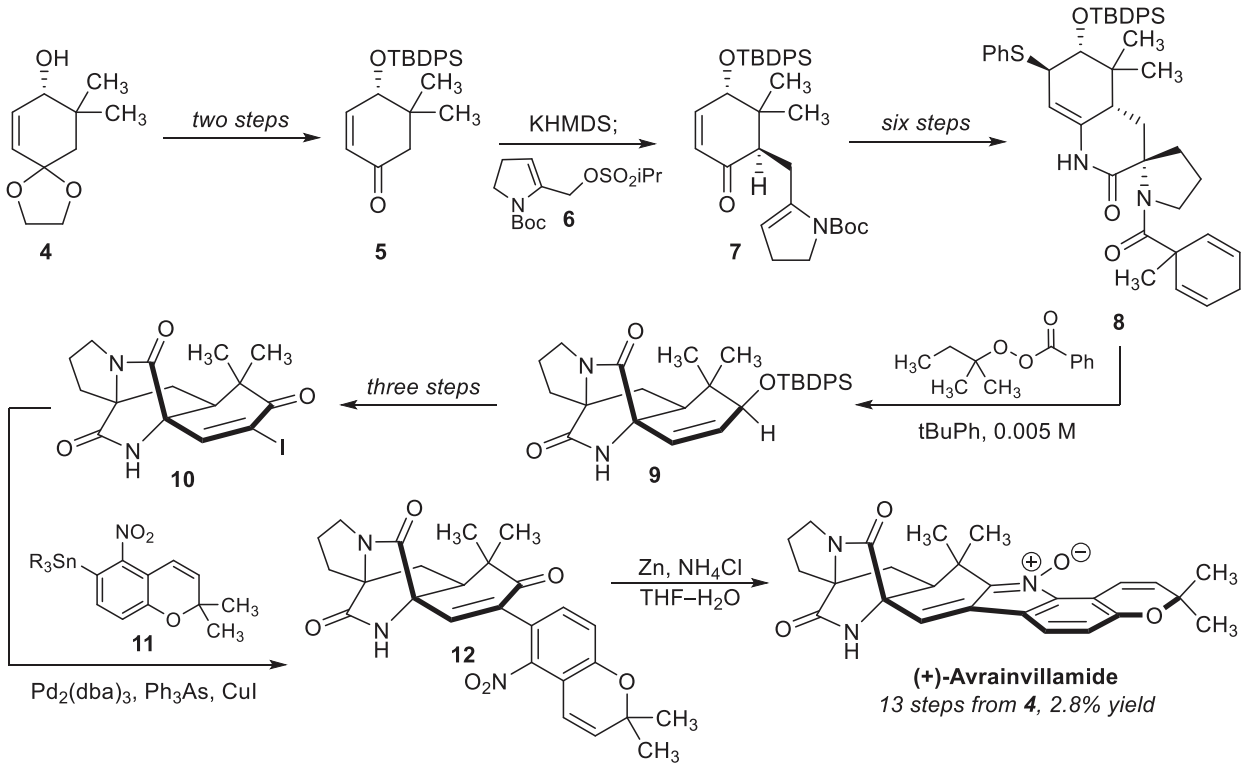

Armed with a convergent synthetic route to avrainvillamide, efforts turned towards the synthesis of novel avrainvillamide analogs and the identification of key structure-activity relationships. Avrainvillamide analogs can be broadly classified into three groups: analogs in which the α,β-unsaturated nitrone functionality has been removed or shielded from attack by nucleophiles (**13–15**, Figure 1.3); analogs containing modified aromatic groups (**16–19**, Figure 1.4); and analogs in which the bridged 2,5-diketopiperazine structure has been modified or removed (**3**, **20–22**, Figure 1.5). These studies revealed that the α,β-unsaturated nitrone of

[6] For revised procedures for the synthesis of avrainvillamide, refer to Appendix III.

avrainvillamide is essential for its antiproliferative activity, as reduction of this group, as in analog **13**, or shielding it from nucleophiles, as in **14**, significantly reduced biological activity. [7]

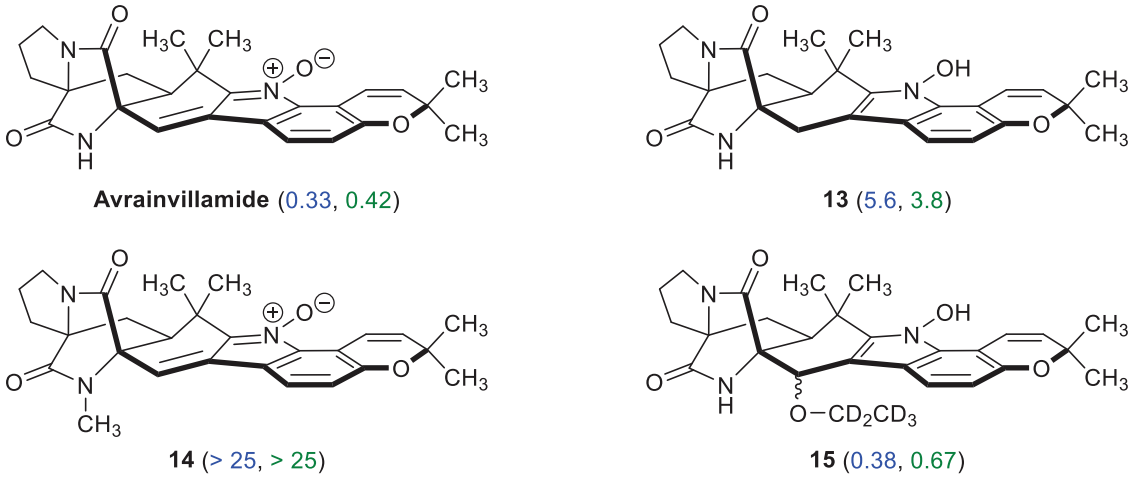

Figure 1.3 Avrainvillamide analogs bearing modified 3-alkylidene-3*H*-indole-1-oxide core structures. Values in parentheses indicate 72-hour GI_{50} values (in μM) against LNCaP (in blue) and T–47 D (in green) cancer cell lines.

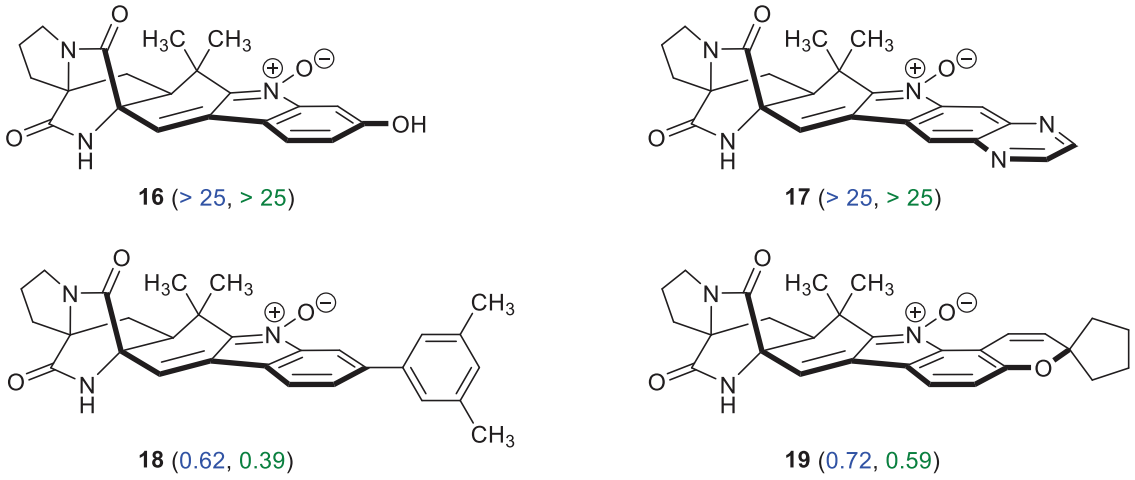

Figure 1.4 Avrainvillamide analogs bearing modified aromatic groups. Values in parentheses indicate 72-hour GI_{50} values (in μM) against LNCaP (in blue) and T–47 D (in green) cancer cell lines.

On the other hand, the adduct between avrainvillamide and ethanol-d_5 (**15**) was approximately equipotent to avrainvillamide, consistent with the hypothesis that the 1,5-addition of

[7] Herzon. S. B. Enantioselective Syntheses of Avrainvillamide and Stephacidin B. Ph. D. Dissertation, Harvard University, May 2006.

nucleophiles to avrainvillamide is reversible under physiological conditions. It was also observed that the incorporation of polar functionalities in the aromatic portion of the molecule (analogs **16** and **17**) completely abolished activity in whole-cell assays, whereas a range of hydrophobic and aromatic substituents were tolerated (analogs **18** and **19**).[8] Although the bridged 2,5-diketopiperazine motif greatly increased the potency of avrainvillamide analogs, analogs bearing simplified diketopiperazine systems (as in **20**), as well as compounds lacking this group entirely, (analogs **3** and **21**) were found to retain modest antiproliferative activity.[9] Lastly, analogs containing simplified, acyclic nitrone core structures (such as **22**) did not exhibit antiproliferative activity; this was not unexpected since these compounds had previously been demonstrated to be unreactive towards nucleophiles.[7]

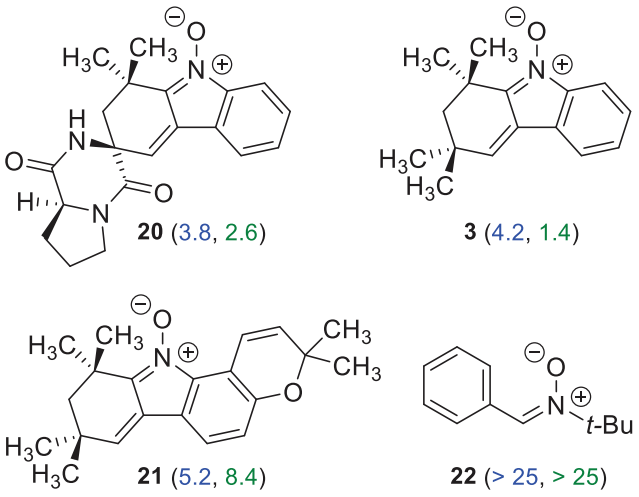

Figure 1.5 Avrainvillamide analogs lacking the bridged 2,5-diketopiperazine structural group. Values in parentheses indicate 72-hour GI_{50} values (in μM) against LNCaP (in blue) and T–47 D (in green) cancer cell lines.

The synthesis of avrainvillamide also enabled a detailed examination of its reactivity towards nucleophiles. In addition to its dimerization to form stephacidin B under mild

[8] Siegrist, R.; Chan, K. P.; Myers. A. G. Harvard University, *Unpublished work*, 2006-2008.

[9] Herzon, S. B.; Siegrist, R.; Chan, K. P.; Myers, A. G. Harvard University, *Unpublished work*, 2005-2009.

conditions,[5] it was also found that avrainvillamide readily formed adducts with both oxygen- and sulfur-based nucleophiles, including methanol, ethanol, coenzyme A, and glutathione.[3,10] This last observation was particularly exciting, as it suggested that the biological activity of avrainvillamide may be mediated by its ability to covalently modify cysteine residues of proteins *in vivo*.

1.2 Identification of Nucleophosmin as a Cellular Target of Avrainvillamide

Although the antiproliferative activity of avrainvillamide and stephacidin B were well established, the cellular mechanisms responsible for this activity remained unknown. Based on the observation that avrainvillamide readily formed adducts with sulfur nucleophiles, initial efforts focused on the identification of protein binding partners of avrainvillamide using activity-based probes (Figure 1.6). These probes were readily accessible from the original synthetic route to avrainvillamide, and were shown to be approximately equipotent to avrainvillamide in whole-cell antiproliferative assays.[11]

Analysis of human cancer cells that were treated with the dansylated avrainvillamide probe **22** revealed that the fluorescent signal appeared to concentrate in the nucleoli and cytoplasm of cells. Simultaneous affinity-isolation experiments using the biotin-avrainvillamide conjugate **23** identified a small pool of putative target proteins, including one predominantly nucleolar protein, nucleophosmin. Subsequent competition assays employing a panel of fully synthetic avrainvillamide analogs revealed a strong correlation between their nucleophosmin

[10] Herzon, S. B.; Siegrist, R.; Wulff, J. E.; Myers, A. G. Harvard University, *Unpublished work*, 2006-2008.

[11] Wulff. J. E.; Siegrist, R.; Myers, A. G. The Natural Product Avrainvillamide Binds to the Oncoprotein Nucleophosmin. *J. Am. Chem. Soc.* **2007**, *127*, 14444-14451.

binding affinities and their antiproliferative activites in whole-cell assays.[11] nucleophosmin was unique in this regard – a similar correlation was not observed for any of the other proteins identified in initial experiments. Avrainvillamide was the first small molecule reported to interact with nucleophosmin; despite considerable interest in nucleophosmin as a potential therapeutic target, small molecule ligands of nucleophosmin remain scarce in the literature.

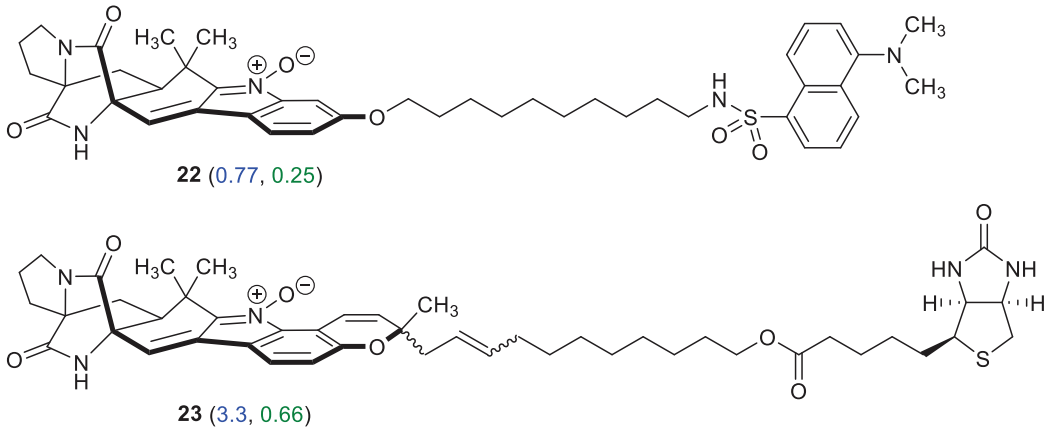

Figure 1.6. Chemical structures of the fluorescent avrainvillamide probe **22** and affinity-isolation probe **23**. Values in parentheses indicate 72-hour GI_{50} values (in μM) against LNCaP (in blue) and T–47 D (in green) cancer cell lines.

Once nucleophosmin had been identified as a cellular target of avrainvillamide, efforts turned towards identifying the specific residue (or residues) responsible for this interaction. Initial affinity-isolation experiments revealed that the interaction between nucleophosmin and probe **23** was abolished in the presence of iodoacetamide, thus preliminary studies focused on the three cysteine residues found in nucleophosmin residues – cys^{21}, cys^{104}, and cys^{275}. Three nucleophosmin constructs were prepared, each bearing a single cysteine-to-alanine point mutation, for evaluation in binding assays. Subsequent affinity-isolation experiments revealed that the C275A mutation in nucleophosmin (but neither the C21A nor the C104A mutation) reduced isolation of nucleophosmin, indicating that avrainvillamide interacts with nucleophosmin exclusively at cys^{275}.[11]

At the time of this discovery, two structures of nucleophosmin had been reported in the literature – a crystal structure of residues 16-124 of *Xenopus laevis* nucleolar protein 38 (NO38, a nucleophosmin homolog),[12] and a solution-phase NMR structure of residues 254-294 of human nucleophosmin.[13] To obtain further insight into the nature of the avrainvillamide-nucleophosmin interaction, efforts were directed towards trying to obtain a crystal structure of avrainvillamide bound to nucleophosmin. Several truncation constructs of nucleophosmin were prepared in order to eliminate regions of the protein that were predicted to interfere with crystallization, however, these efforts ultimately proved unsuccessful. Undeterred, collaborators in the Shakhnovich group performed a computational docking study between avrainvillamide and the published NMR structure of the C-terminal domain of nucleophosmin. A series of energy-minimized structures were produced, including one in which the chromene moiety of avrainvillamide projects into a well-defined hydrophobic pocket of nucleophosmin (Figure 1.7).[14] However, although this model provided support for several of the empirically determined structure-activity relationships, particularly those involving substitution of the chromene group, it did not account for the importance of the complex 2,5-diketopiperazine structure, and was thus of limited utility for the rational design of novel avrainvillamide analogs.

[12] Namboodiri, V. M.; Akey, I. V.; Schmidt-Zachmann, M. S.; Head, J. F.; Akey, C. W. The Structure and Function of Xenopus NO38-core, a Histone Chaperone in the Nucleolus. *Structure*. **2004**, *12*, 2149-2160.

[13] Grummitt. C. G.; Townsley, F. M.; Johnson, C. M.; Warren, A. J.; Bycroft, M. Structural Consequences of Nucleophosmin Mutations in Acute Myeloid Leukemia. *J. Biol. Chem.* **2008**, *283*, 23326-23332.

[14] Kutchukian, P.; Chan, K. P.; Meketa, M.; Myers, A. G.; Shakhnovich, E. Harvard University, *Unpublished work*, 2008.

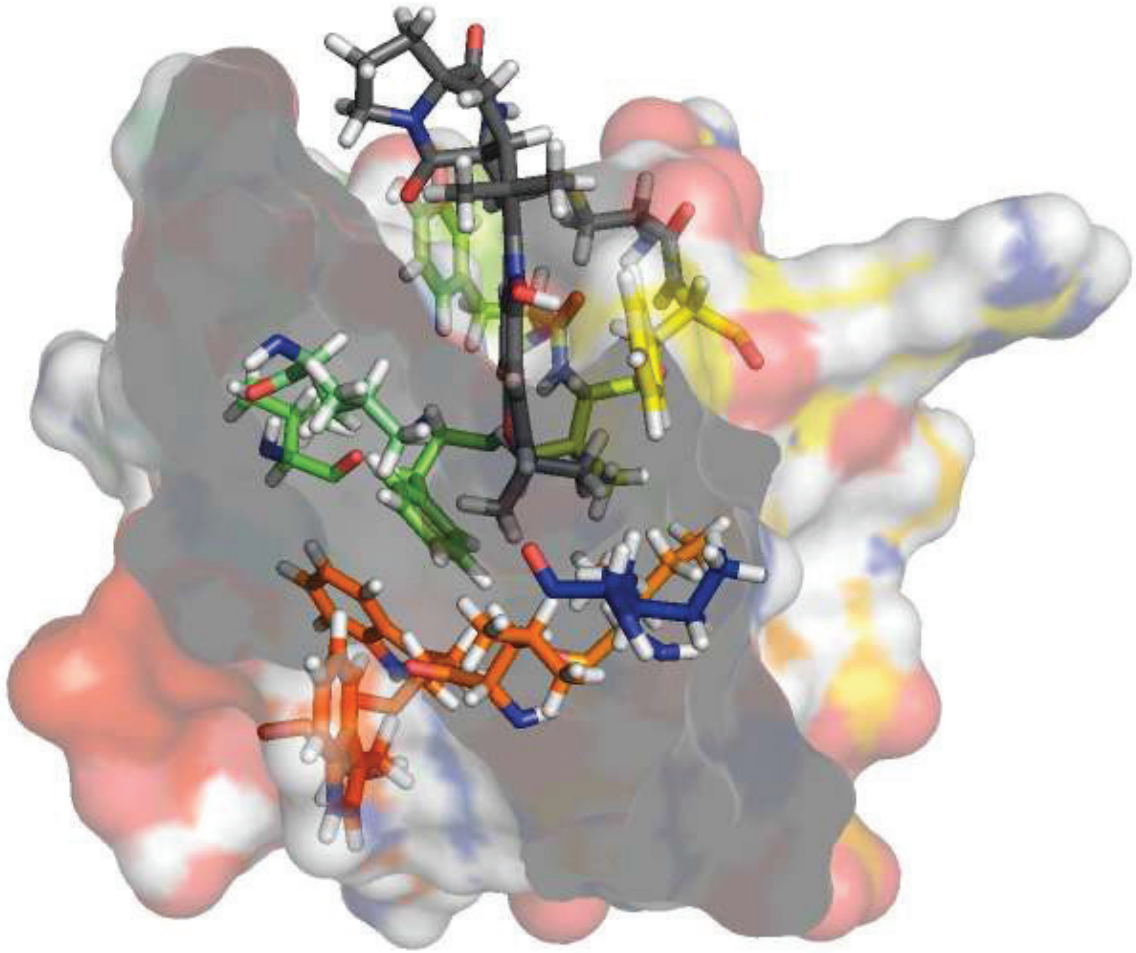

Figure 1.7 Energy-minimized structure of avrainvillamide bound to the C-terminal domain of nucleophosmin. Key branched-chain and aromatic amino acids defining the hydrophobic pocket of nucleophosmin are depicted as sticks. Carbon atoms of avrainvillamide are colored grey; carbon atoms of nucleophosmin residues are colored according to their position within the primary structure of nucleophosmin, ranging from red (gly^{254}) to blue (leu^{294}).

1.3 Structure and Function of Nucleophosmin

Nucleophosmin (NPM1, also known as B23, numatrin, or NO38) is a nucleolar phosphoprotein with a myriad of roles in cellular biology. Three NPM1 isoforms have been

identified in humans, each arising from alternative 3' exon splicing of the *NPM1* gene.[15] The primary isoform, NPM1.1, comprises 294 amino acids; the notation "NPM1" as used in this text refers to NPM1.1. The 265 amino acid NPM1.2 and 259 amino acid NPM1.3 (Figure 1.7) proteins have poorly understood roles in cellular biology and will not be discussed further.

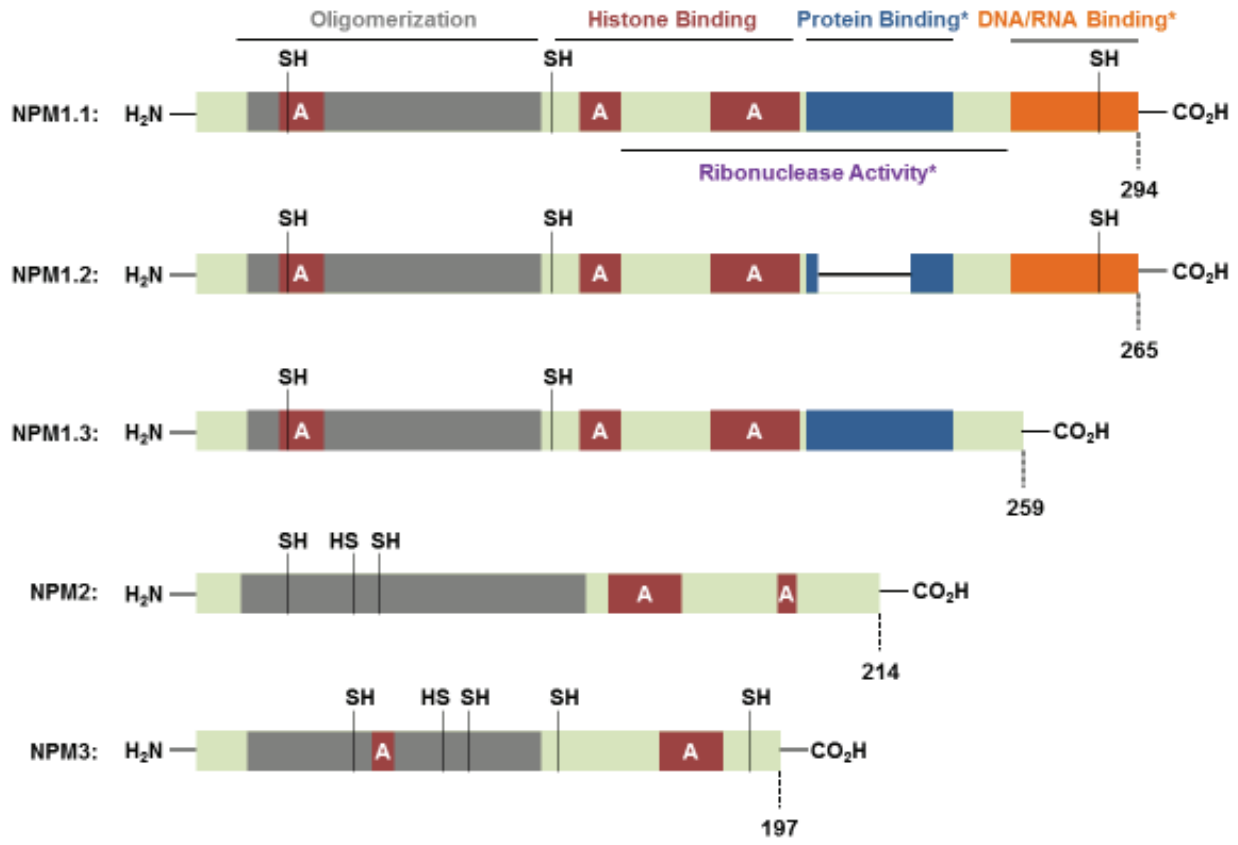

Figure 1.8. Schematic functional domain structures of nucleophosmin isoforms 1, 2, and 3 and nucleoplasmins 2 and 3. Asterisks (*) indicate functional domains unique to NPM1.

Initial analyses of the structural domains of NPM1 (Figure 1.8) led to its classification as a member of the nucleoplasmin family of chaperone proteins, which includes nucleoplasmins 2 and 3 (NPM2 and NPM3, respectively).[16] All three proteins share a moderately conserved N-

[15] Umekawa, H.; Chang, J. H.; Correia, J. J.; Wang, D.; Wingfield, P. T.; Olson, M. O. J. Nucleolar Protein B23: Bacterial Expression, Purification, Oligomerization and Secondary Structures of Two Isoforms. *Cell Mol. Biol. Res.* **1993**, *39*, 635-645.

[16] Frehlick, L. J.; Eirín-López, J. M.; Ausió, J. New Insights Into the Nucleophosmin/Nucleoplasmin Family of Nuclear Chaperones. *BioEssays*, **2007**, *29*, 49-59.

terminal domain (residues 16–104 of NPM1) that enables the formation of homooligomers[12] and multiple highly acidic, unstructured domains (residues 26–39, 120–134, and 161–189 of NPM1) that are thought to mediate interactions between this family of proteins and their basic protein substrates.[17] Several chaperone substrates of NPM1 have been characterized; these include histones[18] and preribosomal particles, including 60S ribosomes and a small subset of ribosomal proteins.[19,20] On the other hand, NPM1 is distinguished from NPM2 and NPM3 by the presence of two additional domains – a stretch of basic residues flanking the third acidic domain, and a hydrophobic three-helix bundle at its extreme C-terminus.[21] These unique domains of NPM1 are associated with its ability to bind nucleic acids,[22] ribonuclease activity,[23] and its predominant nucleolar, rather than nuclear, localization.[24] Several post-translational modifications of NPM1 have been described in the literature; one in particular (thr[199]-phosphorylation) was found to be important in the context of avrainvillamide biology, and is discussed in Chapter 2.

---

[17] Szebeni, A.; Olson, M. O. Nucleolar Protein B23 has Molecular Chaperone Activities. *Protein Sci*. **1999,** *8*, 905-912.

[18] Okuwaki, M.; Matsumoto, K.; Tsujimoto, M.; Nagata, K. Function of Nucleophosmin/B23, a Nucleolar Acidic Protein, as a Histone Chaperone. *FEBS Lett*. **2001**, *506*, 272-276.

[19] Maggi, L. B.; Kuchenruether, M.; Dadey, D. Y. A.; Schwope, R. M.; Grisendi, S.; Townsend, R. R.; Pandolfi, P. P.; Weber, J. D. Nucleophosmin Serves as a Rate-Limiting Nuclear Export Chaperone for the Mammalian Ribosome. *Mol. Cell Biol.* **2008**, *28*, 7050-7065.

[20] Yu, Y.; Maggi, L. B.; Brady, S. N.; Apicelli, A. J.; Dai, M. S.; Lu, H.; Weber, J. D. Nucleophosmin is Essential for Ribosomal Protein L5 Nuclear Export. *Mol. Cell Biol.* **2006**, *26*, 3798-3809.

[21] Hingorani, K.; Szebeni, A.; Olson, M. O. Mapping the Functional Domains of Nucleolar Protein B23. *J. Biol. Chem*. **2000**, *275*, 24451–24457.

[22] Wang, D.; Baumann, A.; Szebeni, A.; Olson, M. O. The Nucleic Acid Binding Activity of Nucleolar Protein B23.1 Resides in its Carboxy-terminal End. *J. Biol. Chem.* **1994**, *269*, 30994-30998.

[23] Herrera, J. E.; Savkur, R.; Olson, M. O. The Ribonuclease Activity of Nucleolar Protein B23. *Nucleic Acids Res.* **1995**, *23*, 3794-3797.

[24] Peculis, B. A.; Gail, J. G. Localization of the Nucleolar Protein NO38 in Amphibian Oocytes. *J. Cell Biol.* **1992**, *116*, 1-14.

The chaperone functionality of NPM1 is essential for several critical cellular processes, including chromatin assembly and remodeling[25] and ribosome biogenesis.[19] NPM1, however, also possesses several essential non-chaperone activities, although many of these additional functionalities are dependent on the ability of NPM1 to shuttle between the nucleolus, nucleus, and cytoplasm. For example, NPM1, through its interactions with the nuclear export factor exportin-1, is an essential regulator of centrosome duplication.[26] Furthermore, NPM1 has been implicated in DNA transcription,[27,28] and is thus a key regulator of growth and proliferation. NPM1-deficient mice exhibit late-stage embryonic lethality resulting from defects in ribosome synthesis and hematopoiesis.[29] On the other hand, immortalized mouse embryo fibroblasts lacking NPM1 are viable and proliferate *in vitro*, provided that expression of tumor protein p53 (p53) is also ablated.[30]

[25] Okuwaki, M.; Sumi, M.; Hisaoka, M.; Saotome-Nakamura, A.; Akashi, S.; Nishimura, Y.; Nagata, K. Function of Homo- and Hetero-oligomers of Human Nucleoplasmin/Nucleophosmin Family Proteins NPM1, NPM2 and NPM3 During Sperm Chromatin Remodeling. *Nucleic Acids Res.* **2012**, *40*, 4861-4878.

[26] Wang, W.; Budhu, A.; Forgues, M.; Wang, X. W. Temporal and Spatial Control of Nucleophosmin by the Ran-Crm1 Complex in Centrosome Duplication. *Nat. Cell Biol.* **2005**, *7*, 823-830.

[27] Swaminathan, V.; Kishore, A. H.; Febitha, K. K.; Kundu, T. K. Human Histone Chaperone Nucleophosmin Enhances Acetylation-Dependent Chromatin Transcription. *Mol. Cell Biol.* **2005**, *17*, 7534-7545.

[28] Li, Z.; Boone, D.; Hann, S. R. Nucleophosmin Interacts Directly With c-Myc and Controls c-Myc-induced Hyperproliferation and Transformation. *Proc. Natl. Acad. Sci. USA*. **2008**, *105*, 18794-18799.

[29] Grisendi, S.; Bernardi, R.; Rossi, M.; Cheng, K.; Khandker, L.; Manova, K.; Pandolfi, P. P. Role of Nucleophosmin in Embryonic Development and Tumorigenesis. *Nature*. **2005**, *437*, 147-153.

[30] Colombo, E.; Bonetti, P.; Denchi, E. L.; Martinelli, P.; Zamponi, R.; Marine, J. C.; Helin, K.; Falini, B.; Pelicci, P. G. Nucleophosmin is Required for DNA Integrity and p19Arf Protein Stability. *Mol. Cell Biol.* **2005**, *25*, 8874–8886.

1.4 Subcellular Localization of Nucleophosmin

NPM1 readily translocates between the nucleolus, nucleus, and cytoplasm in its role as a molecular chaperone protein. The subcellular localization of NPM1 is mediated by several

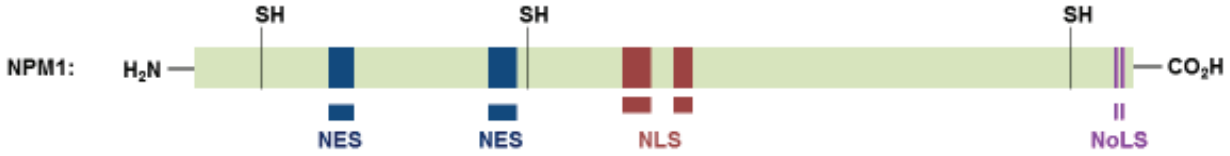

Figure 1.9. Schematic representation of the localization sequences mediating the intracellular transport of NPM1.

trafficking sequences present within the protein (Figure 1.9) and is controlled by several dynamic processes; its subcellular localization thus reflects the balance between the factors directing the protein to the various subcellular compartments. NPM1 contains a bipartite nuclear localization sequence (NLS) located at positions 134–142 and 150–155,[21] two leucine-rich nuclear export sequences (NES) located at positions 42–49 and 94–102,[21] and a nucleolar localization sequence (NoLS) that comprises residues trp^{288} and trp^{290}.[31] Due to the relative strength of the NoLS in comparison to the NLS and NES, NPM1 predominantly localizes within nucleoli. Indeed, owing to its strong affinity for this organelle and its ability to bind a wide range of proteins and nucleic acids, NPM1 is a critical structural component of the nucleolus.[32]

The precise roles of the various localization sequences of NPM1 have been studied extensively through the use of green fluorescent protein (GFP)-tagged nucleophosmin constructs (Table 1.1).[26] For example, while the wild-type GFP–NPM1 protein displays the expected nucleolar localization, fusion proteins bearing deletions of one or both of the NLS are observed

[31] Nishimura, Y.; Ohkubo, T.; Furuichi, Y.;Umekawa, H. Tryptophans 286 and 288 in the C-terminal Region of Protein B23.1 are Important for its Nucleolar Localization. *Biosci. Biotechnol. Biochem.* **2002**, *66*, 2239-2242.

[32] Amin, M. A.; Matsunaga, S.; Uchiyama, S.; Fukui, K. Depletion of Nucleophosmin Leads to Distortion of Nucleolar and Nuclear Structures in HeLa Cells. *Biochem. J.* **2008**, *415*, 345-351.

in both the cytoplasm and the nucleolus (but not the nucleus). The NES domains of NPM1 mediate its export from the nucleus by the nuclear export receptor exportin-1 (Xpo1, also known as chromosome region maintenance homolog 1, Crm1).[20,26] Deletion or mutation of the NES results in translocation of the corresponding GFP–NPM1 proteins from the nucleolus to the nucleus. It is not immediately apparent that inhibition of the nuclear export of NPM1 should interfere with its nucleolar localization; this observation is attributed to an accumulation of excess NPM1 in the nucleolus, eventually overcoming the ability of the nucleolus to retain the protein.

Table 1.1. The subcellular localization of previously studied GFP–NPM1 fusion proteins bearing mutations to the various NPM1 trafficking sequences.

Entry	Mutation	Description	Localization
1	None	Wild-type	nucleolus
2	Δ134–142	NLS1 Deletion	nucleolus, cytoplasm
3	Δ150–155	NLS2 Deletion	nucleolus, cytoplasm
4	L100,102A	NES2 Mutation	nucleolus, nucleus
5	Δ94–102	NES2 Deletion	nucleolus, nucleus
6	W288,290G	NoLS Mutation	nucleolus, nucleus

The NoLS of NPM1 deserves special treatment. This sequence comprises two key tryptophan residues located within a right-handed three-helix bundle at the extreme C-terminus of NPM1.[31] This folded structure is stabilized by hydrophobic interactions between several branched-chain and aromatic amino acids, including phe^{268}, phe^{276}, tyr^{271}, and the aforementioned tryptophan residues. Mutation of the two tryptophan residues results in destabilization of this domain and diffuse nuclear localization of the protein (Table 1.1, Entry 6). However, it has also been observed that the GFP–NPM1–F268,276A double mutant, which exhibits an unfolded NPM1 C-terminal domain, is excluded from nucleoli, demonstrating that destabilization of the three-helix bundle is sufficient to displace NPM1 from the nucleolus, even

if both tryptophan residues are present.[13] On the other hand, the GFP–NPM1–K263,267A fusion protein is observed to localize throughout the nucleus despite possessing a properly folded NPM1 C-terminal domain, indicating that correct folding of this domain, while necessary, is not sufficient to ensure the proper localization of NPM1.[13]

Despite considerable progress in understanding the roles of the various localization sequences in NPM1, the specific binding partners responsible for maintaining its nucleolar localization have long remained elusive. Recently, however, it was reported that the C-terminal domain of NPM1 forms binary complexes with short G-quadruplex DNA oligonucleotides;[33] subsequent chromatin immunoprecipitation and sequencing experiments demonstrated that NPM1 interacts with G-quadruplex ribosomal DNA (rDNA) in living cells.[34] This interaction is stabilized by interactions between the phosphate backbone of the rDNA and basic amino acids of NPM1, including lys[267], which may explain the aberrant localization of the GFP–NPM1–K263,267A protein. However, it was also shown that an unstructured basic region of NPM1 immediately adjacent to the C-terminal three-helix bundle greatly contributes to the stability of NPM1-rDNA complexes,[35] suggesting that the nucleolar localization of NPM1 may not be entirely determined by the status of its NoLS and C-terminal domain.

[33] Gallo, A.; Lo Sterzo, C.; Mori, M.; Di Matteo, A.; Bertini, I.; Banci, L.; Brunori, M., Federici, L. Structure of Nucleophosmin DNA-binding Domain and Analysis of Its Complex with a G-quadruplex Sequence from the c-Myc Promoter. *J. Biol. Chem.* **2012**, *287*, 26539-26548.

[34] Chiarella, S.; De Cola, A.; Scaglione, G. L.; Carletti, E.; Graziano, V.; Barcaroli, D.; Lo Sterzo, C.; Di Matteo, A.; Di Ilio, C.; Falini, B.; Arcovito, A.; De Laurenzi, V.; Federici, L. Nucleophosmin Mutations Alter its Nucleolar Localization by Impairing G-quadruplex Binding at Ribosomal DNA. *Nucleic Acids Res.* **2013**, *41*, 3228-3239.

[35] Federici, L.; Arcovito, A.; Scaglione, G. L.; Scaloni, F.; Lo Stero, C.; Di Matteo, A.; Falini, B.; Giardina, B.; Brunori, M. Nucleophosmin C-terminal Leukemia-associated Domain Interacts with G-rich Quadruplex Forming DNA. *J. Biol Chem.* **2010**, *285*, 37138-37149.

1.5 Nucleophosmin in Cancer

In addition to its essential functions in normal cellular growth and proliferation, NPM1 has also been associated with both tumor suppressor and oncogenic activity. NPM1 regulates the stability and activity of p53 and p14ARF tumor suppressor proteins, and is known to activate apoptotic pathways mediated by these proteins in response to nucleolar or nuclear stress factors.[36,37] NPM1 underexpression is linked to tumorigenesis, possibly through impairment of tumor suppressor pathways.[29] On the other hand, NPM1 overexpression is frequently observed in a diverse array of solid tumors and is also associated with increased cancer cell proliferation and, in many cases, poor patient prognosis.[38,39,40] The precise mechanisms linking NPM1 overexpression to increased cancer cell growth proliferation are not fully understood, but are thought to involve a combination of factors including NPM1-mediated increases in ribosome synthesis and activity,[41] enhancement of the transcriptional activity of NPM1 binding partners

[36] Kurki, S.; Peltonen, K.; Latonen, L.; Kiviharju, T. M.; Ojala, P. M.; Meek, D; Laiho, M. Nucleolar Protein NPM Interacts with HDM2 and Protects Tumor Suppressor Protein p53 From HDM2-mediated Degradation. *Cancer Cell.* **2004**, *5*, 465-475.

[37] Brady, S. N.; Yu, Y.; Maggi, L. B.; Webber, J. D. ARF Impedes NPM/B23 Shuttling in an Mdm2-Sensitive Tumor Suppressor Pathway. *Mol. Cell Biol.* **2004**, *21*, 9327-9338.

[38] Liu, Y.; Zhang, F.; Zhang, X.; Qi, L.; Yang, L.; Guo, H.; Zhang, N. Expression of Nucleophosmin/NPM1 Correlates with Migration and Invasiveness of Colon Cancer Cells. *J. Biomed. Sci.* **2012**, *19*, 53-62.

[39] Yun, J. P.; Miao, J.; Chen, G. G.; Tian, Q. H.; Zhang, C. Q.; Xiang, J.; Fu, J.; Lai, P. B. Increased Expression of Nucleophosmin/B23 in Hepatocellular Carcinoma and Correlation with Clinicopathological Parameters. *Br. J. Cancer*. **2007**, *96*, 477-484.

[40] Naoe, T.; Suzuki, T.; Kiyoi, H.; Urano, T. Nucleophosmin: A Versatile Molecule Associated with Hematological Malignancies. *Cancer Sci.* **2006**, *97*, 963-969.

[41] Ruggero, D; Pandolfi, P. P. Does the Ribosome Translate Cancer? *Nat. Rev. Cancer.* **2003**, *3*, 179-192.

such as c-Myc and NF-κB,[28,42] and the ability of NPM1 to sequester and inactivate tumor suppressor proteins.[36,43]

NPM1 mutations of clinical importance have been studied extensively in patients with acute myeloid leukemia (AML). *NPM1* gene mutations are among the most common genetic abnormalities in AML, occurring in an estimated 35-60% of adult AML patients[44,45,46] and are considered "founder" mutations in AML – they are thought to play key roles in the initiation and progression of AML, are relatively stable over the course of the disease, and are associated with a distinct gene and micro RNA (miRNA) signatures.[47] In the absence of other genetic mutations, particularly mutations in the fms-like tyrosine kinase 3 (FLT3) gene, NPM1 mutations in AML are associated with a favorable prognosis and improved response to traditional induction chemotherapy.[44,46,48] Despite considerable molecular heterogeneity, the vast majority of these

---

[42] Dhar, S. K.; Lynn, B. C.; Daosukho, C. Saint Clair, D. K.; Identification of Nucleophosmin as an NF-kappaB Co-activator for the Induction of the Human SOD2 Gene. *J. Biol. Chem.* **2004**, *274*, 28209-28219.

[43] Sportoletti, P.; Grisendi, S.; Majid, S. M.; Cheng, K. Clohessy, J. G.; Viale, A.; Teruya-Feldstein, J.; Pandolfi, P. P. NPM1 is a Haploinsufficient Suppressor of Myeloid and Lymphoid Malignancies in the Mouse. *Blood*. **2008**, *111*, 3859-3862.

[44] Falini, B.; Nicoletti, I.; Martelli, M. F.; Mecucci, C. Acute Myeloid Leukemia Carrying Cytoplasmic/Mutated Nucleophosmin (NPMc+ AML): Biologic and Clinical Features. *Blood*. **2007**, *109*, 874-885.

[45] Falini, B.; Mecucci, C.; Tiacci, E.; Alcalay, M.; Rosati, R.; Pasqualucci, L.; La Starza, R.; Diverio, D.; Colombo, E.; Santucci, A. Cytoplasmic Nucleophosmin in Acute Myelogenous Leukemia with a Normal Karyotype. *New Engl. J. Med*. **2004**, *352*, 254-266.

[46] Jain, P.; Kantarjian, H.; Patel, K.; Faderl, S.; Garcia-Manero, G.; Benjamini, O.; Borthakur, G.; Pemmaraju, N.; Kadia, T.; Daver, N. Mutated NPM1 in Patients with Acute Myeloid Leukemia in Remission and Relapse. *Leukemia and Lymphoma*. **2014**, *55*, 1337-1344.

[47] Garzon, R.; Garofalo, M.; Martelli, M. P.; Briesewitz, R.; Wang, L.; Fernandez-Cymering, C.; Volinia, S.; Liu, C.; Schnittger, S.; Haferlach, T.; Liso, A.; Diverio, D.; Mancini, M.; Meloni, G.; Foa, R.; Martelli, M. F.; Mecucci, C.; Croce, C. M.; Falini, B. Distinctive microRNA Signature of Acute Myeloid Leukemia Bearing Cytoplasmic Mutated Nucleophosmin. *Proc. Natl. Acad. Sci. USA*. **2008**, *105*, 3945-3950.

[48] Döhner, K.; Schlenk, R. F.; Habdank, M.; Scholl, C.; Rücker, F. G.; Corbacioglu, A.; Bullinger, L.; Fröhling, S.; Döhner H. Mutant Nucleophosmin (NPM1) Predicts Favorable Prognosis in Younger Adults with Acute Myeloid Leukemia and Normal Cytogenetics: Interaction with Other Gene Mutations. *Blood.* **2005**, *106*, 3740-3746.

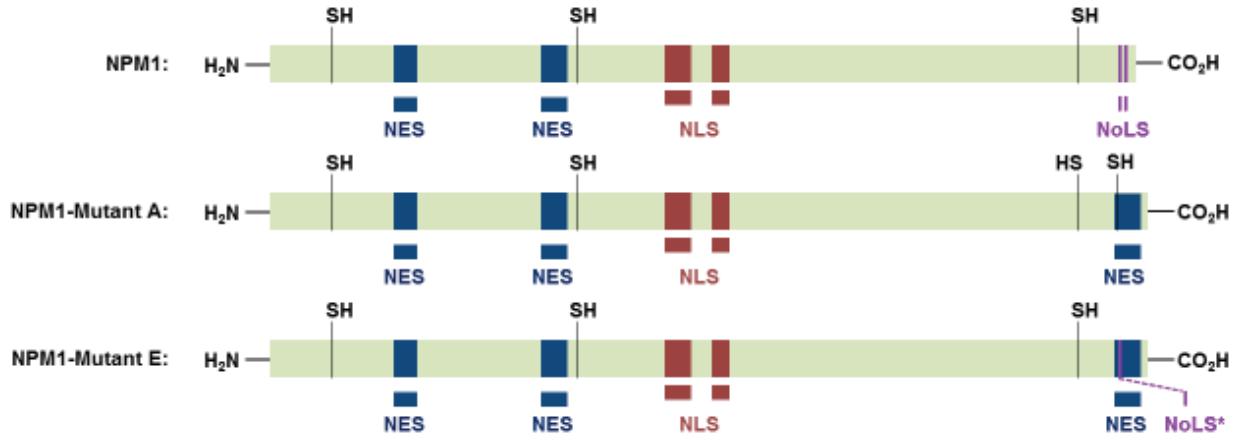

Figure 1.9. Schematic representation of the subcellular localization sequences present in two AML-associated NPMc+ variants. NoLS* indicates a partial NoLS present in NPM1–Mutant E resulting from retention of trp[288].

mutations arise from the presence of a 4-nucleotide insert in exon 12 of the *NPM1* gene.[44,45] The resultant reading-frame shift causes loss of one or both of trp[288] and trp[290], and thereby partial or whole loss of the NoLS, as well as the introduction of a third leucine-rich NES at the extreme C-terminus of the mutant protein (Figure 1.9). The combination of loss of nucleolar targeting and enhanced Crm1-mediated nuclear export of NPM1, but neither mutation alone, results in aberrant, cytoplasmic localization of the protein.[49] As with wild-type NPM1, the factors contributing to the altered trafficking of AML-associated NPM1 variants have been studied extensively through the use of GFP-tagged NPM1 fusion proteins (Table 1.2). AML patients typically possess one copy each of the wild-type and mutant *NPM1* genes,[44,45] however, both forms of the NPM1 protein are observed in the cytoplasm due to the formation of NPM1-NPMc+ heterooligomers through the conserved NPM1 N-terminal domain;[44,45,49] the formation of these

[49] Falini, B.; Bolli, N.; Shan, J.; Martelli, M. P.; Liso, A.; Pucciarini, A.; Bigerna, B.; Pasqualucci, L.; Mannucci, R.; Rosati, R.; Gorello, P.; Diverio, D.; Roti, G.; Tiacci, E.; Cazzaniga, G.; Biondi, A.; Schnittger, S.; Haferlach, T.; Hiddemann, W.; Martelli, M. F.; Gu, W.; Mecucci, C.; Nicoletti, I. Both Carboxy-terminus NES Motif and Mutated Tryptophan(s) are Crucial for Aberrant Nuclear Export of Nucleophosmin Leukemic Mutants in NPMc+ AML. *Blood*. **2006**, *107*, 4514-4523.

oligomers also results in a loss of NPM1 functionality in numerous cellular contexts.[44,50] The observation of NPM1 in the cytoplasm of AML cells also provides a rapid histochemical method for the detection of *NPM1* gene mutations in AML patients. *NPM1* gene mutations are associated with a positive response to traditional chemotherapy and increased long-term patient survival rates, and are thus clinically important prognostic indicators in AML. Indeed, AML patients exhibiting cytoplasmic NPM1 are identified as the distinct AML subclass NPMc+ by the World Health Organization.

Table 1.2. Primary structures of the extreme C-terminus of AML-associated NPMc+ variants and the subcellular localization of GFP-tagged NPMc+-derived fusion proteins. The NoLS is in purple; the NPMc+-specific NES is in blue.

Entry	1° Structure	Description	Localization
1	281-QEAIQDL**W**Q**W** RKSL-COOH	Wild-type	nucleolus
2	281-QEAIQD**L**CLA **V**EE**V**S**L**RK-COOH	Mutant A	cytoplasm
3	281-QEAIQD**LW**L**W** **V**EE**V**S**L**RK-COOH	Mutant A-NoLS^{+}	nucleolus
4	281-QEAIQD**L**CGA GEEGS**L**RK-COOH	Mutant A-NES^{-}	nucleus
5	281-QEAIQD**LW**QS **L**AQ**V**S**L**RK-COOH	Mutant E	nucleolus, cytoplasm

1.6 Nucleophosmin as a Therapeutic Target in Cancer

Due to its prominent roles in the initiation and progression of AML and other human cancers, NPM1 is emerging as a novel target for therapeutic intervention.[51] However, despite considerable interest, only three small molecules, including avrainvillamide, have been demonstrated to bind to NPM1 in cancer cell antiproliferation. NSC348884 (**24,** Figure 1.10)

[50] Czepiel,K.; Nichol, K.; Tippy, M.; Abayasekara, N.; Lee, J.; Wajswol, E.; Khanna, A.; Berliner, N.; Khanna-Gupta, A. Haploinsufficiency of NPM1 in AML Derived NPM1 Mutant (NPMc+) Expressing Cells Contributes to Aberrant C/EBPα Activity. *Blood*. **2014**, *124*, 21-30.

[51] Balusu, R.; Fiskus, W.; Rao, R.; Chong, D. G.; Nalluri, S.; Mudunuru, U.; Ma, H.; Chen, L.; Venkannagari, S.; Ha, K.; Abhyankar, S.; Williams, C.; McGuirk, J.; Khoury, H. J.; Ustun, C.; Bhalla, K. N. Targeting Levels or Oligomerization of Nucleophosmin 1 Induces Differentiation and Loss of Survival of Human AML Cells with Mutant NPM1. *Blood*. **2011**, *118*, 3096-3106.

is a synthetic polybenzimidazole that inhibits NPM1 oligomerization and induces p53-mediated apoptosis in leukemic cells.[52] More recently, the Waldmann group has reported a cascade synthesis of natural product-inspired indoloquinolizines such as **25**, which were revealed to be potent modulators of centrosome integrity.[53] These compounds, however, were demonstrated to bind to Crm1 with higher affinity than NPM1; specific consequences of the indoloquinolizine-NPM1 interaction were not investigated further. Indeed, leptomycin B (LMB), a specific Crm1 ligand, is also known to deregulate centrosome duplication;[26] it is thus possible that the biological activity of these compounds is primarily (or entirely) mediated by Crm1. Two non-

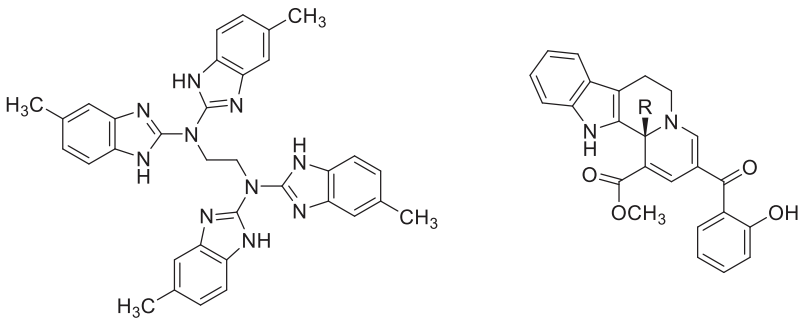

Figure 1.10. Chemical structures of two NPM1-binding small molecules.

small molecule modulators of NPM1 have also been described — a synthetic 76-nucleotide RNA aptamer, which, like NSC348884, inhibits NPM1 oligomerization, induces apoptosis, and sensitizes cells towards DNA-damaging agents,[54] and a peptide derived from the human immunodeficiency virus (HIV) Rev protein, which was demonstrated to inhibit tumor growth in

[52] Qi, W.; Shakalya, K.; Stejskal, A.; Goldman, A.; Beeck, S.; Cooke, L.; Mahadevan, D. NSC348884, a Nucleophosmin Inhibitor Disrupts Oligomer Formation and Induces Apoptosis in Human Cancer Cells. *Oncogene*. **2008**, *27*, 4210-4220.

[53] Dückert, H.; Pries, V.; Khedkar, V.; Menninger, S.; Hübel, K.; Ziegler, S.; Kumar, K.; Waldmann, H. Natural Product-inspired Cascade Synthesis Yields Modulators of Centrosome Integrity. *Nat. Chem. Biol.* **2012**, *8*, 179-184.

[54] Jian, Y.; Gao, Z.; Sun, J.; Shen, Q.; Feng, F.; Jing, Y.; and Yang, C. RNA Aptamers Interfering with Nucleophosmin Oligomerization Induce Apoptosis of Cancer Cells. *Oncogene*. **2009**, *28*, 4201-4211.

mice.[55] As a result of both the complexity of NPM1 biology and the lack of molecules known to interact with NPM1, the hypothesis that NPM1 is a viable therapeutic target remains untested in clinical contexts. The altered trafficking of NPM1 in NPMc+ AML has also been identified as a potential point of therapeutic intervention.[56] It has been demonstrated that small molecule inhibitors of Crm1-mediated nuclear export induce nuclear retention of NPMc+ proteins.[57,58] These Crm1 inhibitors, however, do not interact with NPM1 or NPMc+, and do not restore NPMc+ proteins to the nucleolus. Indeed, while small molecules that target the N-terminal domain of NPM1, such as NSC348884, presumably interact with the corresponding (conserved) domain of NPMc+ proteins, small molecules that specifically interact with the mutated C-terminal domain of AML-associated NPMc+ proteins have not been described in the literature.

1.7 Research Strategy

Although the main goal of our research on avrainvillamide could be stated briefly, the avrainvillamide problem was certainly a daunting one. In short, we sought to determine the mechanisms underlying the antiproliferative activity of avrainvillamide. This simple statement could then be expanded in numerous directions. What are the functional consequences of the interaction between avrainvillamide and NPM1? Does avrainvillamide affect the biological

[55] Chan, H. J.; Weng, J. J.; Yat, B.; Yung, M. Nucleophosmin/B23-binding Peptide Inhibits Tumor Growth and Up-regulates Transcriptional Activity of p53. *Biochem. Biophy. Res. Commun.* **2005**, *333*, 396-403.
[56] Falini, B.; Gionfriddo, I.; Cecchetti, F.; Ballanti, S.; Pettirossi, V.; Martelli, M. P. Acute Myeloid Leukemia with Mutated Nucleophosmin (NPM1): Any Hope for a Targeted Therapy? *Blood Rev.* **2011**, *6*, 247-254.

[57] Ranganathan, P.; Yu, X.; Na, C.; Santhanam, R.; Shacham, S.; Kauffman, M.; Walker, A.; Klisovic, R.; Blum, W.; Caligiuri, M.; Croce, C. M.; Marcucci, G.; Garzon, R. Preclinical Activity of a Novel CRM1 Inhibitor in Acute Myeloid Leukemia. *Blood*. **2012**, *120*, 1765-1773.

[58] Etchin, J.; Sun, Q.; Kentsis, A.; Farmer, A.; Zhang, Z. C.; Sanda, T.; Mansour, M. R.; Barcelo, C.; McCauley, D.; Kauffman, M.; Shacham, S.; Christie, A. L.; Kung, A. L.; Rodig, S. J.; Chook, Y. M.; Look, A. T. Antileukemic Activity of Nuclear Export Inhibitors that Spare Normal Hematopoietic Cells. *Leukemia*. **2013**, *27*, 66–74.

activity of targets other than NPM1? Can the *in vitro* antiproliferative activity of avrainvillamide be translated into a clinically relevant therapeutic strategy? At the outset, we had little data to rely on. Although we were confident that NPM1 was a primary cellular target of avrainvillamide, the biological consequences of this interaction remained unclear. The multiple cellular functions of NPM1 and the lack of easily quantifiable NPM1 enzymatic activity only served to complicate our analysis, which was further impeded by both the scarcity of NPM1-interacting small molecules as well as the dearth of literature reports of NPM1 as a point of therapeutic intervention in cancer.

Nevertheless, we identified several potential leads to follow. First and foremost among these was the altered trafficking of NPMc+ proteins in AML, since these variants exhibit mutations proximal to the avrainvillamide-binding residue of NPM1. We also sought to obtain further proof of the formation of an avrainvillamide-NPM1 complex, and ideally, to characterize differences between the interactions of avrainvillamide and NPM1 and NPMc+ proteins. Our studies on the intracellular transport of NPM1 subsequently led us to explore Crm1 as a secondary target of avrainvillamide; this was also supported by the prior identification of Crm1 as a potential binding partner of avrainvillamide in affinity-isolation assays employing probe **23**. We were then able to examine the effects of avrainvillamide on cellular processes that are mediated by both NPM1 and Crm1, eventually leading to the discovery that avrainvillamide deregulates mitosis through its effects on these two proteins. Finally, we studied the effects of avrainvillamide on NPM1 phosphorylation levels, which provided further insights into the mechanisms of action of avrainvillamide.

Chapter 2

The Biological Activity of Avrainvillamide is Mediated by Nucleophosmin and Exportin-1

2.1 Avrainvillamide Binds the C-Terminal Domains of Wild-Type Nucleophosmin and AML-Associated Nucleophosmin Mutants

Despite considerable evidence that nucleophosmin was a cellular target of avrainvillamide, initial efforts were unable to directly observe the formation of an avrainvillamide-nucleophosmin adduct. As discussed in Chapter 1, several truncated NPM1 constructs were prepared for use in co-crystallization experiments that were ultimately unsuccessful. Nevertheless, we saw an opportunity to use these NPM1 constructs to probe the nature of the avrainvillamide-NPM1 interaction by other means.

To this end, we pursued a series of mass spectrometry studies employing the isolated C-terminal domains of NPM1. Initial experiments were conducted in collaboration with Dr. Jeremy Wulff (Bruker Daltronics, Billerica, Massachusetts) using a 12 Tesla Fourier transform ion cyclotron resonance (FT–ICR) solariX XR mass spectrometer, which we hypothesized would enable the study of the largest NPM1 construct (NPM1–C_{108}) prepared during the initial crystallization assays. NPM1–C_{108} contains the C-terminal 108 amino acids (residues 187-294) of human NPM1, and thus contains the full C-terminal three-helix bundle of NPM1 as well as the unstructured region immediately adjacent to it. Gratifyingly, the observed molecular weight (MW) of NPM1–C_{108} (12 157 g mol^{-1}) was in close agreement with the predicted value (12 165 g mol^{-1}) in initial experiments employing the peptide construct alone (Figure 2.1). To our surprise, however, we observed a second peak in the mass spectrum of NPM1–C_{108}; this was ultimately identified as the product of disulfide bond formation between NPM1 and β-mercaptoethanol (Δ MW = +76 g mol^{-1}) which had been used in the preparation and purification of the NPM1 constructs. This disulfide proved to be resistant towards typical biochemical reducing agents (DTT, TCEP; Figure S.1) and was initially considered a nuisance. However, since subsequent

experiments demonstrated that this adduct was unreactive towards avrainvillamide, it ultimately served as a useful control in binding assays employing the NPM1–C_{108} construct.

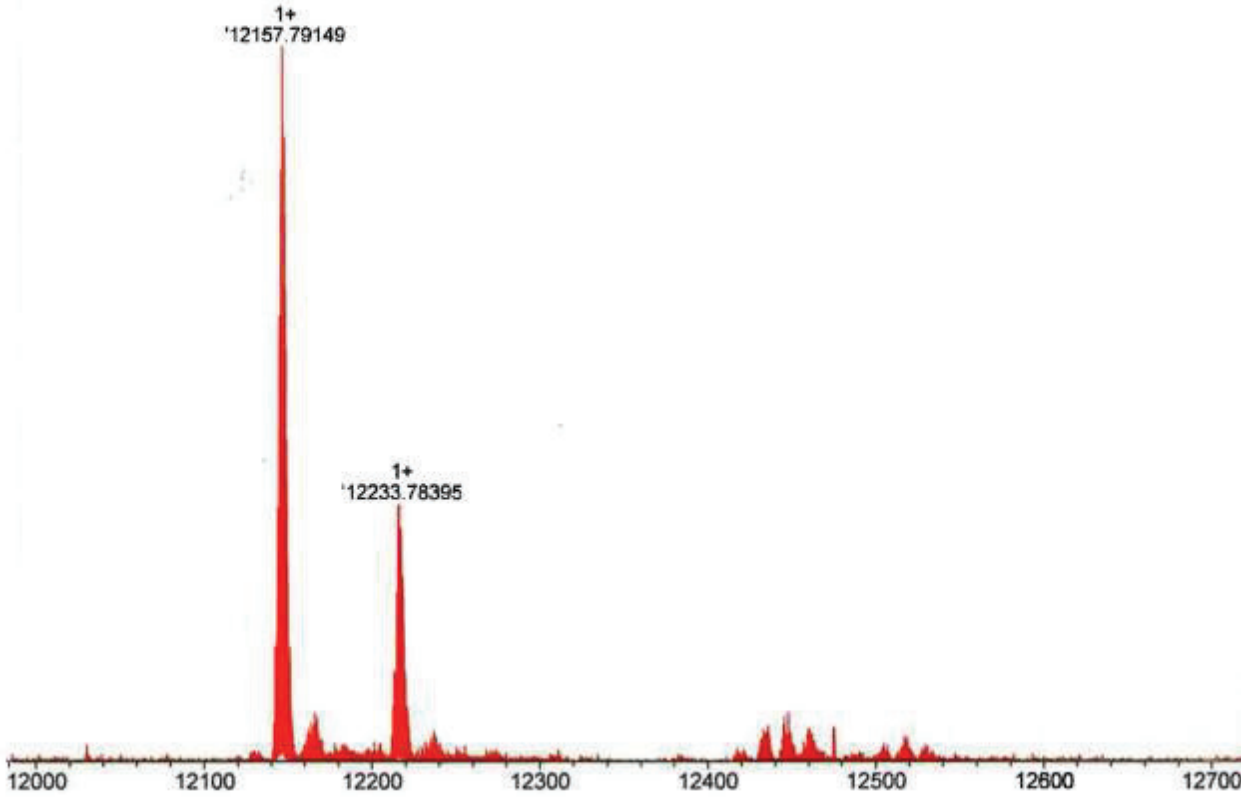

Figure 2.1. Deconvoluted 12 Tesla FT–ICR mass spectrum of the NPM1–C_{108} construct.

To our delight, when DMSO solutions of avrainvillamide (10 eq. relative to NPM1–C_{108}) were added to solutions of the NPM1 construct, we observed the rapid formation of an avrainvillamide-NPM1–C_{108} adduct (Figure 2.2). This complex could be observed within 1 minute at 23 °C, while the fraction of NPM1–C_{108} bound by avrainvillamide appeared to reach a maximal value after approximately 4 hours. Unbound NPM1–C_{108} was always observed under these conditions, even after prolonged incubation with avrainvillamide (24 hours), suggesting that an equilibrium state had been reached. Indeed, increasing the concentration of avrainvillamide strongly reduced the intensity of the unbound NPM1–C_{108} peak (Figure S.2).

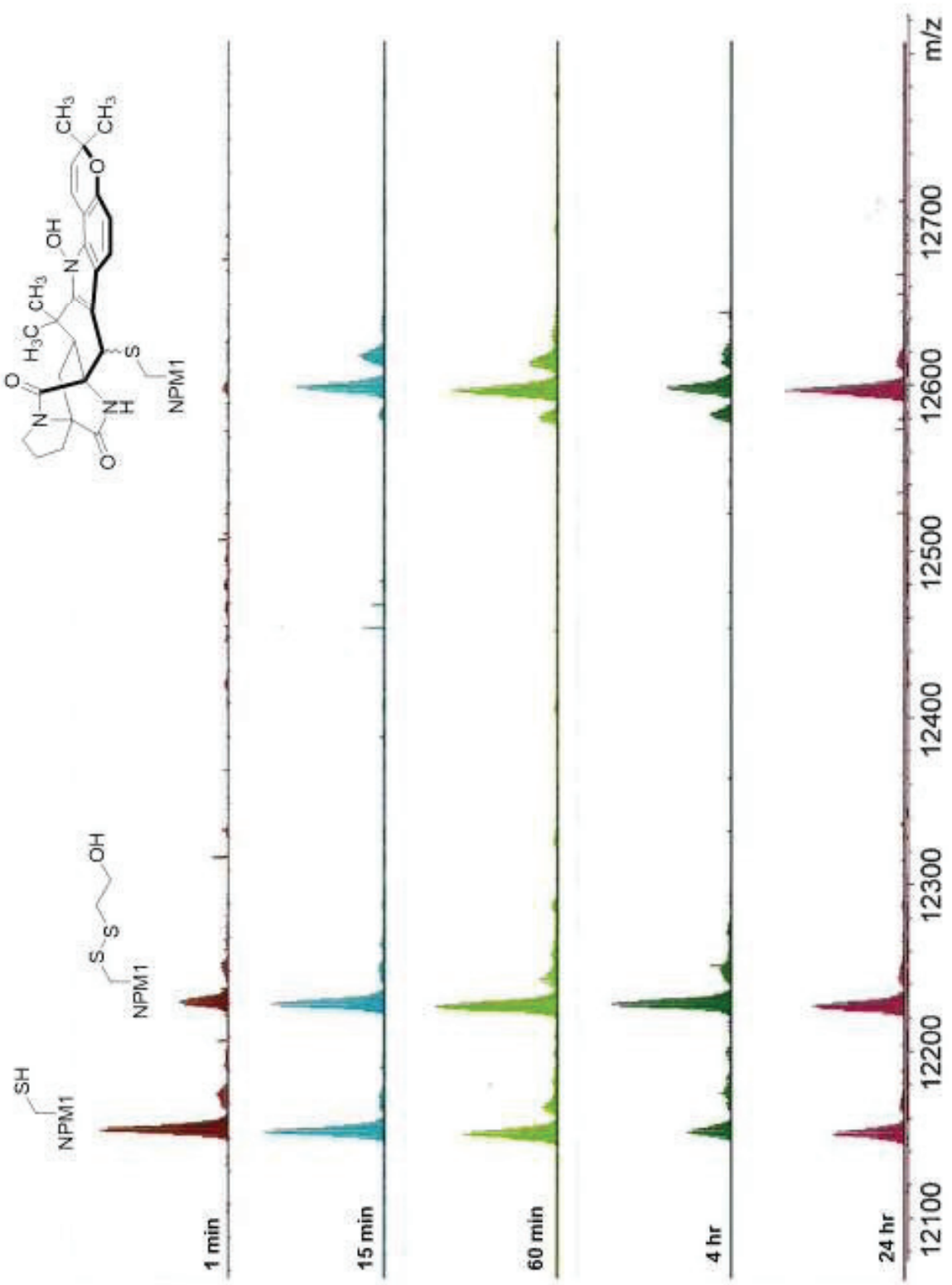

Figure 2.1. Deconvoluted mass spectra of the NPM1–C_{108} construct following treatment with an excess of avrainvillamide (10 eq.). Aliquots of the reaction mixture were removed at the indicated time points, desalted, and analyzed by FT–ICR mass spectrometry.

in the mass spectrum of the resulting solution. Finally, ions corresponding to the avrainvillamide-NPM1–C_{108} adduct were collected and fragmented by electron-transfer dissociation; analysis of the resulting MS-MS spectrum revealed that avrainvillamide alkylated the NPM1 construct exclusively at cys^{275}. While this construct does not contain the other two cysteine residues present in full-length NPM1, these results did indicate that interactions between avrainvillamide and other potentially nucleophilic serine or threonine residues located within this domain of NPM1 are likely of little significance.

We next studied the interactions of several avrainvillamide analogs with NPM1–C_{108} (Figure 2.3). We observed a strong correlation between the bound fraction of NPM1–C_{108} and analog potency in whole-cell antiproliferative assays, in agreement with prior results from competitive affinity-isolation experiments. Competitive mass spectrometry experiments also provided additional insights into the reversibility of the avrainvillamide-NPM1–C_{108} interaction. Thus, when avrainvillamide was added to a solution containing NPM1–C_{108} and analog **28** (and thus a small, but observable, amount of the corresponding adduct), the less potent analog was rapidly displaced from NPM1–C_{108} by avrainvillamide. Similarly, treating a solution of avrainvillamide and NPM1–C_{108} with a large excess of the approximately equipotent analog **18** resulted in the essentially complete replacement of avrainvillamide by analog **18** in the NPM1–C_{108} complex. Notably, these experiments provided the first evidence that the interaction between avrainvillamide and proteins was indeed reversible (as was observed in its reaction with simpler nucleophiles). Taken together, the data strongly supported the hypothesis that the (reversible) interaction between avrainvillamide and NPM1 was a key mediator of the antiproliferative activity of avrainvillamide.

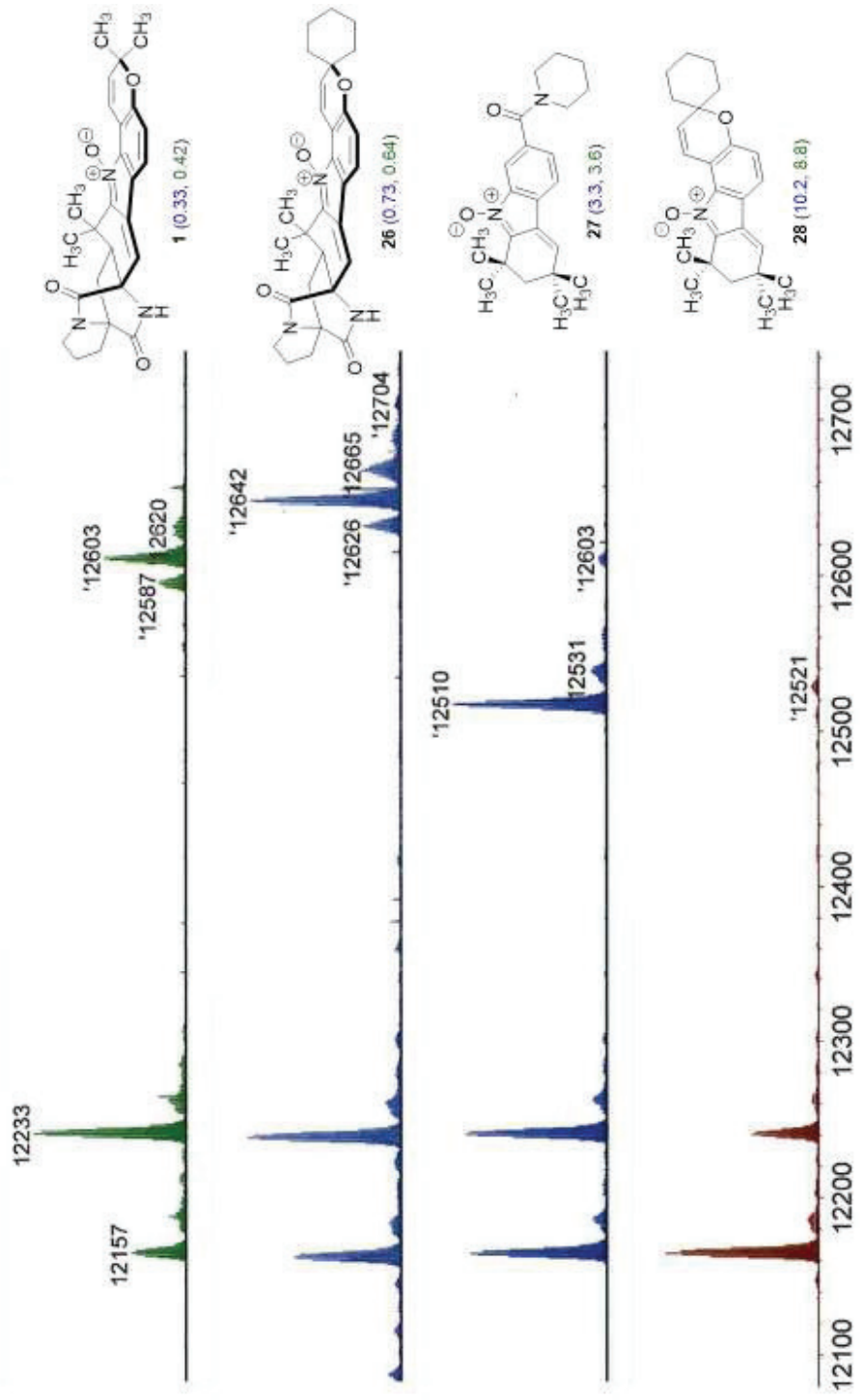

Figure 2.3. Deconvoluted mass spectra of the NPM1–C_{108} construct following treatment with avrainvillamide or analogs **26-28**. Aliquots of each reaction mixture were removed 4 hr after the addition of the indicated small molecule, desalted, and analyzed by FT–ICR mass spectrometry. Values in parentheses indicate 72-hr GI_{50} values (in μM) against LNCaP (in blue) and T–47 D (in green) cells.

Despite the wealth of data we had obtained through our collaboration with Bruker, several factors contributed to our decision to conduct further mass spectrometry experiments elsewhere. Among these were inconsistent instrument availability (which often required waiting several months between experiments) and issues with instrument performance (we were unable to obtain high-quality data on multiple occasions). The use of nanospray injection with the solariX instrument required a sample desalting step immediately prior to sample injection, limiting our ability to conduct time-resolved experiments. Lastly, over the course of our experiments we found that optimal results were obtained by collecting ions with a relatively narrow range of m/z values, limiting our ability to obtain reproducible quantitative data.

Around this time Dr. Sunia Trauger joined the Bauer Core Facility at Harvard. Dr. Trauger was instrumental in enabling us to conduct detailed mass spectrometric studies using an Agilent 6220 LC-TOF instrument that was available at Harvard. To compensate for the reduced resolving power of this instrument, we chose to study NPM1–C_{52} peptides rather than the longer NPM1–C_{108} construct. These peptides contain the complete C-terminal three-helix bundle of NPM1, and analysis of reconstituted solutions of the peptides by circular dichroism (CD) spectroscopy verified that they exhibited the expected secondary structures (*vide infra*). The NPM1–C_{52} peptides had the additional advantage that they could be prepared by standard synthetic means, obviating the need for the purification of the constructs from expression lysates. In particular, the preparation of the peptides eliminated the need for β-mercaptoethanol during synthesis and purification, and thus the mass spectrum of each NPM1–C_{52} peptide analyzed exhibited a single peak after spectral deconvolution.

We first sought to validate the use of the shorter NPM1–C_{52} peptide. As was observed for the NPM1–C_{108} construct, an avrainvillamide-NPM1–C_{52} adduct was observed within 1 minute

at 23 °C, and the fraction of NPM1–C_{52} bound by avrainvillamide appeared to reach its maximum value (88%) within 2 hr (Figure 2.4 A). The fraction of NPM1–C_{52} bound by avrainvillamide was again strongly dependent on the molar ratio of avrainvillamide to peptide construct and a correlation was observed between NPM1–C_{52} binding affinity and analog potency in antiproliferative assays. Given this strong similarity between the data obtained from the NPM1–C_{52} and the NPM1–C_{108} construct, we thus elected to use the shorter peptide in subsequent binding experiments.

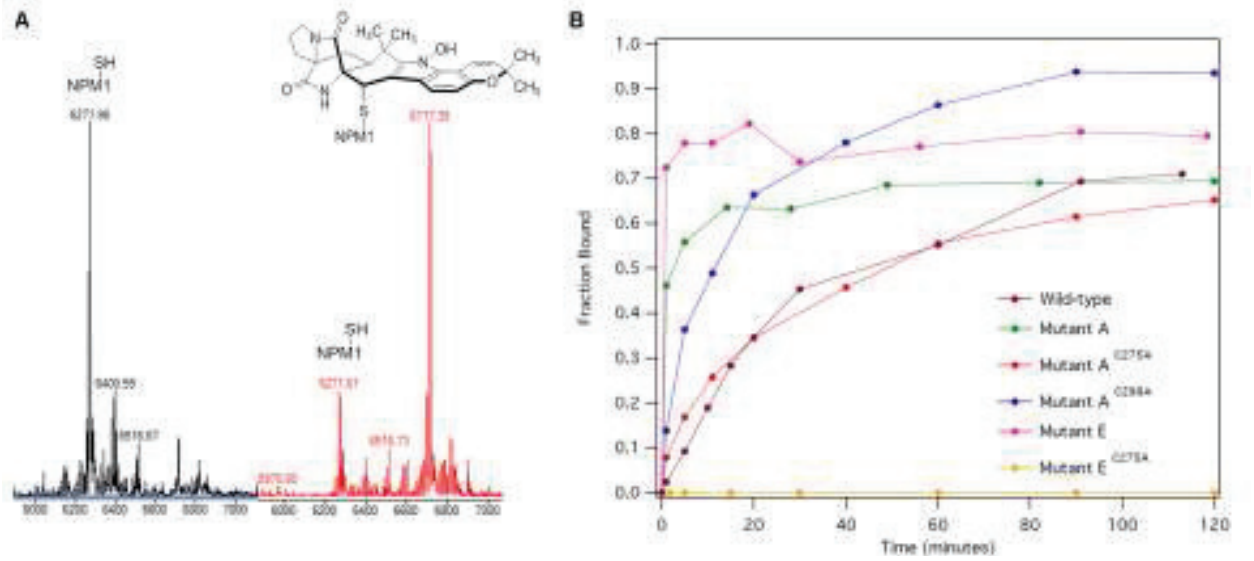

Figure 2.4. **A**. Deconvoluted ESI-TOF mass spectrum of the NPM1–C_{52} construct in the absence (black trace) or presence (red trace) of avrainvillamide (3 eq., 2 hr). **B.** Fraction of NPM1–C_{52} (NPM1–C_{56} for NPMc+ variants) peptide bound by avrainvillamide as a function of time.

A main focus of these experiments was to determine how changes in the primary and secondary structures of NPM1 impacted its reactivity towards avrainvillamide. Specifically, given the considerable structural differences between the C-terminal domains of wild-type NPM1 and AML-associated NPMc+ variants, we hypothesized that avrainvillamide may display selectivity for one form of the protein. To this end, we studied the reaction between avrainvillamide and each of seven NPM1 C-terminal domains. Thus, avrainvillamide (150 μM,

3 eq. relative to NPM1)[59] was added to a 50 μM solution of NPM1–C_{52} peptide at 23 °C; reaction progress was monitored by mass spectrometry at fixed intervals. These initial binding assays demonstrated that avrainvillamide binds the unfolded C-terminal domains of NPM1–Mutant A and NPM1–Mutant E in addition to the corresponding structured domain of wild-type NPM1; furthermore, avrainvillamide alkylates peptides derived from NPMc+ proteins more rapidly than the parent NPM1–C_{52} domain (Figure 2.4 B). On the other hand, difference between the steady-state bound fractions of the various NPM1 C-terminal domains was far less pronounced. The cysteine-mutated peptides revealed that, in addition to cys^{275}, cys^{288} of NPM1–Mutant A, a residue not present in wild-type NPM1, is also alkylated by avrainvillamide under these conditions. For the parent NPM1–Mutant A–C_{56} peptide, which contains both cysteine residues, the product of a single alkylation was the major product observed under the initial conditions studied. However, an adduct between NPM1–Mutant A–C_{56} and two molecules of avrainvillamide was observed when increased concentrations of avrainvillamide were used (500 μM, 10 eq. relative to NPM1; refer to Appendix IV for spectra). Finally, no complexes were observed between avrainvillamide and the NPM1–Mutant A–C275,288A–C_{56} nor the NPM1–Mutant E-C275A–C_{56} peptides, consistent with our previous results indicating that avrainvillamide interacts with the C-terminal domain of NPM1 exclusively through cysteine residues.

The apparent kinetic selectivity of avrainvillamide for the C-terminal domain of NPMc+ variants was subsequently explored in detail by measuring the relative rates of formation of the various avrainvillamide-NPM1 peptide complexes. To accomplish this we studied the reaction between avrainvillamide and the NPM1 peptides at early time points (ca. 1–10 minutes), when

[59] The smaller ratio of avrainvillamide to NPM1 used in these experiments enabled the more reproducible quantitation of NPM1 binding affinity at early time points.

the rates of formation of the adducts followed pseudo-first-order kinetics. In agreement with our previous observations, the rates of alkylation of the NPM1–Mutant A–C_{56} and NPM1–Mutant E–C_{56} peptides were both approximately 4.6-fold higher than the rate of alkylation of the wild-type NPM1–C_{52} peptide (Table 2.1). The C275A mutation in the NPM1–Mutant A–C_{56} peptide resulted in a 3.5-fold reduction in reaction rate, whereas the corresponding C288A mutation only

Table 2.1 Relative rates of formation of the NPM1–C_{52}- or NPM1–C_{56}-avrainvillamide complexes. Results are reported as the mean ± standard deviation of three independent experiments.

NPM1 Variant	Modifications	Relative Rate
Wild-type	-	1.0 ± 0.1[a]
Mutant A	-	4.6 ± 0.7
	C275A	1.3 ± 0.2
	C288A	3.6 ± 0.1
	C275A, C288A	0[b]
Mutant E	-	4.6 ± 0.3
	C275A	0[b]

[a]: By definition
[b]: The corresponding avrainvillamide-NPM1–C_{56} complexes were not observed under any circumstances.

reduced the reaction rate by 1.3-fold, indicating that cys^{275} is indeed the primary avrainvillamide binding site within the C-terminal domain of NPM1–Mutant A. Direct competition studies further supported these claims; thus avrainvillamide bound a greater fraction of NPM1–Mutant A–C_{56} than wild-type NPM1–C_{52} in solutions containing equimolar amounts of both peptides and a substoichiometric amount of avrainvillamide. Similarly, avrainvillamide displayed a pronounced selectivity for NPM1–Mutant A–C288A–C_{57} in solutions containing both the NPM1–Mutant A–C288A–C_{57} and NPM1–Mutant A–C275A–C_{56} peptides (refer to Appendix IV for spectra). Taken together, our data indicates that cys^{275} of NPM1–Mutant A is the primary

avrainvillamide binding site of NPM1–Mutant A, and furthermore, that this residue is alkylated more rapidly than the corresponding site in wild-type NPM1. Notably, this represented the first report of a small molecule that interacts with the mutated C-terminal domain of AML-associated NPMc+ variants.

2.2 Avrainvillamide Relocalizes AML-Associated NPM1 Mutants to the Nucleolus of Leukemic Cells

Our discovery that avrainvillamide binds the C-terminal domain of NPMc+ proteins, combined with the clinical significance of NPM1 mutations in AML patients led us to explore the effects of avrainvillamide on the subcellular localization of NPMc+ proteins in cultured human cancer cells. To this end, we chose to study the effects of avrainvillamide in OCI–AML2 cells, which are homozygous for wild-type NPM1, and in OCI–AML3 cells, which are heterozygous wild-type NPM1/NPM1–Mutant A.[60] Avrainvillamide exhibited moderate antiproliferative activity against both cell lines (GI_{50} values at 72 hr of 0.35 ± 0.09 μM and 0.52 ± 0.15 μM for OCI–AML2 and OCI–AML3 cells, respectively), however, the antiproliferative activity of avrainvillamide against these leukemic cell lines showed a strong dependence on initial cell seeding density. For each cell line, cells were treated with increasing concentrations of avrainvillamide, then the cells were fixed, stained for total NPM1, nucleolin (as a nucleolar marker), and DNA (as a nuclear marker), then imaged on a fluorescence microscope.

[60] Quentmeier, H.; Martelli, M.; Dirks, W.; Bolli, N.; Liso, A.; MacLeod, R.; Nicoletti, I.; Mannucci, R.; Pucciarini, A; Bigerna, B. Cell Line OCI/AML3 Bears Exon-12 NPM Gene Mutation-A and Cytoplasmic Expression of Nucleophosmin. *Leukemia.* **2005**, *19*, 1760-1767.

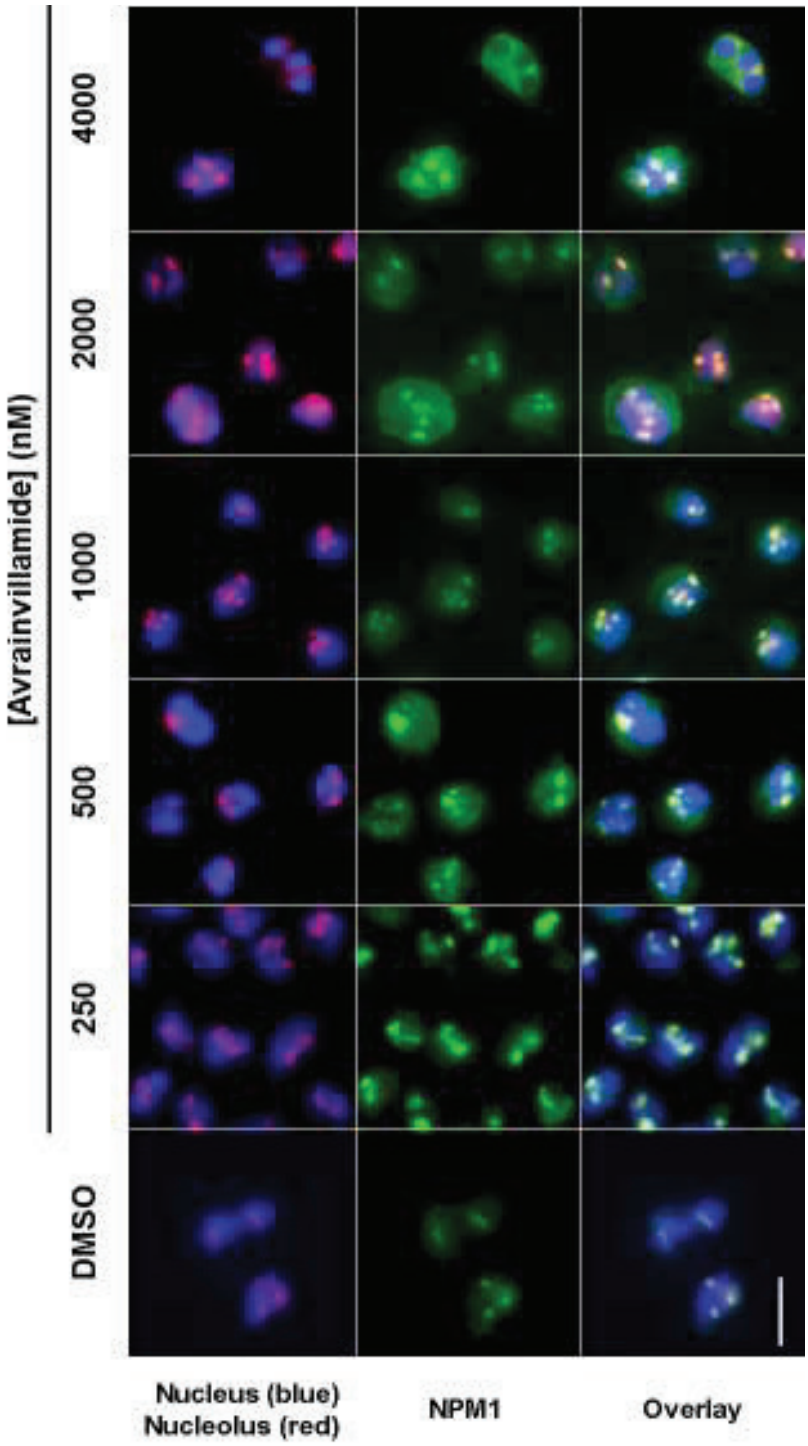

Figure 2.5. Representative immunofluorescence microscopy images of OCI–AML2 cells following treatment with DMSO (vehicle control) or varying concentrations of avrainvillamide (48 hr). Colors: green, NPM1; red, nucleolin (nucleolar marker); blue, DNA (nuclear marker). Scale bar = 10 μm.

As expected, NPM1 was observed predominantly in the nucleoli of OCI–AML2 cells; this localization phenotype was unaffected by treatment with sublethal concentrations of avrainvillamide (Figure 2.5). In contrast, NPM1 was observed in both the cytoplasm and nucleoli of untreated OCI–AML3 cells. When these cells were exposed to sublethal doses of avrainvillamide, NPM1 was observed to concentrate in nucleoli, although NPM1 was also observed diffusely throughout nuclei (Figure 2.6). This remarkable phenotype is markedly different from the phenotype induced by leptomycin B (LMB), a specific inhibitor of Crm1-mediated nuclear export (which relocalizes NPMc+ proteins to the nuclei, but not nucleoli),[61] suggesting that avrainvillamide mediates the relocalization of NPMc+ proteins by a mechanism that is either partially or wholly Crm1-independent.

At the highest concentration of avrainvillamide studied (4.0 μM, 48 hr), which induced an apoptotic phenotype in both cell lines, we observed condensed or fragmented nuclei and a loss of nucleolar structure. The subcellular localization of NPM1 in apoptotic cells, however, was remarkably different between the two cell lines. NPM1 was excluded from the nuclei of apoptotic OCI–AML2 cells, whereas NPM1 was apparently retained in the highly condensed nuclei of OCI–AML3 cells. We also observed an apparent reduction in nucleolin expression levels in OCI–AML3, but not OCI–AML2 cells, suggesting that the mechanisms underlying the antiproliferative activity of avrainvillamide in leukemic cells may be cell line- (and potentially NPM1 mutational status-) dependent.

[61] Bolli, N.; Nicoletti, I.; De Marco, M. F.; Bigerna, B.; Pucciarini, A.; Mannucci, R.; Martelli, M. P.; Liso, A.; Mecucci, C.; Fabbiano, F.; Martelli, M. F.; Henderson, B. R.; Falini, B. Born to be Exported: COOH-terminal Nuclear Export Signals of Different Strength Ensure Cytoplasmic Accumulation of Nucleophosmin Leukemic Mutants. *Cancer Res.* **2007**, *67*, 6230-6237.

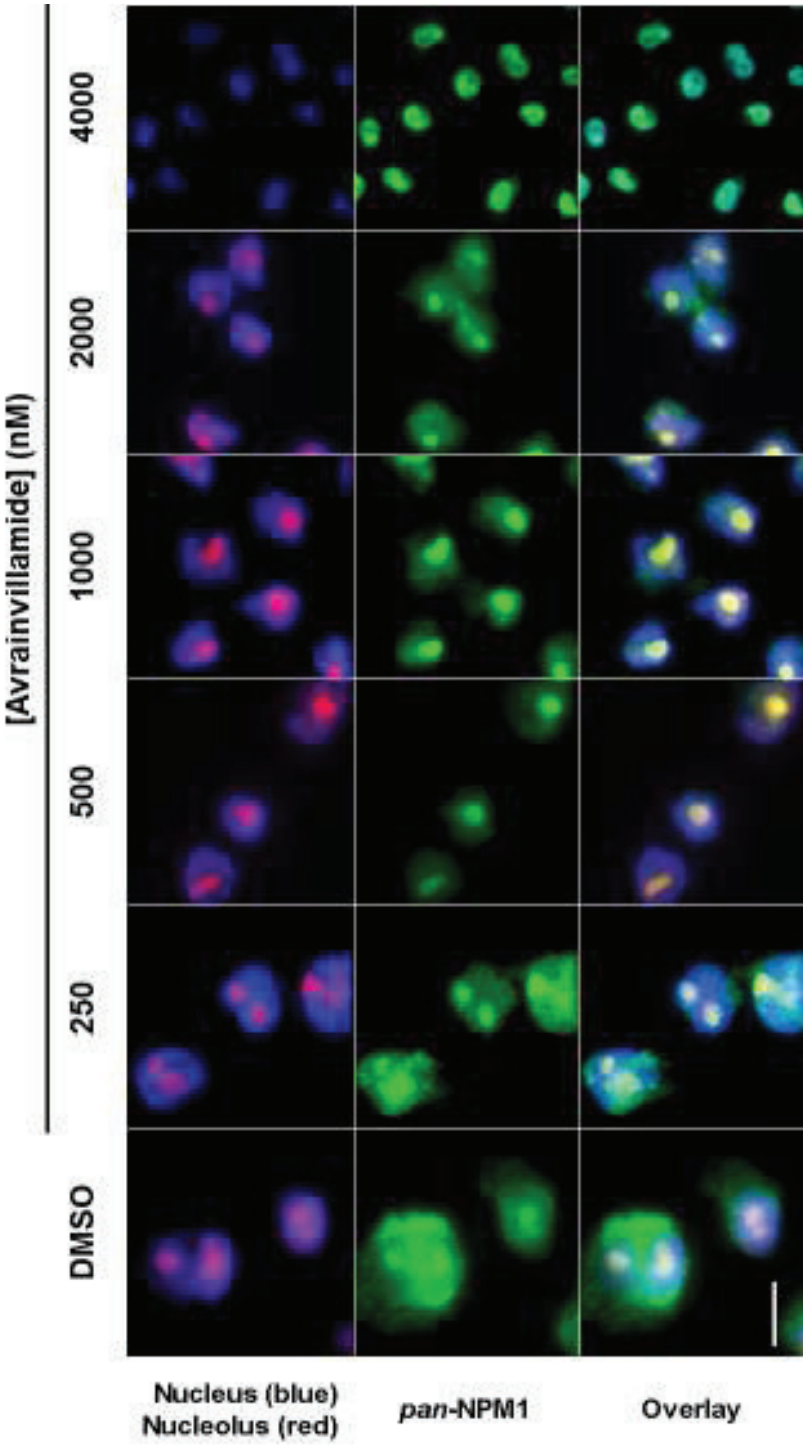

Figure 2.6. Representative immunofluorescence microscopy images of OCI–AML3 cells following treatment with DMSO (vehicle control) or varying concentrations of avrainvillamide (48 hr). Colors: green, *pan*-NPM1; red, nucleolin (nucleolar marker); blue, DNA (nuclear marker). Scale bar = 10 μm. Quantitative relocalization data (as a percentage of cells) is available in Appendix I.

2.3 The Relocalization of NPMc+ Variants to Nucleoli of Cancer Cells Is Mediated by the Interaction of Avrainvillamide and Cys^{275} of NPMc+ Proteins.

To gain further insight into the molecular interactions responsible for the observed relocalization of NPMc+ proteins to the nucleoli of leukemic cells, we studied the effects of avrainvillamide treatment on the subcellular localization of a series of eGFP–NPM1 fusion proteins (Figure 2.7). These constructs consist of an eGFP fluorescent marker tagged to the N-termini of full-length NPM1 proteins; the NPM1 proteins correspond to the NPM1 and NPMc+ C-terminal domains studied in the previously described mass spectrometry binding experiments. These constructs were synthesized by site-directed mutagenesis using a previously described eGFP–NPM1 plasmid[26] as the template. An extensive screen of mutagenesis reaction conditions revealed that the addition of 0.5% (v/v) DMSO was essential for successful amplification of the parent plasmid; it was also observed that longer (50 – 60 bp) primers bearing centrally located mutations performed most efficiently in these reactions. The subcellular localizations of the eGFP–NPM1 fusion proteins were evaluated in the HCT–116 colon cancer cell line; this cell line was selected since it exhibited moderate sensitivity towards avrainvillamide (GI_{50} = 1.10 ± 0.04 μM) and was readily transfected with the synthesized plasmids.

We first sought to revisit our results from the two OCI–AML cell lines. Thus, HCT–116 cells were separately transfected with plasmids encoding either the eGFP–NPM1 protein or the eGFP–NPM1–Mutant A protein and then dosed with either DMSO (as a vehicle control), avrainvillamide (1 μM, 24 hr), or LMB (100 nM, 4 hr). Following dosing, the cells were fixed, stained for nucleolin and DNA, and imaged using a fluorescence microscope. In agreement with

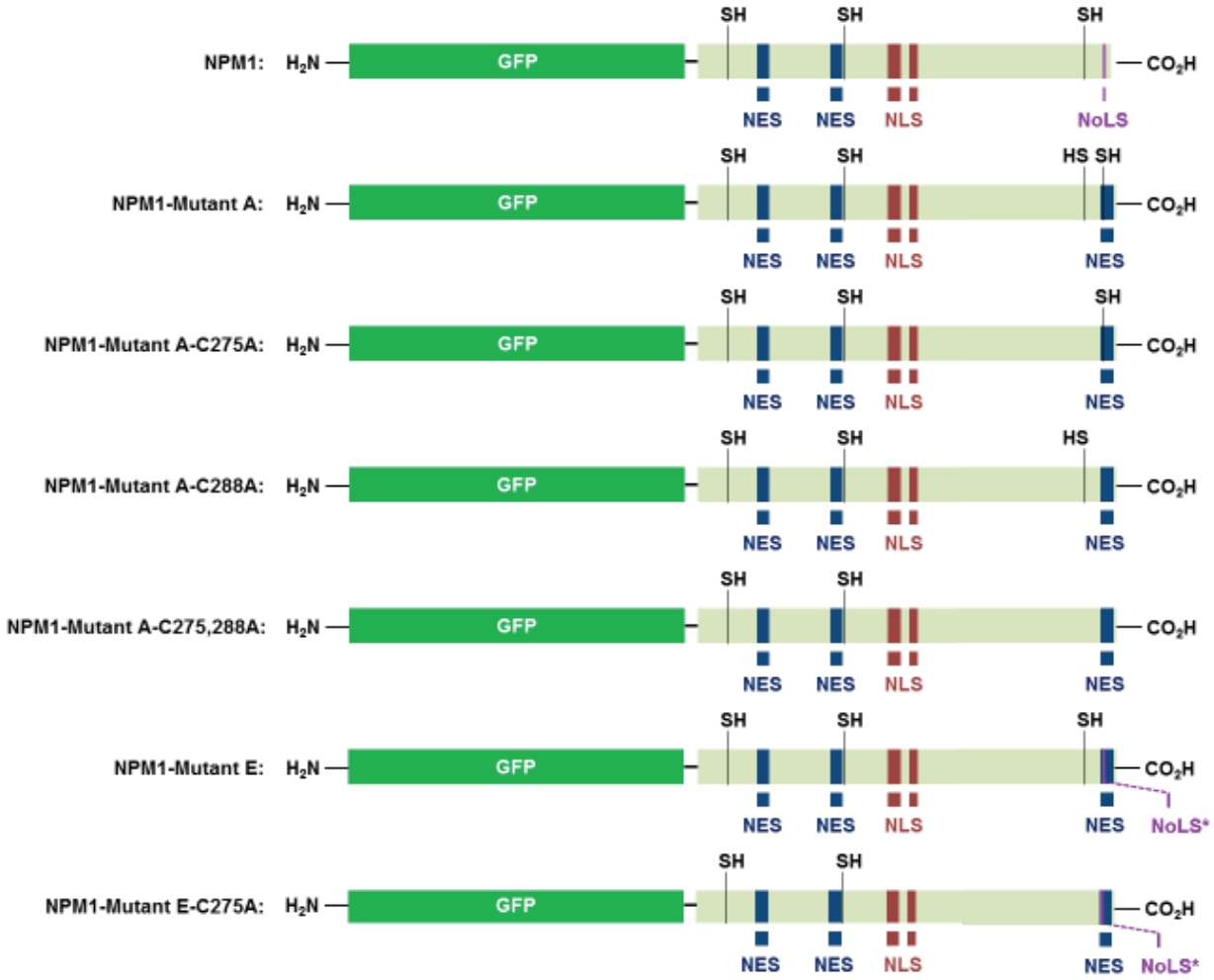

Figure 2.7. Schematic representations of the eGFP–NPM1 and eGFP–NPMc+ fusion proteins used in subcellular localization experiments. Localization sequences are indicated by colored bands; cysteine residues are indicated by –SH groups. NoLS* indicates a partial NoLS present in NPM1–Mutant E resulting from retention of trp[288].

literature reports[26,49] and our previous observations, the eGFP–NPM1 protein was observed exclusively in nucleoli of control cells; this localization phenotype was unaffected by treatment with either avrainvillamide or LMB (Figure 2.8). On the other hand, the eGFP–NPM1–Mutant A protein localized primarily within the cytoplasm, but was observed to relocalize to nucleoli upon treatment with avrainvillamide, mirroring our results in the OCI–AML3 cell line.

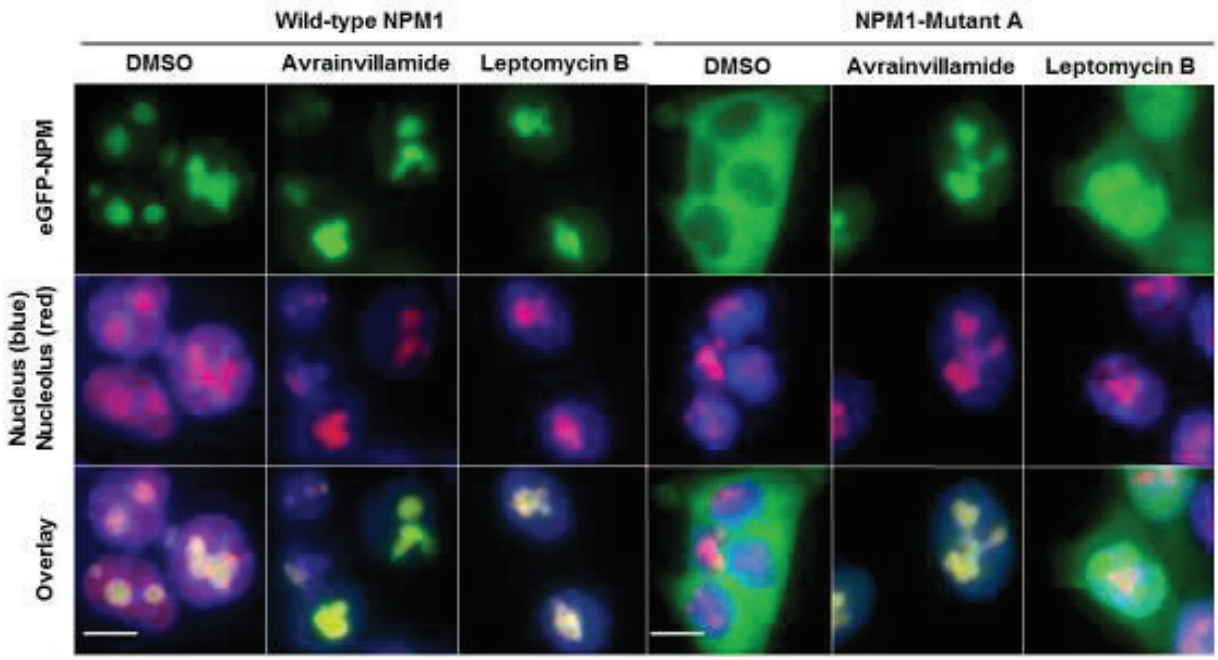

Figure 2.8. Representative immunofluorescence microscopy images demonstrating the subcellular localization of the eGFP–NPM1 (wild-type) and eGFP–NPM1–Mutant A proteins following treatment with either DMSO (vehicle control), avrainvillamide (1 μM, 24 hr), or leptomycin B (100 nM, 4 hr). Colors: green, eGFP; red, nucleolin (nucleolar marker); blue, DNA (nuclear marker). Scale bars = 10 μm. Quantitative relocalization data (as a percentage of cells) is available within Appendix I.

We next sought to identify the molecular interactions responsible for the observed relocalization of NPM1–Mutant A proteins to nucleoli following treatment with avrainvillamide. Since our mass spectrometry experiments revealed that avrainvillamide binds to both cys^{275} and cys^{288} of NPM1–Mutant A, we next studied the effects of avrainvillamide treatment on the subcellular localization of the eGFP–NPM1–Mutant A–C275A and eGFP–NPM1–Mutant A–C288A proteins. The eGFP–NPM1–Mutant A–C275A protein, like the parent eGFP–NPM1–Mutant A protein, localized predominantly within the cytoplasm. Unlike its unmodified counterpart, however, the eGFP–NPM1–Mutant A–C275A protein localized within nuclei, but not specifically nucleoli, following treatment with avrainvillamide (Figure 2.9).

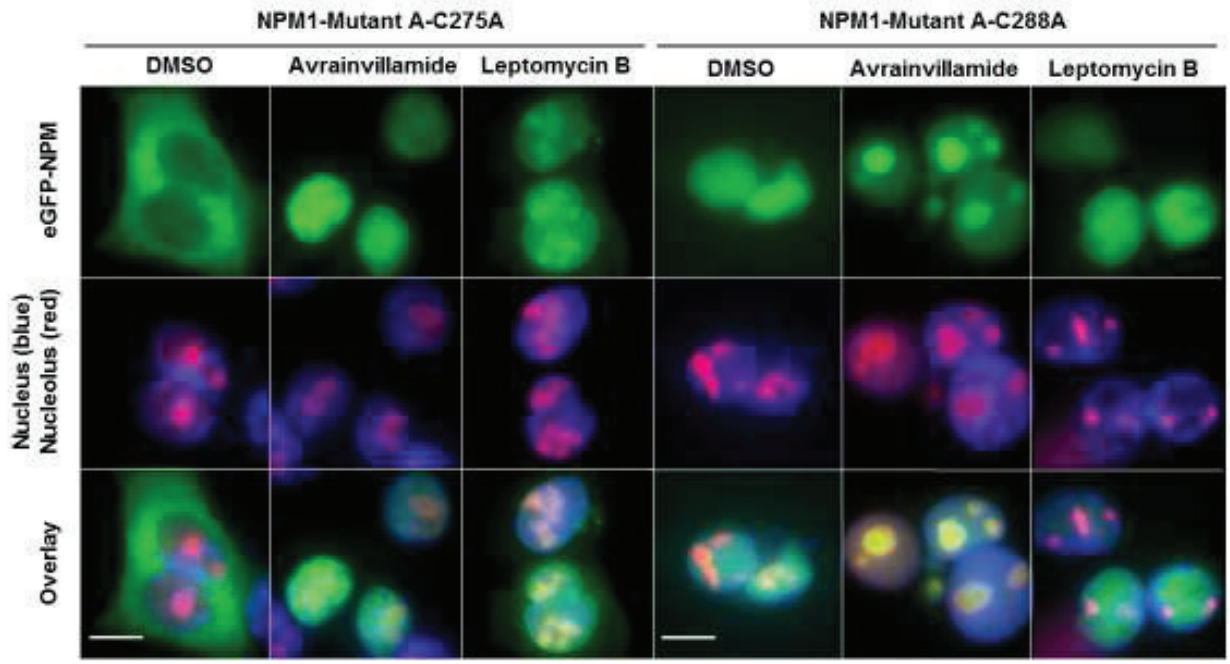

Figure 2.9. Representative immunofluorescence microscopy images demonstrating the subcellular localization of the eGFP–NPM-Mutant A–C275A and eGFP–NPM1–Mutant A–C288A proteins following treatment with either DMSO (vehicle control), avrainvillamide (1 μM, 24 hr), or leptomycin B (100 nM, 4 hr). Colors: green, eGFP; red, nucleolin (nucleolar marker); blue, DNA (nuclear marker). Scale bars = 10 μm. Quantitative relocalization data (as a percentage of cells) is available within Appendix I.

On the other hand, the eGFP–NPM1–Mutant A–C288A protein was found to localize within the nuclei of control cells. This observation is not readily explained in terms of the multiple localization sequences present in NPM1–Mutant A, however, one literature report notes that this protein localizes within nucleoli of leukemic cells.[62] Thus, while the specific subcellular localization of this protein may be cell line-specific, evidence does support the hypothesis that the C288A mutation in NPM1–Mutant A interferes with the ability of Crm1 to recognize its C-terminal NES. When cells expressing this protein were treated with avrainvillamide, the eGFP signal concentrated within nucleoli, as was observed for the eGFP–NPM1–Mutant A construct.

[62] Huang, M.; Thomas, D.; Li, M. X.; Feng, W.; Majeti, R.; Mitchell, B. S. Role of Cysteine 288 in Nucleophosmin Cytoplasmic Mutations: Sensitization to Toxicity Induced by Arsenic Trioxide and Bortezomib. *Leukemia*. **2013**, *27*, 1970-1980.

We studied the effects of LMB on the subcellular localization of each eGFP–NPM1 construct in order to account for the possibility that avrainvillamide mediates the relocalization of NPMc+ proteins indirectly. In particular, Crm1 possesses a solvent-accessible cysteine, cys^{528} (cys^{529} in yeast), which is located within the cargo protein binding site. This residue, one of twenty cysteines in Crm1, is specifically and irreversibly alkylated by the α,β-unsaturated δ-lactone functionality of LMB (certain crystal structures of the resulting adduct also show that the lactone is also opened by a water molecule), thereby preventing the binding and export of substrate proteins, including NPM1 and NPM1–Mutant A (Figure 2.10).[63] As Crm1 was identified as a potential cellular target of avrainvillamide,[11] we recognized the possibility that avrainvillamide may indirectly affect the subcellular localization of NPMc+ proteins in an NPM1–independent manner, by interacting with Crm1.

A direct comparison between avrainvillamide- and LMB-treated cells, however, quickly revealed significant phenotypic differences between the two cell populations. As expected based on literature precedent,[61] LMB treatment resulted in nuclear, but not nucleolar, retention of the NPM1–Mutant A protein; furthermore, this localization phenotype was unaffected by the C275A mutation in NPM1–Mutant A. LMB did not affect the subcellular localization of the NPM1–Mutant A–C288A protein; this was expected since this protein is not exported from the nucleus by Crm1. In particular, LMB treatment never afforded a nucleolar localization phenotype for any of the NPM1–Mutant A constructs examined, demonstrating a critical difference between LMB and avrainvillamide.

[63] Kudo, N.; Matsumori, N.; Taoka, H.; Fujiwara, D.; Schreiner, E. P.; Wolff, B.; Yoshida, M.; Horinouchi, S. Leptomycin B Inactivates CRM1/Exportin 1 by Covalent Modification at a Cysteine Residue in the Central Conserved Region. *Proc. Natl. Acad. Sci. USA.* **1999**, *96*, 9112-9117.

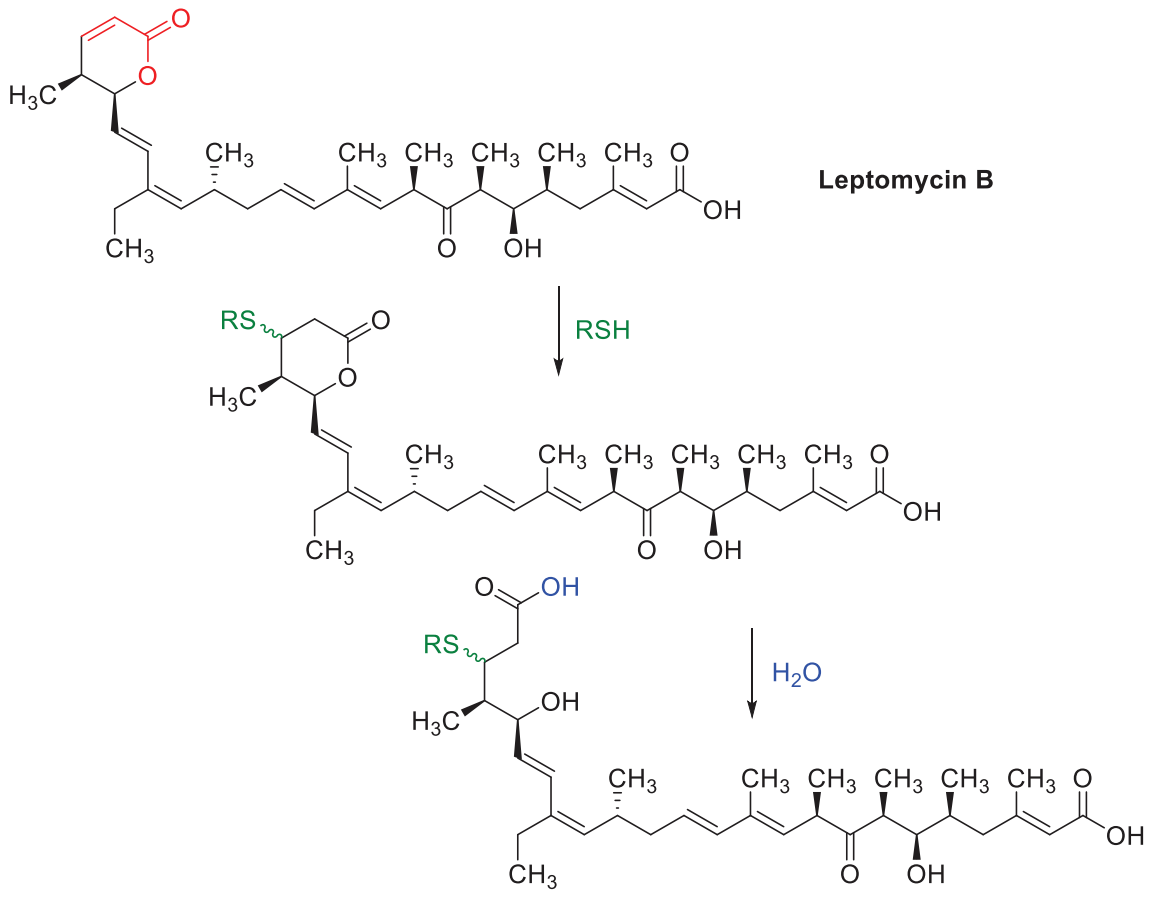

Figure 2.10. Mechanism for the irreversible alkylation of cys[528] of human Crm1 by LMB. The lactone hydrolysis step is nonessential for inhibition of Crm1 export activity, but has been observed in several LMB-Crm1 co-crystal structures.

Taken together, these results greatly increased our understanding of the mechanisms responsible for the observed relocalization of NPMc+ variants upon treatment with avrainvillamide. The comparison of avrainvillamide to LMB demonstrated that avrainvillamide modulates NPMc+ localization through mechanisms that are Crm1-independent. This claim is supported by the observation that avrainvillamide relocalizes the eGFP–NPM1–Mutant A–C288A protein to nucleoli despite our obseervation that this protein is retained in the nucleus (and thus is not subjected to enhanced Crm1-mediated nuclear export as is the case for the eGFP–NPM1–Mutant A protein). Our data also indicates that there are critical functional

differences between of cys^{275} and cys^{288} of NPM1–Mutant A. Specifically, the interaction between avrainvillamide and cys^{275} (but not cys^{288}) of NPM1–Mutant A mediates the relocalization of this protein to nucleoli, since mutation of this residue uniquely results in an altered avrainvillamide-induced NPM1–Mutant A localization phenotype. Indeed, since it was subsequently shown that avrainvillamide inhibits Crm1-mediated nuclear export (*vide infra*), it is possible that the interaction between avrainvillamide and cys^{288} of NPM1–Mutant A does not have any functional consequences in the context of the subcellular localization of NPM1–Mutant A. Finally, to complete the series of eGFP–NPM1–Mutant A constructs, we studied the subcellular localization of the eGFP–NPM1–Mutant A–C275,288A protein (Figure 2.11). This construct localized within the nuclei (but not specifically within nucleoli) of control cells, as was observed for the eGFP–NPM1–Mutant A–C288A protein, and did not relocalize upon treatment with either avrainvillamide or LMB. This result was fully consistent with our previous observations, since this protein did not bind avrainvillamide in our initial mass spectrometric assays and is not exported out of the nucleus by Crm1. Finally, to address the possibility that the effects of avrainvillamide on the subcellular localization of the eGFP–NPM1 fusion proteins were cell line dependent, we repeated the entire series of experiments in HeLa S3 cells (72-hour $GI_{50} = 4.1 \pm 0.3$ μM) and obtained qualitatively identical results (refer to Appendix I for images).

We also conducted a similar series of experiments using the less common NPM1–Mutant E variant. In contrast to the NPM1–Mutant A protein, NPM1–Mutant E contains a W290S mutation and retains trp^{288}, resulting in a partial, but not total, cytoplasmic NPM1 localization phenotype. Additionally, the NPM1–Mutant E variant does not contain a fourth cysteine residue, thus only two eGFP–tagged constructs were prepared—eGFP–NPM1–Mutant E and eGFP–NPM1–Mutant E-C275A.

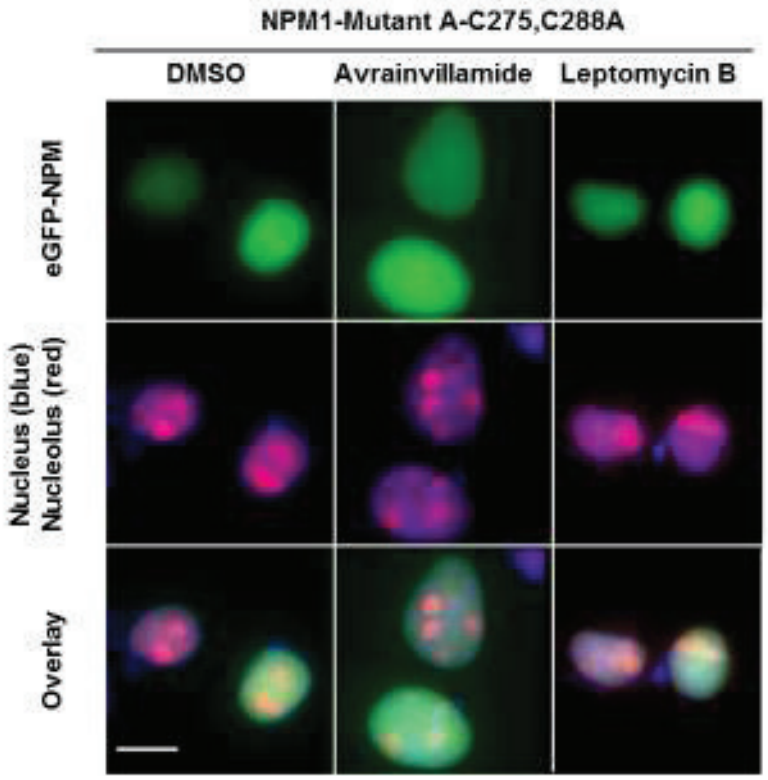

Figure 2.11. Representative immunofluorescence microscopy images demonstrating the subcellular localization of the eGFP–NPM-Mutant A–C275,288A protein following treatment with either DMSO (vehicle control), avrainvillamide (1 μM, 24 hr), or leptomycin B (100 nM, 4 hr). Colors: green, eGFP; red, nucleolin (nucleolar marker); blue, DNA (nuclear marker). Scale bar = 10 μm.

In agreement with previous reports,[49] the eGFP–NPM1–Mutant E protein was observed to localize within both the cytoplasm and nucleoli, but not within the nucleoplasm (Figure 2.12). Avrainvillamide treatment fully restored nucleolar localization of this construct, as was observed for the eGFP–NPM1–Mutant A protein. Unlike the corresponding experiments employing NPM1–Mutant A constructs, however, this localization phenotype was not affected by the presence of a C275A mutation. Thus, the eGFP–NPM1–Mutant E-C275A protein displayed the same localization phenotype as the unmodified eGFP–NPM1–Mutant E protein and was also restored to nucleoli upon treatment with avrainvillamide. Since the C-terminal domain of the

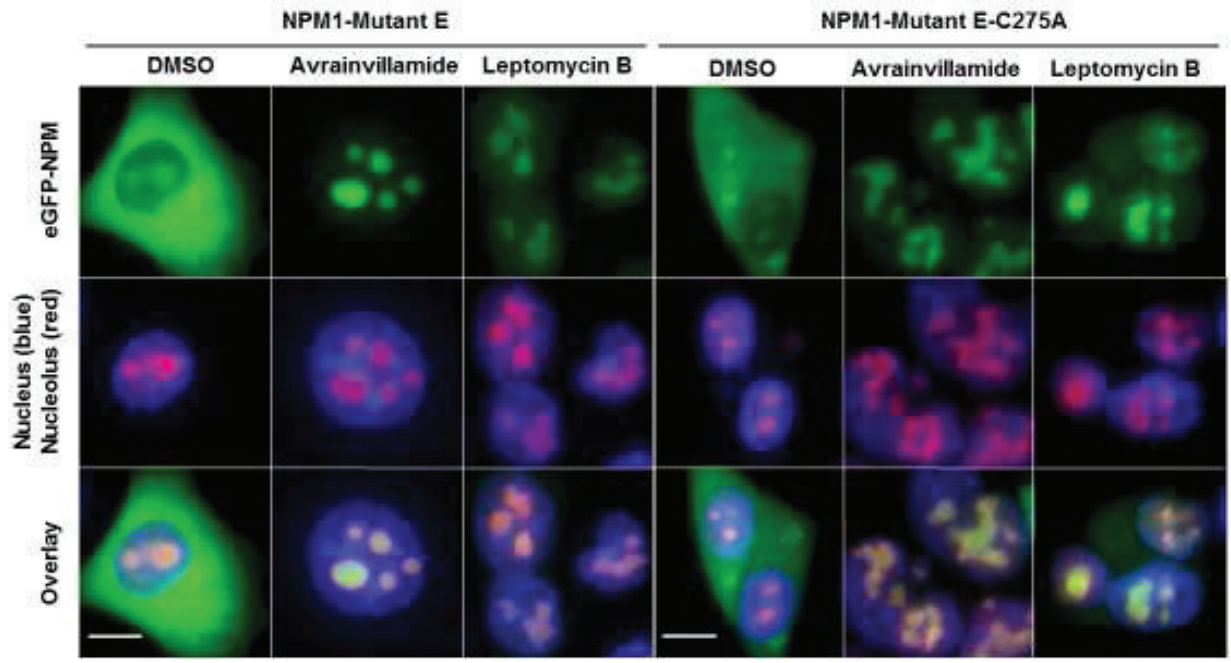

Figure 2.12. Representative immunofluorescence microscopy images demonstrating the subcellular localization of the eGFP–NPM-Mutant E and eGFP–NPM1–Mutant E-C275A proteins following treatment with either DMSO (vehicle control), avrainvillamide (1 μM, 24 hr), or leptomycin B (100 nM, 4 hr). Colors: green, eGFP; red, nucleolin (nucleolar marker); blue, DNA (nuclear marker). Scale bars = 10 μm. Quantitative relocalization data (as a percentage of cells) is available within Appendix I.

NPM1–Mutant E-C275A protein was unreactive towards avrainvillamide in direct binding assays, this observation led us to explore the possibility that NPM1 was not the sole cellular target of avrainvillamide. In particular, it was observed that the NPM1 localization phenotype induced by avrainvillamide in cells expressing eGFP–NPM1–Mutant E variants was identical to the phenotype induced by LMB. LMB is able to restore the NPM1–Mutant E protein to nucleoli due to the presence of a weak NoLS, which is capable of targeting this protein to nucleoli in the absence of hyperactive Crm1-mediated nuclear export processes.

The discovery that avrainvillamide is capable of restoring NPMc+ proteins to the nucleoli of cancer cells indicated that avrainvillamide, through its ability to bind the C-terminal domain of NPM1, possesses remarkable and unique biological activity. Our results clearly demonstrated

not only that this activity is partially mediated by interactions between avrainvillamide and cys^{275} of NPM1–Mutant A, but also that such an interaction cannot account for all of the observed effects of avrainvillamide on the subcellular localization of NPMc+ variants. We thus turned our efforts towards developing a better understanding of the cellular mechanisms underlying the avrainvillamide-mediated relocalization of NPMc+ proteins. At this point we sought to address two main goals—identifying the cellular component or components responsible for retaining avrainvillamide-bound NPMc+ proteins in the nucleolus as well as determining the cellular targets responsible for the NPM1–independent biological activities of avrainvillamide.

2.4 Avrainvillamide Does Not Affect the Secondary Structure of Isolated NPM1 C-Terminal Domains.

Although our mutagenesis studies demonstrated that the specific interaction between avrainvillamide and cys^{275} of NPM1–Mutant A was essential for the nucleolar relocalization of this protein following treatment with avrainvillamide, the mechanisms responsible for this activity remained unclear. It is thought that the nucleolar localization of NPM1 is dependent on both the tertiary structure of the C-terminal domain of NPM1 and the ability of this domain to interact with G-quadruplex rDNA. Consistent with this hypothesis, the NPM1–Mutant A protein possesses an unfolded C-terminal domain due to the W288C and W290A mutations and does not bind to short G-quadruplex rDNA oligonucleotides.[13,34] Similarly, the NPM1–Mutant E protein exhibits a partially destabilized C-terminal domain due to the W290S mutation,[13] however, the interactions between this domain of NPM1–Mutant E and G-quadruplex rDNA have not been previously studied.

The folding dynamics of the NPM1, NPM1–Mutant A, and NPM1–Mutant E C-terminal domains have also been studied extensively. It has been demonstrated that the C-terminal domains of the NPM1–Mutant A and NPM1–Mutant E proteins do not assume random coil structures, but rather, both proteins retain some degree of secondary structure in their "unfolded" forms (it should be noted, however, that no structural data is available for either protein). It is hypothesized that the partially folded structures may exist in equilibrium with fully folded states; therefore, a small molecule that specifically binds to the folded C-terminal domain of NPMc+ proteins may induce refolding of this domain and thereby correct the aberrant localization of the corresponding full-length proteins.[64] Experimental evidence supporting this hypothesis, however, has not yet been obtained. Furthermore, while all known nucleolar NPM1 proteins (or more properly, GFP–tagged NPM1 proteins) possess a correctly folded NPM1 C-terminal domain, as discussed in Chapter 1, the proper folding of this domain does not ensure the nucleolar localization of NPM1. Therefore, it also remains to be determined whether a hypothetical folded NPM1–Mutant A C-terminal domain is capable of targeting this protein to the nucleolus, potentially by its ability to bind to G-quadruplex rDNA. Finally, it should be noted that avrainvillamide binds to unfolded NPMc+ C-terminal domains more rapidly than to the folded NPM1 C-terminal domain in initial mass spectrometry experiments, although we did not assess the effects of avrainvillamide on the secondary structures of these domains at that time.

We thus sought to determine whether avrainvillamide directly influenced the secondary structure of the NPM1 and NPMc+ C-terminal domains. Specifically, since the folded structure of this domain is stabilized by interactions between hydrophobic and aromatic amino acids, we

[64] Scaloni, F.; Gianni, S.; Federici, L.; Falini. B.; Brunori, M. Folding Mechanism of the C-terminal Domain of Nucleophosmin: Residual Structure in the Denatured State and its Pathophysiological Significance. *FASEB J.* **1999**, *23*, 2360–2365.

hypothesized that the chromene portion of avrainvillamide may provide additional stabilizing interactions within this domain, possibility offsetting the destabilization induced by loss of one or both tryptophan residues. Indeed, inspection of the computed structure of avrainvillamide docked into the C-terminal domain of NPM1 suggests that the aromatic core of avrainvillamide may form favorable π-stacking interactions with tyr^{271} and phe^{276}, while the C-14 geminal dimethyl group projects into a pocket flanked by ile^{247} and leu^{287}.

We elected to model our studies on the effects of avrainvillamide on the C-terminal structure of NPM1 on previous literature reports in which the secondary structures of the NPM1, NPM1–Mutant A, and NPM1–Mutant E were assessed by circular dichroism (CD) spectroscopy.[13] As an initial control, we obtained the CD spectrum of a buffered aqueous solution (containing 5% acetonitrile) of the NPM1–C_{52} peptide used in our mass spectrometry binding assays, and found that it did indeed show the presence of an α-helix structural element, as expected (Figure 2.13 A). The CD spectrum of the NPM1–C_{52} peptide did not show any significant changes when measured in the presence of an excess of avrainvillamide (10 eq. relative to NPM1–C_{52}), indicating that avrainvillamide does not destabilize this domain when bound to cys^{275} of NPM1 (Figure 2.14 A).

In agreement with expectations, CD spectra of the NPM1–Mutant A–C_{56} and NPM1–Mutant E-C_{56} domains showed a lack of α-helical structure (Figure 2.13 B); as reported, neither peptide produced a prototypical random coil spectrum. As was observed for the NPM1–C_{52} peptide, obtaining either spectrum in the presence of avrainvillamide did not reveal any significant changes, indicating that the interaction between avrainvillamide and the NPM1 peptide is not sufficient to refold either protein. On the other hand, both proteins exhibited an α-helical structure in the presence of 2,2,2-trifluoroethanol, indicating that the native NPM1 folded

structure is attainable for the NPMc+ proteins. Recognizing the abiotic nature of these experiments, we attempted to retest our hypothesis in more biologically relevant contexts. We first varied the temperature of the peptide solutions, however, no significant changes in the CD spectra of either peptide were observed, even after prolonged heating at 37 °C. Similarly, heating the NPM1 C-terminal peptides to 95 °C (to eliminate any residual secondary and tertiary structures) followed by slow cooling to 23 °C in the presence of avrainvillamide failed to induce any changes in the CD spectra of both peptides.

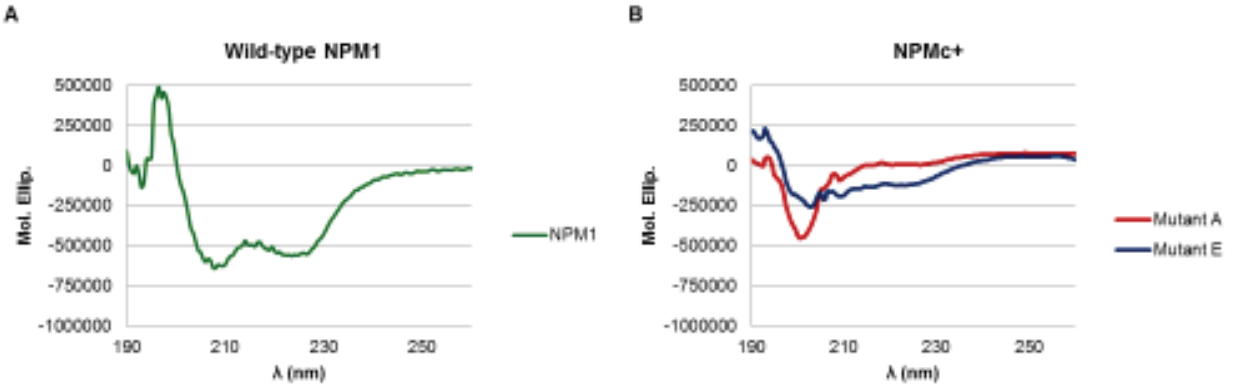

Figure 2.13. CD spectra of the C-terminal domains of (**A**) wild-type NPM1 and (**B**) NPMc+ variants NPM1–Mutant A and NPM1–Mutant E.

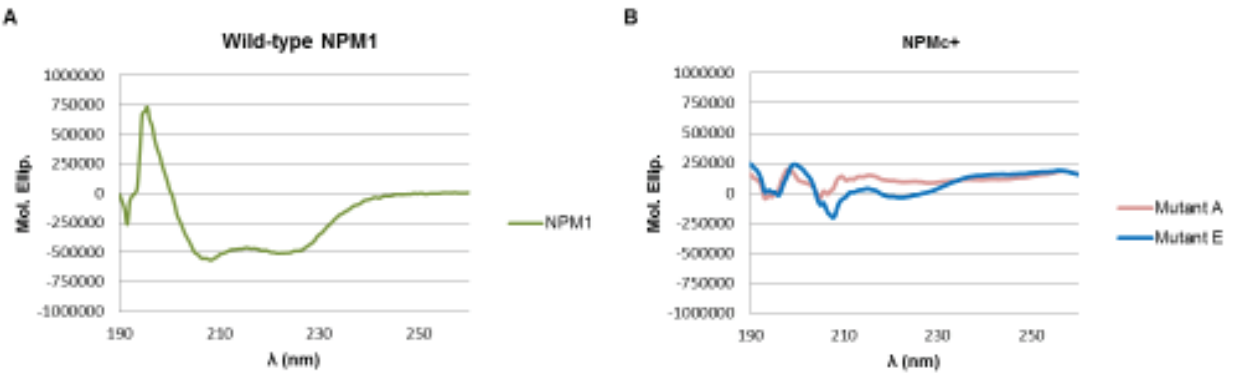

Figure 2.14. CD spectra of the C-terminal domains of (**A**) wild-type NPM1 and (**B**) NPMc+ variants NPM1–Mutant A and NPM1–Mutant E following incubation with 3 eq. avrainvillamide.

We also considered the possibility that avrainvillamide does not induce the refolding of NPMc+ proteins on its own, but may facilitate dynamic NPM1 folding processes mediated by other cellular components. Since the C-terminal domain of NPM1 is known to interact with G-quadruplex rDNA, we thus repeated the above series of experiments in the presence of a short G-quadruplex rDNA oligonucleotide (5'-GGG GTG GGG GGG AGG G-3', "13079nt") known to interact with the C-terminal domain of (wild-type) NPM1.[34] Unfortunately, these experiments also failed to detect any effects of avrainvillamide on the C-terminal structure of the NPM1–Mutant A and NPM1–Mutant E peptides (refer to Appendix I for spectra). While these experiments appear to indicate that avrainvillamide does not alter the secondary structure of NPM1 and NPMc+ proteins in simplified contexts, we cannot exclude the possibility that avrainvillamide influences dynamic NPM1 folding processes mediated by other, as yet unidentified cellular components.

2.5 Avrainvillamide Does Not Alter the Interaction Between the C-Terminal Domain of NPM1 Proteins and G-Quadruplex rDNA.

Although our results indicated that avrainvillamide did not alter the C-terminal structure of NPM1 and NPMc+ proteins, the possibility remained that avrainvillamide induces nucleolar retention of NPMc+ proteins by restoring binding interactions between the C-terminal domains of these proteins and G-quadruplex rDNA. We thus elected to study the effects of avrainvillamide on the NPM1–G-quadruplex rDNA interaction by means of an electrophoretic mobility shift assay (EMSA). For the nucleic acid component of the EMSA we selected 13079nt on the basis of its known *in vitro* and *in vivo* interactions with the C-terminal domain of wild-

type NPM1.[34] Initial control EMSA experiments involving 13079nt and the NPM1–C_{52} peptide revealed that complex formation was extremely sensitive to minor changes to the rDNA species. In particular, both 5'- and 3'-biotinylation of 13079nt resulted in complete inhibition of NPM1 binding activity. It was therefore necessary to employ ^{32}P labelling of the 13079nt in order to preserve its interactions with the NPM1–C_{52} peptide.

We next incubated the NPM1–Mutant A and NPM1–Mutant E peptides with the 13079nt in the presence and absence of avrainvillamide. In agreement with literature reports, the NPM1–Mutant A–C_{56} peptide did not appear to interact with the G-quadruplex rDNA.[34] On the other hand, we observed evidence of the formation of a complex between the NPM1–Mutant E–C_{56} peptide and 13079nt; this marked the first known observation of this binding interaction. Avrainvillamide did not appear to alter the interactions between the NPM1 peptide and 13079nt for any of the NPM1 C-terminal domains studied (Figure 2.15). Thus, an excess of avrainvillamide (10 eq. relative to NPM1) did not inhibit complex formation between the 13079nt and the NPM1–C_{52} or NPM1–Mutant E–C_{56} peptides, nor was avrainvillamide found to induce complex formation between the 13079nt and the NPM1–Mutant A–C_{56} peptide. Although these results still did not aid our understanding of the mechanisms responsible for the observed relocalization of NPMc+ by avrainvillamide, they did demonstrate that avrainvillamide does not disrupt the interaction between NPM1 G-quadruplex rDNA. This last observation is particularly striking, given the extreme sensitivity of the 13079nt–NPM1 interaction to minor structural perturbations. Furthermore, it has been hypothesized by others[65] that avrainvillamide may inhibit the interaction between NPM1 and G-quadruplex rDNA, and therefore displace NPM1 from nucleoli; however, our results clearly demonstrate that avrainvillamide has no

[65] Federici, L. University of Chieti, Chieti, Italy. *Personal communication*. 2012.

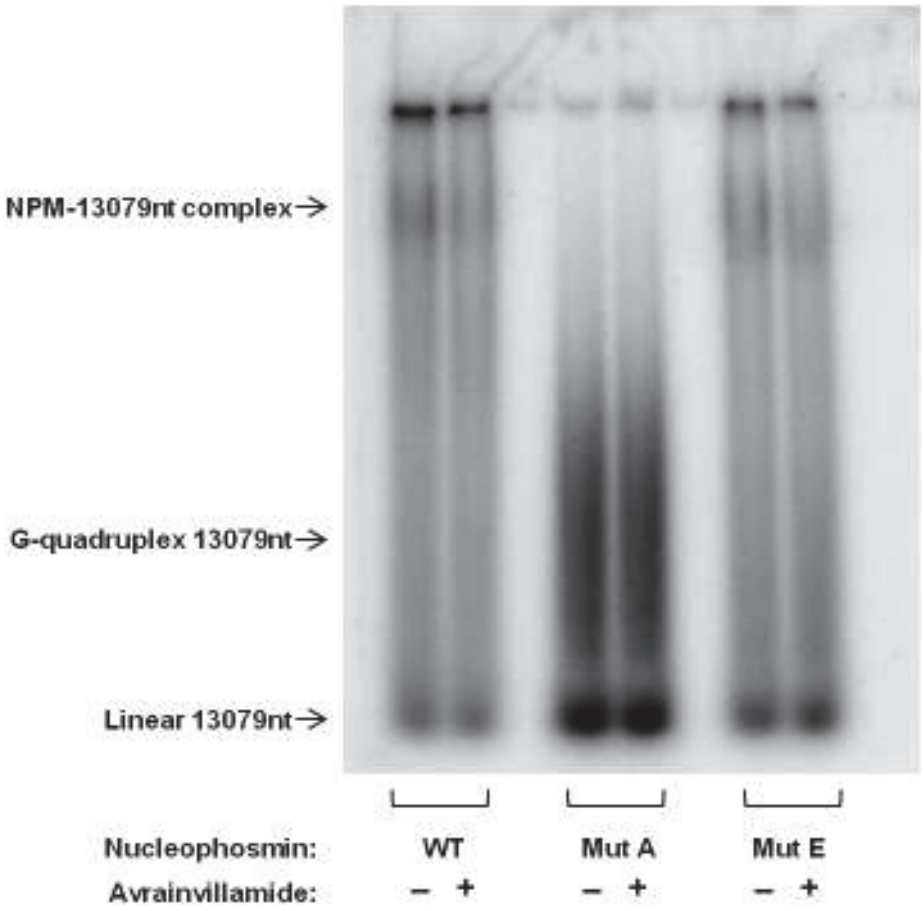

Figure 2.15. Electrophoretic mobility shift assay between the NPM1–C_{52} and NPM1–C_{56} peptides and the G-quadruplex 13079nt oligonucleotide.

negative effects on the secondary structure of the C-terminal domain of NPM1 nor its interactions with G-quadruplex rDNA. Indeed, our claim was supported by work conducted by the Federici group, who subsequently found that avrainvillamide did not appear to influence the G-quadruplex rDNA binding affinities of the NPM1-C_{70} and NPM1-Mutant A-C_{70} peptides as measured by surface plasmon resonance.[65]

The negative results we obtained in the CD and EMSA experiments leave us unable to propose a complete mechanistic model for the observed relocalization of certain NPMc+ proteins to nucleoli. We hypothesize that avrainvillamide, when bound to cys^{275}, but not cys^{288}, of

specific NPMc+ proteins functions as a surrogate NoLS, potentially through its ability to stabilize the native C-terminal fold of NPM1 through interactions of its hydrophobic core with branched-chain and aromatic residues. However, if avrainvillamide does indeed stabilize a native C-terminal folded structure in NPMc+ proteins, it does so through its influence on dynamic folding processes mediated by as yet unidentified cellular components. Lastly, avrainvillamide does not destabilize the C-terminal folded structure of wild-type NPM1 and does not appear to inhibit the interaction between wild-type NPM1 and G-quadruplex rDNA, suggesting that low concentrations of avrainvillamide do not alter cellular processes mediated by the C-terminal domain of NPM1.

2.6 Avrainvillamide Inhibits Crm1-Mediated Nuclear Export of Proteins Other Than NPM1.

Although we could not determine the nucleolar binding partners responsible for the avrainvillamide-mediated nucleolar retention of NPMc+ proteins, the observation that avrainvillamide treatment altered the subcellular localization of an NPMc+ protein to which it did not bind (the NPM1–Mutant E-C275A protein) led us to explore other potential cellular targets of avrainvillamide. Given the identification of Crm1 as a potential cellular target of avrainvillamide in initial affinity-isolation assays and the identical NPM1–Mutant E localization phenotypes induced by avrainvillamide and LMB, Crm1 was identified as a candidate target protein. To determine whether avrainvillamide inhibited Crm1-mediated nuclear export on a global level we studied the subcellular localization of other Crm1 export substrates. Based on previous literature reports, we initially chose to use a cytoplasmic GFP–tagged HIV-Rev protein

construct as a marker for Crm1 activity.[66] However, we were concerned about the known interaction between Rev and NPM1, and thus elected to also study the subcellular localization of Ran binding protein 1 (RanBP1), an endogenously expressed Crm1 export substrate that has no known interactions with NPM1.[67]

We analyzed Crm1 export activity by fluorescence microscopy, using similar protocols to those we had developed previously to study the subcellular localization of NPMc+ proteins. Cells expressing the given protein were treated with DMSO, avrainvillamide, or LMB, then fixed and stained for DNA as a nuclear marker. For experiments employing RanBP1 as the indicator for Crm1 activity, an additional staining step was required to enable visualization of RanBP1 itself. For both proteins, examination of control cells revealed the predicted cytoplasmic localization of the Crm1 cargo protein, and as expected, LMB treatment resulted in complete nuclear retention of both proteins. Avrainvillamide treatment was also observed to induce nuclear retention of both proteins, although avrainvillamide appeared to be less effective than LMB in this regard (Figure 2.16). Nonetheless, these experiments demonstrated that the interaction between avrainvillamide and Crm1 has functional consequences in cancer cells, and thus may also play a role in determining the antiproliferative effects of avrainvillamide.

To obtain further evidence of the interaction between avrainvillamide and Crm1, we also sought to directly observe the interaction between avrainvillamide and Crm1. To this end we obtained a Crm1 construct comprising residues trp^{491}–ala^{557} of human Crm1. Unfortunately, all attempts to visualize this construct or its avrainvillamide adduct by mass spectrometry were

[66] Love, D. C.; Sweitzer, T. D.; and Hanover, J. A. Reconstitution of HIV-1 Rev Nuclear Export: Independent Requirements for Nuclear Import and Export, *Proc. Natl. Acad. Sci. USA.* **1998**, *95*, 10608-10613.

[67] Plafker, K.; Macara, I. G. Facilitated Nucleocytoplasmic Shuttling of the Ran Binding Protein RanBP1. *Mol. Cell Biol*. **2000**, *20*, 3510-3521.

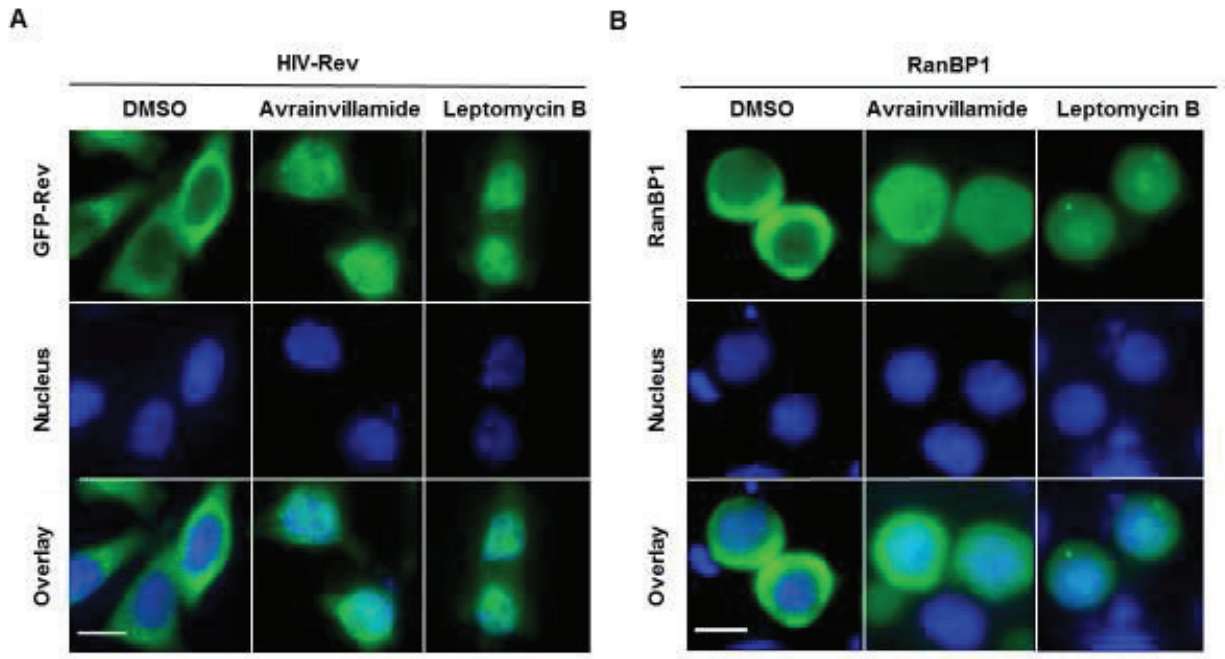

Figure 2.16. Representative immunofluorescence microscopy images demonstrating the subcellular localization of (**A**) a GFP–Rev construct and (**B**) RanBP1 following treatment with either DMSO (vehicle control), avrainvillamide (1 μM, 24 hr), or leptomycin B (100 nM, 4 hr). Colors: green, (**A**) GFP, (**B**) RanBP1; blue, DNA (nuclear marker). Scale bars = 10 μm. Quantitative relocalization data (as a percentage of cells) is available within Appendix II.

unsuccessful. We were, however, able to demonstrate that avrainvillamide binds to an 18-amino acid corresponding to residues glu^{513}–gln^{530} of human Crm1 that is also alkylated by LMB (refer to Appendix IV for spectra).[68]

2.7 Avrainvillamide Displaces Threonine-199-Phosphorylated NPM1 From Centrosomes and Deregulates Mitosis.

Despite the striking observation that avrainvillamide is capable of inducing an apparent wild-type NPM1 localization phenotype, the implications of this activity in the context of

[68] Kudo, N.; Matsumori. N.; Taoka, H.; Fukiwara, D.; Schreiner, E. P.; Wolff, B.; Yoshida, M.; Horinouchi, S. Leptomycin B Inactivates Crm1/Exportin 1 by Covalent Modification at a Cysteine Residue in the Central Conserved Region. *Proc. Natl. Acad. Sci.* **1999**, *96*, 9112-9117.

avrainvillamide-induced cancer cell antiproliferation remained unclear. This was especially true since we did not observe a significant difference in antiproliferative response towards avrainvillamide between the wild-type NPM1 OCI–AML2 cell line and the NPMc+ OCI–AML3 cell line, and since avrainvillamide induced identical relocalization phenotypes in the HCT–116 and HeLa S3 cell lines despite a roughly four-fold difference in GI_{50} value in antiproliferation assays. Indeed, it was hypothesized that the apparent restoration of a wild-type NPM1 subcellular localization phenotype may enhance cell survival by correcting NPM1 haploinsufficiency in certain nucleolar processes arising from the presence of the cytoplasmic NPMc+ protein.[44,50] We thus considered the possibility that the ability of avrainvillamide to mediate the subcellular localization of NPMc+ protein is not directly related to its antiproliferative activity. We thus sought to identify other NPM1– and Crm1-dependent cellular processes that were modulated by treatment with avrainvillamide.

The interaction between NPM1 and Crm1 has been demonstrated to play a critical role in regulating centrosome duplication during mitosis. While Crm1 primarily functions as a nuclear export factor and shuttles between the nucleus and cytoplasm, a small fraction of Crm1 is maintained at the centrosomes. This centrosomal fraction of Crm1 is capable of recruiting NPM1 to the centrosomes through interactions between Crm1 and the NES motifs of NPM1. While the centrosomal localization of NPM1 is thus mediated by Crm1, it is also highly dependent on both the cellular phase and the phosphorylation state of NPM1.

During the G_1 and S phases of the cell cycle, a small fraction of NPM1 associates with unduplicated centrosomes (Figure 2.17). This association is maintained through late G_2 phase, when NPM1 is phosphorylated on thr^{199} by the Cyclin-dependent kinase (Cdk) 2/cyclin E complex, triggering its dissociation from the centrosome. This dissociation of NPM1 from

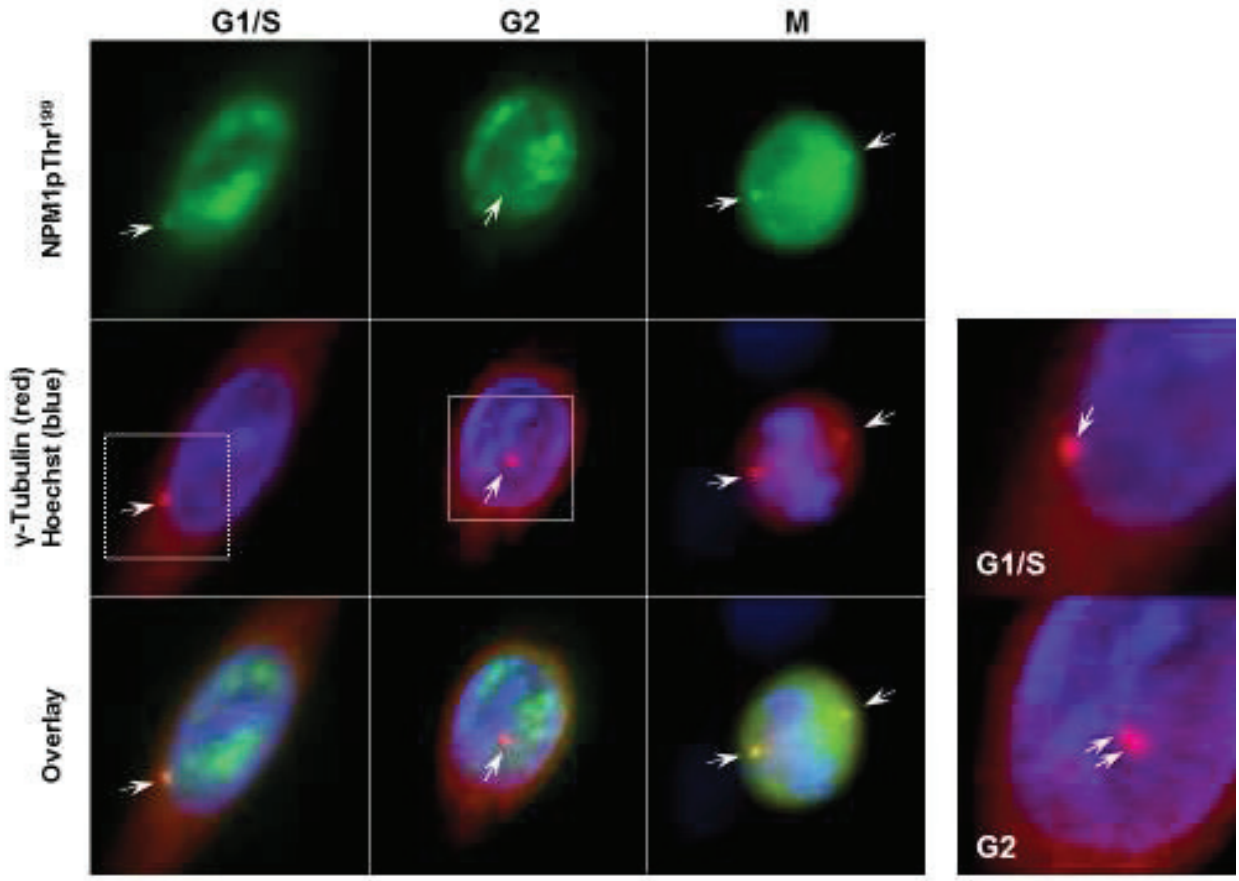

Figure 2.17. Representative immunofluorescence microscopy images depicting the centrosomal localization of thr[199]-phosphorylated-NPM1 throughout the cell cycle in untreated HCT–116 cells.NPM1 associates with centrosomes during G1/S phase and M phase, but is displaced from the centrosomes during late G2/early M phase, thus allowing centrosome duplication to occur. Colors: green, thr[199]-phosphorylated NPM1; red, γ–tubulin (centrosomal marker); blue, DNA. Insets show magnification of the boxed areas in G1/S and G2 phase, allowing visualization of centrosomes before (G1/S) and after (G2) duplication.

unduplicated centrosomes precedes entry into M phase and is required for the subsequent duplication of the centrosomes. Following centrosome duplication, thr[199]-phosphorylated NPM1 then reassociates with centrosomes during metaphase, thereby ensuring that centrosome duplication occurs exactly once during each mitotic phase. Finally, thr[199] of NPM1 is dephosphorylated during late M/early G1 phase, allowing the next centrosome duplication cycle to begin. Precise control of the phosphorylation state (on thr[199]) of NPM1 as well as its centrosomal localization (or lack thereof) during mitosis are thus critical regulatory factors in

centrosome duplication.[26] Consistent with these observations, expression of the non-phosphorylatable NPM1–T199A mutant results in an inhibition of centrosome duplication, monopolar mitotic spindles, and eventual cellular death.[69] On the other hand, LMB treatment displaces NPM1 from both duplicated and unduplicated centrosomes during all phases of the cell cycle and results in enhanced centrosome duplication and an accumulation of supernumerary centrosomes.[26]

We thus sought to determine whether avrainvillamide altered the subcellular localization of thr^{199}-phosphorylated NPM1 during the various phases of the cell cycle. In order to obtain temporal resolution of the subcellular localization of thr^{199}-phosphorylated NPM1, we first worked to identify an appropriate method for the synchronization of cell populations in these experiments. Although the cell cycle phase of a given cell is typically readily determined by immunofluorescence microscopy by analyzing centrosome and DNA staining, this method is clearly inappropriate for assessing changes in cell cycle behavior. Additionally, since a random population of cells typically contains only a small fraction of mitotic cells, we were hopeful that a robust synchronization procedure would also improve our ability to image mitotic cells. Indeed, mitotic cells could be isolated and imaged in large numbers by either physical methods (mitotic shake-off) or by chemical treatment (such as with nocodazole). However, since these cells had by definition already entered mitosis, the effects of avrainvillamide treatment on this first, partial mitosis were unclear at best. By the time these populations of cells had entered their second mitotic phase, synchronicity was reduced, largely eliminating any benefits obtained by the synchronization procedure. In contrast, when cells were blocked in S phase by means of a

[69] Tokuyama, Y.; Horn, H. F.; Kawamura, K.; Tarapore, P.; Fukasawa, K. Specific Phosphorylation of Nucleophosmin on Thr199 by Cyclin- dependent Kinase 2-Cyclin E and Its Role in Centrosome Duplication. *J. Biol. Chem.* **2001**, *276*, 21529-21537.

double thymidine block, synchronization was generally maintained through the first mitotic phase, enabling an assessment of the effects of avrainvillamide over a complete mitotic phase. With a robust synchronization protocol in place, one final hurdle remained before we were fully prepared to conduct these experiments. Initial control experiments revealed that the use of solutions of formaldehyde as a fixative for sample preparation inhibited immunostaining of γ–tubulin, which was used as a centrosome marker. A screen of several fixatives and fixation conditions, including glutaraldehyde solutions (either alone or in combination with formaldehyde), organic solvents (acetone, methanol), and combinations of formaldehyde and organic solvents revealed that fixing cells in cold (–20 °C) methanol for precisely 7 minutes yielded optimal results and was also compatible with co-immunostaining of thr^{199}-phosphorylated NPM1.

With optimized synchronization and immunostaining procedures in place, we were able to determine the effects of avrainvillamide treatment on the subcellular localization of thr^{199}-phosphorylated NPM1 over the course of the cell cycle, and in particular, during mitosis. As previously discussed, cells were synchronized in S phase using a double thymidine block, then were directly released into medium containing either DMSO (vehicle control) or avrainvillamide (1 μM). Cells were then fixed at predetermined time points; these were selected based on initial, avrainvillamide-free assays to coincide with specific phases of the cell cycle. Following fixation, the cells were immunostained for thr^{199}-phosphorylated NPM1, γ–tubulin, and DNA and imaged using a fluorescence microscope.

Avrainvillamide was found to displace thr^{199}-phosphorylated NPM1 from the centrosomes during all phases of the cell cycle, consistent with its Crm1-binding activity (Figure 2.18). The effects of this activity prior to the first mitotic phase (which occurred between 6 and 8

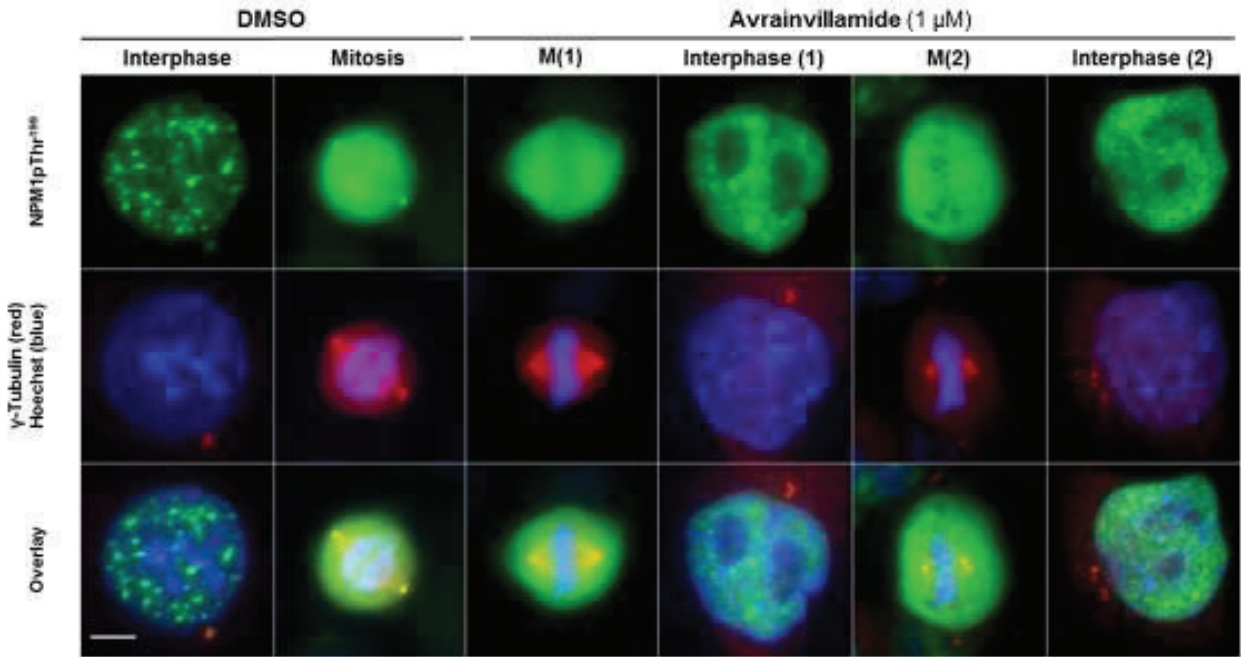

Figure 2.18. Representative immunofluorescence microscopy images of HCT–116 cells treated with either DMSO (vehicle control) or avrainvillamide and imaged during the indicated phases. Numbers in parentheses indicate the number of cell cycles elapsed following release from the double thymidine block. Colors: green, thr^{199}-phosphorylated NPM1; red, γ–tubulin (centrosomal marker); blue, DNA. Scale bar = 10 μm. Quantitative data (percentage of cells exhibiting supernumerary centrosomes) is available within Appendix II.

hours after release from the double thymidine block), however, were unclear, since the cells did not exhibit any morphological abnormalities at this time. Indeed, while inhibition of the interaction between NPM1 and centrosomes may facilitate premature entry into mitosis, thr^{199}-phosphorylation of NPM1 does not regulate cell cycle behavior during S and early G_2 phases. The activity of avrainvillamide was most apparent during mitosis, when thr^{199}-phosphorylated NPM1 failed to localize at duplicated centrosomes during metaphase, although no other morphological abnormalities were observed during the first post-block mitotic phase. Despite the lack of apparent aberrations during the first mitotic cycle, we observed supernumerary centrosomes in a significant fraction of cells during the subsequent G_1 phase, indicating that aberrant centrosome reduplication did indeed occur during the first mitotic cycle. The presence of supernumerary centrosomes occasionally resulted in tripolar mitotic morphologies, suggesting

that the effects of avrainvillamide on the centrosomal localization of thr[199]-phosphorylated NPM1 resulted in the deregulation of centrosome duplication and by extension, mitosis Indeed, while a fraction of avrainvillamide-treated cells exhibited normal, bipolar mitotic morphologies in which supernumerary centrosomes clustered to two spindle poles (Figure 2.19, panel "a"),

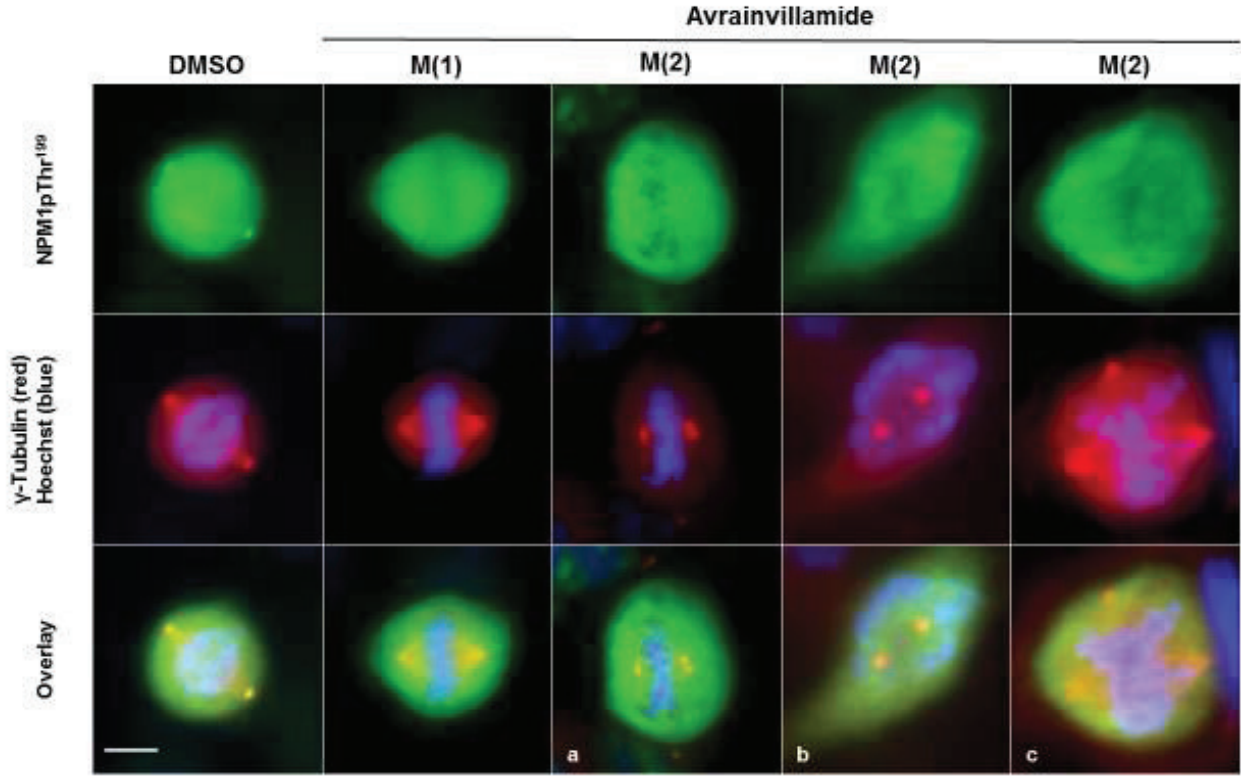

Figure 2.19. Immunofluorescence microscopy images depicting normal mitotic morphology as observed in DMSO-treated cells, as well as several examples of aberrant mitotic morphologies resulting from treatment with avrainvillamide. Numbers in parentheses indicate the number of cell cycles elapsed following release form the double thymidine block. Colors: green, thr[199]-phosphorylated NPM1; red, γ–tubulin (centrosomal marker); blue, DNA. Scale bar = 10 μm).

avrainvillamide treatment was also found to induce abnormal mitotic phenotypes. These include cells in which extra centrosomes did not cluster to one of two spindle poles (Figure 2.19, panel "b") as well as cells which were observed to undergo tripolar mitosis (Figure 2.19, panel "c"). When dosing times were extended, avrainvillamide-treated cells continued to accumulate supernumerary centrosomes, however, at the longest time points studied (48 hours),

essentially no mitotic cells were observed. Notably, previous flow cytometry experiments showed that avrainvillamide (2 μM, 24 hr) induced G_2/M phase arrest in the T–47 D breast cancer cell line.[70] Taken together, our results suggest that avrainvillamide induces G_2 phase arrest. The mechanisms underpinning avrainvillamide-induced G_2 phase arrest, however, remain unclear at this time.

The observation that avrainvillamide deregulates mitosis was exciting, since it provided the first evidence that avrainvillamide influences an essential cellular process. However, since this activity could be ascribed to interactions between avrainvillamide and Crm1, we were still unable to account for the observed correlation between the ability of avrainvillamide analogs to bind NPM1 and their antiproliferative activities, particularly since a corresponding correlation was not observed for Crm1. We thus considered that the effects of avrainvillamide on cell cycle behavior, like its inhibition of the nuclear export of RanBP1, represent off-target activities, and continued our search for NPM1–mediated (and Crm1-independent) cellular processes that were modulated by avrainvillamide.

2.8 Avrainvillamide Increases Cellular Levels of Thr^{199}-Phosphorylated NPM1.

During our studies on the effects of avrainvillamide on the subcellular localization of thr^{199}-phosphorylated NPM1, we observed an apparent increase in cellular levels of thr^{199}-phosphorylated NPM1 (Figure 2.20 A). In order to confirm this finding, we cultured cells in the presence of DMSO (vehicle control) or varying concentrations of avrainvillamide (0.5–4 μM), then lysed the cells and measured the relative amounts of thr^{199}-phosphorylated NPM1 present within nucleoplasm and cytoplasm by immunoblotting. These experiments revealed an apparent

[70] Chan, K. P.; Myers. A. G. Harvard University, *Unpublished work*, 2008.

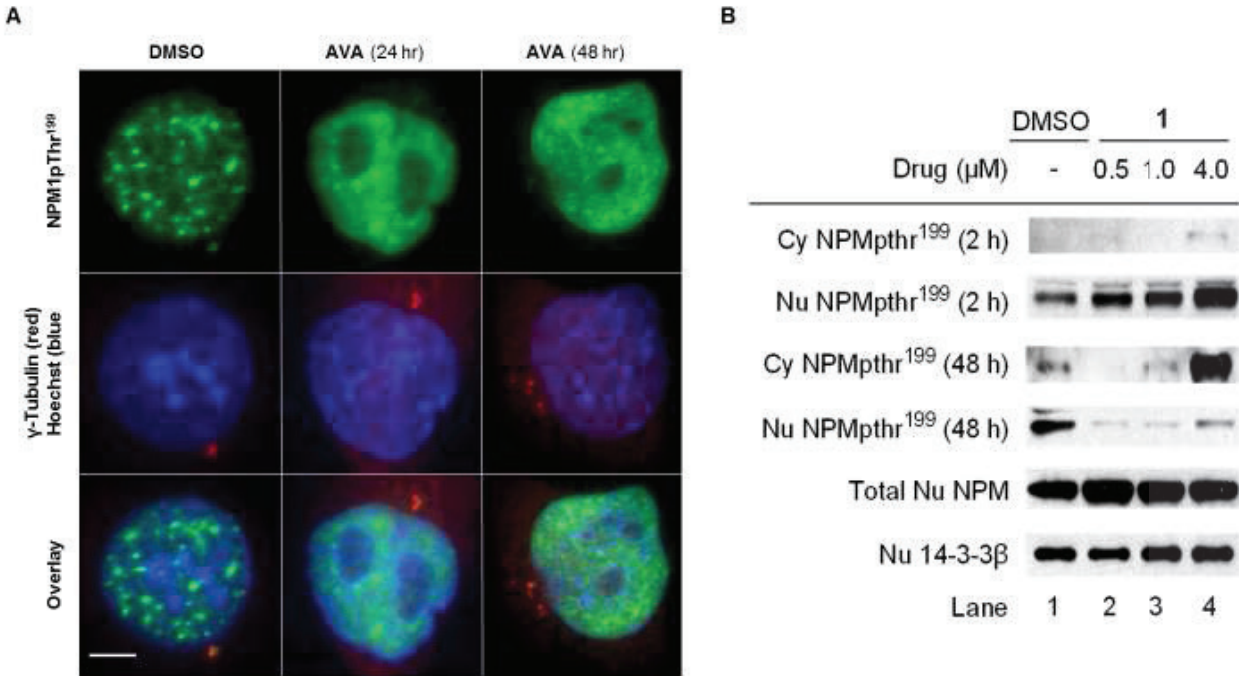

Figure 2.20. **A**. Representative immunofluorescence microscopy images displaying an apparent increase in levels of thr[199]-phosphorylated NPM1 following treatment with avrainvillamide (1 μM) for the indicated amount of time. Numbers in parentheses indicate the number of cell cycles elapsed following release form the double thymidine block. Colors: green, thr[199]-phosphorylated NPM1; red, γ–tubulin (centrosomal marker); blue, DNA. Scale bar = 10 μm). **B**. Immunoblot showing a dose-dependent increase in NPM1 thr[199]-phosphorylation levels following treatment with avrainvillamide. Levels of total NPM1 and 14–3–3β after 48 hr treatment are shown as loading controls. Nu = nuclear. Cy = cytoplasmic.

dose-dependent increase in NPM1 thr[199]-phosphorylation levels mediated by avrainvillamide (Figure 2.20 B). When cells were exposed to subtoxic concentrations of avrainvillamide, thr[199]-phosphorylated NPM1 was retained in the nucleus; increasing either the concentration of avrainvillamide or duration of dosing led to a sharp increase in the amount of cytoplasmic thr[199]-phosphorylated NPM1. Since thr[199]-phosphorylation of NPM1 targets the protein to nuclear speckles,[71] we reasoned that the dramatic increase in aberrantly localized thr[199]-phosphorylated NPM1 may represent an apoptotic phenotype. Indeed, by virtue of its ability to bind to several different nucleolar components, NPM1 is known to play a critical role in the organization and

[71] Tarapore, P.; Shinmura, S.; Suzuki, H.; Tokuyama, Y.; Kim, S.; Mayeda, A.; Fukasawa, K. Thr199 Phosphorylation Targets Nucleophosmin to Nuclear Speckles and Represses Pre-mRNA Processing. *FEBS Letters*. **2006**, *580*, 399–409.

stabilization of nucleoli (and by extension, nuclei). Depletion of NPM1 from nucleoli, for example, by NPM1–targeting siRNA, destabilizes nucleoli and nuclei and induces apoptosis.[32] Since thr[199]-phosphorylation targets NPM1 to nuclear speckles, we thus hypothesize that avrainvillamide functions as a potent modulator of nucleolar stability through its ability to increase NPM1 phosphorylation levels. Indeed, cells treated with avrainvillamide at elevated concentrations for longer time points routinely exhibited defects in nuclear and nucleolar structure (Figure 2.20 A). However, it is important to note that avrainvillamide does not displace NPM1 from nucleoli at lower (subtoxic) concentrations, such as those used in our experiments on the subcellular localization of NPMc+ proteins. Rather, we hypothesize that the observed displacement of NPM1 from nucleoli appears to arise from an accumulation of thr[199]-phosphorylated NPM1 mediated by avrainvillamide and may be directly related to the antiproliferative activity of avrainvillamide.

2.9 Avrainvillamide Inhibits the Dephosphorylation of NPM1 by Protein Phosphatase 1 Beta and Destabilizes Nucleolar and Nuclear Structure.

Our next goal was thus to uncover the mechanisms by which avrainvillamide increases NPM1 thr[199] phosphorylation levels. NPM1 is phosphorylated by several kinases, including Cdk1,[72] Cdk2,[73] Cdk4,[74] and Cdk6,[75] and is dephosphorylated by protein phosphatase 1 beta (PP1β).[76] As

[72] Yu, L. R.; Zhu, Z.; Chan, K. C.; Issaq, H. J.; Dimitrov, D. S.; Veenstra, T. D. Improved Titanium Dioxide Enrichment of Phosphopeptides from HeLa Cells and High Confident Phosphopeptide Identification by Cross-validation of MS/MS and MS/MS/MS Spectra. *J. Proteome Res.* **2007**, *6*, 4150–4162.

[73] Sarek, G.; Jaerviluoma, A.; Moore, H. M.; Tojkander, S.; Vartia, S.; Biberfeld, P.; Laiho, M.; Ojala, P. M. Nucleophosmin Phosphorylation by v-cyclin-CDK6 Controls KSHV Latency. *PLOS Pathol*. **2010**, *6*, e1000818.

discussed above, NPM1 is phosphorylated on thr^{199} primarily by Cdk2/cyclin E, and NPM1 thr^{199} phosphorylation levels generally reach peak levels during mitosis. Indeed, prior to our use of cell synchronization methods to increase counts of mitotic cells in cell cycle analysis experiments, mitotic cells could be rapidly identified from randomly distributed populations by selecting cells with the greatest thr^{199}-phosphorylated NPM1 immunofluorescence signal intensity.

Since we observed a gradual accumulation in thr^{199}-phosphorylated NPM1, we reasoned that it was more likely that avrainvillamide inhibited the dephosphorylation of NPM1 rather than acting as an activator of Cdk2 or any other cellular kinase. We thus decided to determine whether avrainvillamide inhibited the PP1β-mediated dephosphorylation of thr^{199}-phosphorylated NPM1. To accomplish this, HCT–116 cells were treated with okadaic acid, a potent inhibitor of protein phosphatases 1, 2A, and 2B, prior to harvesting in order to increase global protein phosphorylation levels. The cells were then harvested, and thr^{199}-phosphorylated NPM1 was isolated by immunoprecipitation. The NPM1 immunocomplexes were then exposed to solutions of active PP1β, then thr^{199} phosphorylation was assayed by immunoblotting as before. Calyculin A (CA), a known PP1β inhibitor, was employed as a control compound in these experiments and, as expected, strongly attenuated NPM1 dephosphorylation by PP1β. We observed a dose-dependent inhibition of NPM1 dephosphorylation by avrainvillamide, supporting the hypothesis that avrainvillamide increases levels of thr^{199}-phosphorylated NPM1

---

[74] Adon, A. M.; Zeng, X.; Harrison, M. K.; Sannem, S.; Kiyokawa, H.; Kaldis, P.; Saavedra, H. I. Cdk2 and Cdk4 Regulate the Centrosome Cycle and are Critical Mediators of Centrosome Amplification in p53-null cells, *Mol. Cell Biol.* **2010**, *30*, 694–710.

[75] Olsen, J. V.; Vermeulen, M.; Santamaria, A.; Kumar, C.; Miller, M. L.; Jensen, L. J.; Gnad, F.; Cox, J.; Jensen, T. S.; Nigg, E. A.; Brunak, S.; Mann, M. Quantitative Phosphoproteomics Reveals Widespread Full Phosphorylation Site Occupancy During Mitosis, *Sci. Signal*. **2010**, *3*, ra3.

[76] Lin, C. Y.; Tan, B. C.; Liu, H.; Shih, C.; Chein, K.; Lin, C.; Yung, B. Y. Dephosphorylation of Nucleophosmin by PP1β Facilitates pRB Binding and Consequent E2F1-dependent DNA Repair, *Mol. Biol. Cell.* **2010**, *21*, 4409–4417.

by inhibiting its dephosphorylation by PP1β (Figure 2.21 A). LMB treatment did not inhibit NPM1 dephosphorylation, indicating that activity is likely mediated by interactions between avrainvillamide and NPM1, rather than Crm1.

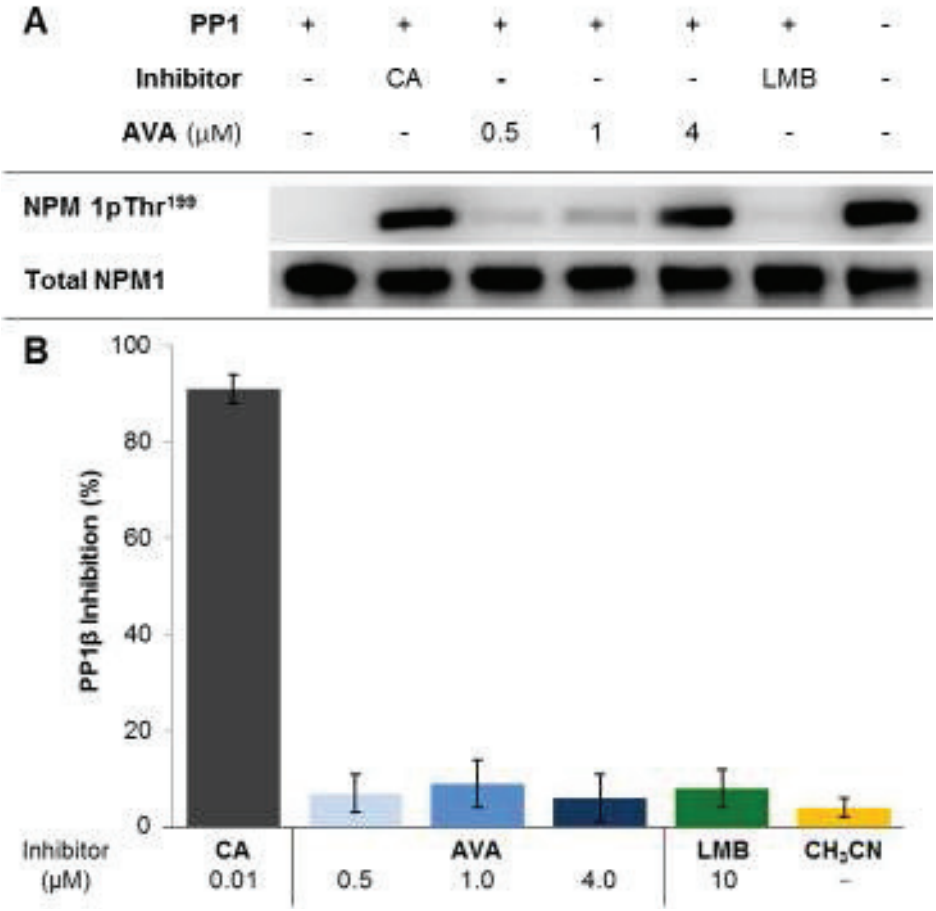

Figure 2.21 A. Results of a PP1β inhibition assay using immunoprecipitated thr[199]-phosphorylated NPM1 as the substrate. CA = calyculin A. **B.** Results of a PP1β inhibition assay employing 4-nitrophenylphosphate as the substrate. Percent inhibition values were calculated relative to control reactions lacking either PP1β (100% inhibition) or inhibitor (0% inhibition). Error bars indicate the mean ± standard deviation of three independent experiments.

In order to exclude the possibility that avrainvillamide inhibits NPM1 dephosphorylation through direct inhibition of PP1β, we conducted a control assay employing 4-

nitrophenylphosphate at the enzyme substrate. As expected, calyculin A completely inhibited the PP1β-mediated release of 4-nitrophenol, whereas neither avrainvillamide nor LMB displayed this activity (Figure 2.21 B). Taken together, our results indicate that avrainvillamide increases cellular levels of thr^{199}-phosphorylated NPM1 by inhibiting the specific action of PP1β on NPM1.

2.10 Conclusions and Future Goals

While there still remain unresolved questions surrounding the biology of avrainvillamide, our research has illuminated several key points and has led to several novel findings. Avrainvillamide is the first small molecule known to restore an apparent wild-type NPM1 localization phenotype in AML cells expressing NPMc+ variants, and we have demonstrated that this activity arises from the specific interaction between avrainvillamide and cys^{275} of NPM1–Mutant A. Avrainvillamide is also the first small molecule demonstrated to interact with the C-terminal domain of NPMc+ variants; we have also shown that avrainvillamide binds AML-associated NPM1 variants more rapidly than wild-type NPM1. This finding suggests that avrainvillamide displays a certain degree of selectivity for specific forms of NPM1, and may be particularly significant in the context of AML biology.

We have also provided the first evidence that the interaction between avrainvillamide and Crm1, previously thought to represent a non-specific binding event, does indeed have functional consequences in cancer cells. Avrainvillamide not only inhibits Crm1-mediated nuclear export, but also interferes with centrosome duplication, presumably by inhibiting the interaction between Crm1 and thr^{199}-phosphorylated NPM1 during metaphase. Simultaneously, avrainvillamide

increases cellular levels of thr^{199}-phosphorylated NPM1 by inhibiting its dephosphorylation by PP1β, thereby removing a negative regulator of premature entry into mitosis. Additionally, and seemingly contrary to our results from studying NPMc+ variants, avrainvillamide-mediated increases in NPM1 thr^{199}-phosphorylation levels serves to indirectly displace it from nucleoli. This in turn leads to a destabilization of nucleolar and nuclear structure, and may represent one mechanism by which avrainvillamide exerts its antiproliferative effects. More importantly, the observation that avrainvillamide can induce nuclear retention of NPM1 and NPMc+ proteins while also displacing NPM1 from nucleoli indicates that avrainvillamide possesses a complex range of biological activities which depend on a range of factors, including NPM1–mutational status, dosing concentration, and dosing duration. Thus, we hypothesize the effects of avrainvillamide on the subcellular localization of NPMc+ proteins and on Crm1 biology may represent subtoxic phenotypes, while the effects of avrainvillamide on the subcellular localization and levels of thr^{199}-phosphorylated NPM1 may be more directly related to its antiproliferative activity.

While the work in our lab has largely focused on the consequences of avrainvillamide treatment on molecular and cellular levels, we also remain focused on evaluating the potential therapeutic utility of avrainvillamide and avrainvillamide analogs. In this context we are indebted to our collaborators in the group of Dr. Bjørn Tore Gjertsen (University of Bergen, Norway), who have simultaneously examined (and continue to examine) the effects of avrainvillamide in clinically relevant contexts. Working in primary AML isolates, the Gjertsen group has succeeded in identifying several subsets of AML cells that exhibit enhanced sensitivity towards avrainvillamide and analog **18**. Furthermore, they have characterized many novel

aspects of the biology of avrainvillamide, including its ability to modulate levels of several key proteins in AML, including NPM1, Crm1, FLT3, and p53.

Avrainvillamide is clearly a remarkable molecule with a range of novel biological activities. We believe that we, through our ability to work at the interface between synthetic chemistry and chemical biology, are in a unique position to further our understanding of its complex functionality. Although we must still address a number of chemical, biological, and clinical questions before we can claim to fully understand the therapeutic potential (or lack thereof) of avrainvillamide, we thus cautiously optimistic that these challenges, through continued research and fruitful collaborations, may be overcome.

Note: Portions of this dissertation are based upon research that has previously published in *ACS Chemical Biology*. These materials are reprinted with permission from: Mukherjee, H.; Chan, K. P.; Andresen, V.; Hanley, M. L.; Gjertsen, B. T.; Myers, A. G. Interactions of the Natural Product (+)-Avrainvillamide with Nucleophosmin and Exportin-1 Mediate the Cellular Localization of Nucleophosmin and its AML-Associated Mutants. *ACS Chem. Biol.* **2015**, *10*, 855 – 863.

Experimental Data

Materials

Small Molecules

Avrainvillamide and avrainvillamide analogs were prepared as previously described with some modifications (*vide infra*).[5,7-11,77] Leptomycin B, calyculin A, and okadaic acid were obtained from LC Laboratories (Woburn, MA). Inhibitors for cell lysate stabilization (Halt™ Protease and Phosphatase Inhibitor Cocktail) were obtained from Life Technologies (Carlsbad, CA). 4-Nitrophenylphosphate was obtained from New England Biolabs (Ipswich, MA). DMSO (Hybri-Max grade) was obtained from Sigma-Aldrich (St. Louis, MO).

Cell Lines and Competent Cells

OCI–AML2 and OCI–AML3 cells were obtained from Deutsche Sammlung von Mikroorganismen und Zellkulturen (Braunschweig, Germany). LNCaP, T–47 D, HCT–116, and HeLa S3 cells were obtained from the American Type Culture Collection (Manassas, VA). Chemically competent *E. coli* cells [Mix and Go – Stain Zymo 5α, genotype: F-φ80 lacZΔM15 Δ(lacZYA-argF) U169 deoR nupG recA1 endA1 hsdR17(rK- mK+) phoA glnV44 (supE44) thi-1 gyrA96 relA1, λ-] were obtained from Zymo Research (Irvine, CA).

[77] As a precaution, all operations involving the handling of α,β-unsaturated nitrone species were conducted in the dark to minimize the occurrence of photochemical rearrangement reactions. Avrainvillamide and avrainvillamide analogs were typically stored as 5 mM solutions in DMSO at –80 °C.

Cell Culture Materials

DMEM, MEM-α, McCoy's 5A medium, and RPMI 1640 were obtained from GE Healthcare Life Sciences (Logan, UT). Opti-MEM, Fetal Bovine Serum (FBS), L-Glutamine, and HEPES buffer were obtained from Life Technologies. Trypsin-EDTA was obtained from Life Technologies. Thymidine, kanamycin (as kanamycin sulfate), SOC medium, LB broth, and LB agar plates containing kanamycin (50 μg/mL) were obtained from Sigma-Aldrich. Standard cell culture flasks and multi-well plates were obtained from Corning (Tewksbury, MA). Lab-Tek chambered coverglasses and poly-L-lysine coated coverglasses were obtained from Thermo-Fisher Scientific (Tewksbury, MA). T4 Polynucleotide Kinase and PP1β were obtained from New England Biolabs. γ-^{32}P-ATP was obtained from Perkin-Elmer (Cambridge, MA).

Other Materials and Reagents

NPM1–C_{108} was produced by Shanghai Medicillon (Shanghai, China) on a contract basis. NPM1 C-terminal peptides and the Crm1 513-530 peptide were obtained from Selleck Chem (Houston, TX). Sources for all primary and secondary antibodies are listed in Table 2.2. The eGFP–NPM1 (wild-type) plasmid was a gift from Xin Wang (Addgene plasmid # 17578). Other eGFP–NPM1 plasmids were synthesized by site-directed mutagenesis (*vide infra*). G-quadruplex DNA oligonucleotides and primers for mutagenesis were obtained from Integrated DNA Technologies (Coralville, IA). KOD Hot Start master mix was obtained from Merck Millipore (Billerica, MA). Cell Titer-Blue assay reagent and Fugene HD were obtained from Promega (Madison, WI). Ultra-pure low-melting agarose, NuPAGE pre-cast 4-12% Bis Tris agarose gels, pre-cast 8% TBE gels, SuperSignal molecular weight protein ladder, NuPAGE LDS sample buffer, NuPAGE

antioxidant, BCA protein assay kit, protein G Dynabeads, TBE buffer (10 x) and MOPS buffer (20 x) were obtained from Life Technologies. Ethidium bromide, paraformaldehyde (prilled), normal goat serum, Triton X-100, Hoechst 33342 trihydrochloride, Fluoromount, Tween 20, Laemmli buffer and bovine serum albumin were obtained from Sigma-Aldrich. Goat anti-mouse IgG and Goat anti-rabbit IgG poly-HRP conjugated antibodies, Bløk-PO blocking buffer, Luminata Forte Western HRP chemiluminescent substrate, Restore Western blot stripping buffer were obtained from Thermo-Fisher Scientific. A plasmid DNA purification kit (Zyppy MidiPrep kit) was obtained from Zymo Research. The preparation of additional buffer solutions is described below.

Table 2.2. Data for the antibodies used in this work. Ms = Mouse; Rb = Rabbit; Go = Goat.

Immunogen	**Host**	**Conjugate**	**Supplier**
Nucleolin	Ms	-	Life Technologies (39-6400)
NPM1	Rb	-	Santa Cruz Biotechnology (sc-6013-R)
RanBP1	Rb	-	Abcam (ab133550)
NPM1 p-T199	Ms	-	Abcam (ab81551)
γ-Tubulin	Rb	-	Abcam (ab11316)
14–3–3β	Ms	-	Abcam (ab18659)
Mouse IgG	Go	Alexa Fluor 555	Life Technologies (A-21424)
Mouse IgG	Go	Alexa Fluor 488	Life Technologies (A-11029)
Rabbit IgG	Go	Oregon Green 488	Life Technologies (O-6382)
Rabbit IgG	Go	Alexa Fluor 647	Life Technologies (A-21235)

Buffer Solutions

Mass Spectrometry (MS) Buffer:

50 mM Ammonium acetate; pH 7.0

Immunofluorescence Antibody Dilution (IFAD) Buffer:

5.0% (w/v) Normal goat serum

137 mM NaCl

2.7 mM KCl

0.2% (w/v) Triton X-100

10 mM Na_2HPO_4

1.8 mM KH_2PO_4; pH 7.4

Kinase Buffer:

10 mM $MgCl_2$

5 mM DTT

70 mM Tris; pH 7.6

Electrophoretic mobility shift assay (EMSA) Buffer:

100 mM KCl

50 mM Tris; pH 7.2

Lysis (RIPA) Buffer:

150 mM NaCl

1.0% (w/v) IGEPAL CA-630

0.5% (w/v) Sodium deoxycholate

0.1% (w/v) Sodium dodecyl sulfate

50 mM Tris; pH 8.0

Circular Dichroism (CD) Buffer:

150 mM KCl

10 mM Ammonium acetate; pH 7.0

Sucrose-hypotonic Buffer:

250 mM Sucrose

0.05% (w/v) Digitonin

1 mM DTT

5 μg/mL leupeptin

200 μM Na_3VO_4

50 mM NaF

1 mM Phenylmethanesulfonyl fluoride

25 mM Tris; pH 6.8

Immunoblot Blocking (IB) Buffer:

5% (w/v) Bovine serum albumin

150 mM NaCl

0.2% (v/v) Tween 20

50 mM Tris; pH 7.6

Phosphatase Assay (PA) Buffer:

1 mM $MnCl_2$

100 mM NaCl

2 mM DTT

0.01% (w/v) Brij 35

50 mM HEPES; pH 7.5

Phosphatase Stop (PS) Solution:

0.67 M Disodium EDTA

1.34 M NaOH

Phosphate-Buffered Saline (PBS):

137 mM NaCl

2.7 mM KCl

10 mM Na_2HPO_4

1.8 mM KH_2PO_4; pH 7.4

Tris-Buffered Saline (TBS)

150 mM NaCl

50 mM Tris; pH 7.6

Tris-Buffered Saline with Tween 20 (TBS-T)

0.2% (v/v) Tween 20 in TBS

Experimental Procedures

General Cell Culture

All cell culture work was conducted in a class II biological laminar flow hood. All media, buffers, and solutions of small molecule were filtered through a 0.2 μm or smaller membrane prior to use. Mammalian cell lines were cultured in standard cell culture flasks with vented caps or in multi-well plates in a non-humidified 37 °C incubator in a fixed atmosphere of 5% CO_2 (in air). For certain immunofluorescence microscopy experiments, cells were alternatively cultured in Lab-Tek chambered coverglasses in humidified chambers within the incubator. Bacterial cells were cultured in a non-humidified 37 °C incubator. LNCaP and T–47 D cells were cultured in RPMI 1640 supplemented with 10% FBS, 2 mM L-glutamine, and 25 mM HEPES buffer (pH 7.4). HeLa S3 cells were cultured in DMEM supplemented with 10% FBS. HCT–116 cells were cultured in McCoy's 5A medium supplemented with 10% FBS. OCI–AML2, OCI–AML3, and U–937 cells were cultured in MEM-α supplemented with 20% FBS.

For routine culture, growth medium was exchanged with fresh medium every 2-3 days. Cells were grown to approximately 80-90% confluency, then were subcultured at a ratio of approximately 1 : 10 (adherent cells) or 1 : 50 (suspension cells). Cells were maintained for a maximum of 15 passages.

Growth Inhibition (GI_{50}) Assays

Note: GI_{50} data for all avrainvillamide analogs against the T–47 D and LNCaP cell lines was obtained by Dr. Jeremy Wulff and Dr. Kok-Ping Chan.

Adherent Cells: Low-passage number cells were grown to approximately 80% confluence, then were treated with a solution of trypsin (0.05% w/v, 37 °C) until most of the cells had dissociated from the flasks (ca. 5-10 minutes). The cell suspension was collected and pelleted by centrifugation (183 × *g*, 4 °C, 10 minutes). The supernatant was discarded and the cells resuspended in fresh growth medium. Small aliquots of this suspension were removed for cell counting using a Scepter 2.0 automated cell counter (EMD Millipore); using these counts a working solution of 5.0×10^4 cells/mL was prepared.

Each GI_{50} assay plate was loaded as follows: To each well on the perimeter of a 96-well plate was added 200 µL fresh medium. To each well in one column of 6 wells of the remaining 6 × 10 space was added 100 µL fresh medium. To each of the remaining 54 wells was added 100 µL of the working suspension of cells. The plates were incubated for 24 hours at 37 °C.

The following day, dosing solutions were prepared by diluting 5 mM stock solutions (in DMSO) of avrainvillamide or avrainvillamide analogs to a working concentration of 50 µM in cell culture medium. Using serial 2-fold dilutions, a total of 8 different dosing solutions were prepared, ranging from 50 µM – 391 nM. A ninth solution containing DMSO only was prepared (vehicle control); DMSO was added to each dosing solution to standardize DMSO concentration across each well (1% v/v). For each assay replicate, 100 µL aliquots of each dilution series (including a DMSO-only solution) were added to a row of the 96-well plate. Each analog was

typically run at least twice on each plate; to minimize positional effects,[78] each analog was also run on at least three plates, varying the position of the analog between the plates. For each assay, two additional plates (control plates) were prepared and dosed with DMSO only in each well. The assay plates were incubated at 37 °C for 72 hours.

Immediately following dosing, each well of one control plate was treated with 20 μL of Cell Titer-Blue reagent. The plate was incubated at 37 °C for 90 minutes, then the fluorescence of each well (560 nm excitation/595 nm emission) was measured using a SpectraMax Gemini XS plate reader. After the 72 hour dosing period had elapsed, the fluorescence of each well of the assay plates was determined in an identical manner. Percent growth inhibition (% GI) was determined for each well using the following formula:

$$\%\,\mathrm{GI} = \frac{(\mathrm{S} - \mathrm{C}_0)}{(\mathrm{C}_t - \mathrm{C}_0)} \times 100\%$$

where S is the sample reading, C_0 is the average reading for the initial control plate, and C_t is the average reading of control plates at the conclusion of the assay. For each analog, % GI was plotted against concentration, and a curve fit was generated using the XLfit4 plug-in (IDBS software) for Microsoft Excel. GI_{50} values represent the concentration at which the resultant curve intersects 50% GI. The curve fit was scaled so that the maximum and minimum % GI values were 100% and 0%, respectively. In order to maximize accuracy and reproducibility, each analog was tested a minimum of six times over a period of at least two weeks. Control readings were typically subtracted row-by-row in order to account for positional effects. New GI_{50} data for avrainvillamide are presented in Table 2.3.

[78] It was observed that cells cultured in wells near the perimeter of the plate routinely grew more rapidly than cells cultured in wells near the center of the plates.

Suspension Cells: GI_{50} values for avrainvillamide against U–937, OCI–AML2, and OCI–AML3 cells were obtained in a similar manner, with the exception that cells from an initial culture could be counted and seeded directly into 96-well plates without the need for treatment with trypsin. Furthermore, suspension cell lines were found to exhibit an antiproliferative response towards avrainvillamide that was dependent on their initial seeding concentration – thus, higher initial seeding concentrations led to higher measured GI_{50} values (the opposite was also true). For consistency, the values reported in Table 2.3 were measured with an initial seeding density of 5.0×10^4 cells/mL, as with the adherent cell lines.

Table 2.3. GI_{50} values for avrainvillamide against a panel of cancer cell lines. Values reported indicate mean ± standard deviation of at least six measurements.

Cell Line	Tissue Source	GI_{50} (μM)
LNCaP	Prostate adenocarcinoma	0.33 ± 0.03
T–47 D	Ductal carcinoma	0.42 ± 0.03
U–937	Histiocytic lymphoma	0.93 ± 0.10
OCI–AML2	Acute myeloid leukemia	0.52 ± 0.15
OCI–AML3	Acute myeloid leukemia (NPMc+)	0.35 ± 0.09
HCT–116	Colon carcinoma	1.10 ± 0.04
HeLa S3	Cervical adenocarcinoma	4.1 ± 0.30

Mass Spectrometry Experiments

Note: For experiments involving the NPM1–C_{108} construct, injection of the sample into the mass spectrometer and data acquisition was performed by Dr. Jeremy Wulff (Bruker Daltronics, Billerica, MA).

NPM1–C_{108} was provided as a solution containing 150 mM NaCl, 2 mM DTT, and 50 mM tris (pH 7.0). Stock solutions of NPM1–C_{108} were diluted with additional buffer to a final concentration of 50 μM, then were treated with DMSO solutions of avrainvillamide or avrainvillamide analogs (5 mM, 10 eq. relative to NPM1). The resulting solutions were incubated at 23 °C for the specified amount of time, then 10 μL aliquots were removed for desalting and MS analysis.

Sample desalting was accomplished using a C_4 Zip Tip (EMD Millipore) containing 0.6 μL of chromatography medium. Prior to use, the Zip Tips were hydrated by repeatedly aspirating/dispensing a solution of 50% acetonitrile and 0.1% formic acid in water through the tip. The sample was loaded onto the Zip Tip by aspirating/dispensing the sample a minimum of 10 times through the tip. The sample was washed by aspirating and dispensing a solution of 0.1% formic acid in water through the tip a minimum of 5 times (using fresh wash solution each time), then the NPM1–C_{108} construct (and/or its avrainvillamide adduct) was eluted by aspirating and dispensing a solution of 60% acetonitrile and 0.1% formic acid in water (once). The eluted samples were immediately loaded onto a solarIX XR 12 Tesla FT–ICR mass spectrometer. Data was acquired continuously until the characteristic signal of the NPM1–C_{108} peptide was observed; once the signal was detected an optimized m/z detection range was selected (typically m/z values between 700 – 1500) for data acquisition. Following data acquisition, spectral deconvolution was performed (maximum entropy method) to provide final spectra.

For experiments using the NPM1–C_{52} and NPM1–C_{56} peptides, lyophilized peptide samples were reconstituted in MS buffer at 23 °C at a final concentration of 50 μM. To each sample was added a solution of avrainvillamide (5 mM in acetonitrile, 3 eq. relative to NPM1). The sample vials were loaded into an autosampler for an Agilent 6220 LC-TOF mass

spectrometer; 2 μL aliquots were injected directly from the sample vials at the specified time points.

For the determination of relative reaction rates, avrainvillamide was added to solutions of C-terminal NPM1 peptides as above. Aliquots of each solution were removed after 1, 5, and 10 minutes to quantify product formation. For each sample, three replicate analyses were performed. For the NPM1–Mutant A, Mutant E, and NPM1–Mutant A–C288A peptides, significant deviations from linearity was observed in the 10 minute samples, thus these time points were disregarded when determining the relative rates. Relative rates were determined by fitting the data points to a line with a fixed intercept at (0 minutes, 0% conversion).

Immunofluorescence Microscopy

Immunofluorescence analysis of suspension cells: Leukemic cells were seeded into 24-well plates at an initial density of 2.5×10^4 cells/well and incubated at 37 °C for 24 hours. The following day, the culture medium was replaced with fresh medium containing DMSO or avrainvillamide at the indicated concentrations and the cells were incubated at 37 °C for the specified amount of time. At the end of the dosing period, each well was charged with a poly-L-lysine coated 12 mm-diameter round coverslip. The cells were transferred onto the coverslips by centrifugation (100 × *g*, 4 °C, 15 minutes). The medium was removed and the cells fixed with a solution of formaldehyde (4% w/v in PBS, freshly prepared from paraformaldehyde; 23 °C, 20 minutes). The coverslips were washed twice with PBS (23 °C, 5 minutes each), the cells were permeablized by treatment with the IFAD buffer (23 °C, 30 minutes). The coverslips were treated with a diluted solution of primary antibodies in IFAD buffer (anti-NPM1 at 1 : 1 000,

anti-nucleolin at 1 : 5 000; 23 °C, 60 minutes). The coverslips were washed twice with PBS, then were treated with a diluted solution of secondary antibodies in IFAD buffer (anti-mouse IgG-Alexa Fluor 555 conjugate at 1 : 2 000, anti-rabbit IgG-Oregon Green 488 conjugate at 1 : 2000; 23 °C, 60 minutes). The coverslips were washed twice with PBS, then nuclei were counter stained by exposing the coverslips to a solution of Hoechst 33342 in PBS (10 μM, 23 °C, 15 minutes). The coverslips were washed four times with PBS, then were immersed briefly in ultra-pure H_2O to remove buffer salts. The coverslips were dried by placing them on edge on a cotton wipe, and then mounted onto microscope slides using 8 μL Fluoromount. The slides were allowed to air-dry overnight at 23 °C, protected from light, prior to imaging. The mounted coverslips were imaged using an Olympus IX71 inverted microscope equipped with an iXon 888 EMCCD camera with excitation at 405, 488, and 532 nm. Each fluorescent dye was imaged individually; the resulting intensity plots were colored and assembled using FIJI (National Institutes of Health) to provide final images.

Experiments employing GFP–tagged fusion proteins: Adherent cells were seeded into 8-chambered Lab-Tek coverglasses at an initial density of 2.5×10^4 cells/well. The coverglasses were incubated at 37 °C in humidified chambers for 24 hours.

Transfection complexes were prepared by adding plasmid DNA (4 μg) to Opti-MEM (100 μL) at 23 °C in a glass vial. Fugene HD (18 μL) was added directly to the solution[79] and the resulting transfection complexes were incubated at 23 °C for 15 minutes. Meanwhile, the cell culture medium was removed from the coverglasses and each chamber was charged with 375 μL of fresh medium. To each well was added 25 μL of transcription complex, then the cells

[79] To minimize potential adsorption of the Fugene HD to surfaces, the pipette tip was placed below the surface of the DNA solution while dispensing the reagent, and the solution was not mixed by pipetting.

incubated in humidified chambers at 37 °C for 48 hours without changing the growth medium. After 48 hours the medium was replaced with fresh medium containing DMSO, avrainvillamide (1 μM), or leptomycin B (100 nM), and the cells incubated for the specified amount of time. After dosing the cells were fixed with formaldehyde, permeablized, and immunostained as described above, with the exception that immunostaining of NPM1 was not performed for experiments employing eGFP–NPM1 constructs, and immunostaining of NPM1 and nucleolin was not performed for experiments employing GFP–Rev. Nuclei were counterstained with Hoechst 33342 as described above. Following the final PBS washes, the chambers were charged with a solution of 3 mM NaN_3 in PBS and imaged directly (without removal of the chambers).

RanBP1 localization experiments: Adherent cells were seeded into 8-chambered Lab-Tek coverglasses at an initial density of 2.5×10^4 cells/well. The coverglasses were incubated at 37 °C in humidified chambers for 24 hours. After 24 hours the medium was replaced with fresh medium containing DMSO, avrainvillamide (1 μM), or leptomycin B (100 nM), and the cells incubated for the specified amount of time. After dosing the cells were fixed with formaldehyde and permeablized as described above. The cells were then treated with a solution of primary antibody (anti-RanBP1, 1 : 1 000 in IFAD buffer; 23 °C, 60 minutes). The cells were washed twice with PBS, then treated with a solution of secondary antibody (anti-rabbit IgG-Oregon Green 488 conjugate, 1 : 2 000 in IFAD buffer, 23 °C, 60 minutes). The cells were washed twice with PBS, nuclei were counterstained and imaged as described above.

Thr^{199}-phosphorylated NPM1 Localization Experiments: Each of a 6-well plate was charged with an 18 mm square coverslip followed by a suspension of 2×10^5 cells. The plates were incubated at 37 °C for 24 hours. After 24 hours the medium was replaced with fresh medium containing 3 mM thymidine and the cells incubated at 37 °C for 17 hours. After

17 hours the medium was replaced with fresh medium and the cells incubated at 37 °C for 12 hours. After 12 hours the cells medium was replaced with fresh medium containing 3 mM thymidine and the cells incubated at 37 °C for 16 hours. After 16 hours the medium was replaced with fresh medium containing either DMSO or avrainvillamide (1 μM) and the cells incubated at 37 °C. Cells were fixed at pre-determined time points selected to coincide with specific phases of the cell cycle. Fixation was performed by washing the coverslips with pre-warmed (37 °C) PBS, then immediately submerging the coverslips in pre-cooled (–20 °C) methanol. The coverslips were incubated at –20 °C for exactly 7 minutes, then the methanol replaced with PBS at 23 °C. The coverslips were incubated at 23 °C for 5 minutes, then non-specific protein-antibody interactions were blocked and the cells simultaneously permeablized by treatment with the IFAD buffer. The coverslips were treated with a diluted solution of primary antibodies in IFAD buffer (anti-NPM1 (phospho-Thr^{199}) at 1 : 1 000, anti-γ–tubulin at 1 : 1 000; 23 °C, 60 minutes). The coverslips were washed twice with PBS, then were treated with a diluted solution of secondary antibodies in IFAD buffer (anti-mouse IgG-Alexa Fluor 488 conjugate at 1 : 2 000, anti-rabbit IgG-Alexa Fluor 647 conjugate at 1 : 2 000; 23 °C, 60 minutes). Nuclei were counterstained and the coverslips washed, mounted and imaged as described above, with the exception that the mounted coverslips were imaged using excitation at 405, 488, and 650 nm.

Site-Directed Mutagenesis

For each mutagenesis reaction, 1 μg plasmid DNA template was added 100 μL KOD Hot Start master mix in a 0.2 mL PCR tube (refer to Table 2.4 for template/primer combinations). To each tube was added forward and reverse PCR primers to achieve a final concentration of 10 μM

each, and DMSO to a final concentration of 0.5% (v/v). The tubes were placed in a thermal cycler programmed as follows:

- 94 °C, 2 minutes.
    - 94 °C, 20 seconds.
    - 54 – 70 °C,[80] 30 seconds.
    - 68 °C, 6 minutes.
    - Repeat indented steps (40 cycles total).
- 4 °C, hold.

Following amplification, template DNA was digested with DpnI (0.5 U/reaction, 37 °C, 60 minutes). The DpnI-treated products were analyzed by electrophoresis on a 1% agarose gel. PCR product solutions determined to contain amplified plasmid DNA (~5.5 kbp) were used directly in bacterial transformation reactions. For each transformation, a 25 µL aliquot of competent cells was thawed at 4 °C for 5 minutes. 1 µL PCR product solution was added to each aliquot, then the cells incubated at 4 °C for 1 minute, 42 °C for 37 seconds, and 4 °C for 1 minute. SOC medium (200 µL) was added to each aliquot of cells, and the cells immediately spread onto LB agar plates containing 50 µg/mL kanamycin. The plates were incubated at 37 °C for 24 hours. Single colonies were selected for amplification and added to culture tubes containing LB broth and 50 µg/mL kanamycin. The liquid cultures were incubated at 37 °C for 17 hours in a shaking incubator, then the cells were pelleted by centrifugation (1 500 × *g*, 4 °C, 15 minutes). Plasmid DNA was isolated from the pelleted cells using the Zyppy Midiprep kit and protocol. Each plasmid DNA sample was sequenced to confirm successful mutagenesis. Samples which contained the desired point mutations were selected for transformation into competent cells as

[80] A temperature gradient was employed in this step; best results were typically obtained at lower temperatures.

above. Single colonies from the resulting plates were amplified in liquid cultures; 700 µL aliquots of each liquid culture were added to 300 µL portions of 50% aqueous glycerol. The glycerol stock suspensions were frozen at –80 °C for long-term storage. Subsequent transfections requiring a synthesized plasmid thus employed plasmid DNA isolated from these frozen glycerol stocks, rather than by repeating the site-directed mutagenesis procedure.

Table 2.4. Template plasmid and primer combinations used in the site-directed mutagenesis reactions. For the eGFP–NPM1–Mutant A–C275,288A double mutant, two rounds of mutagenesis were employed, introducing each of the point mutations in sequence.

Plasmid	Template	Forward Primer	Reverse Primer
eGFP–NPM1–Mutant A	eGFP–NPM1	5'-TCTAGATCCGCTATTTCCTTAAAGAGACTTCCTCCACTGCCAGACAGAGATCTTGAATAG -3'	5'-CTATTCAAGATCTCTGTCTGGCAGTGGAGGAAGTCTCTTTAAGGAAATAGCGGATCTAGA-3'
eGFP–NPM1–Mutant A–C275A	eGFP–NPM1–Mutant A	5'-TTGAATAGCCTCTTGGTCAGTCATCCGGAAAGCATTCTTCACATAATT–3'	5'-AATTATGTGAAGAATGCTTTCCGGATGACTGACCAAGAGGCTATTCAA-3'
eGFP–NPM1–Mutant A–C288A	eGFP–NPM1–Mutant A	5'-TTCCTCCACTGCCAGAGCGAGATCTTGAATAGCCTCTTGGTCAGTCATCCGGAAACA-3'	5'-TGTTTCCGGATGACTGACCAAGAGGCTATTCAAGATCTCGCTCTGGCAGTGGAGGAA-3'
eGFP–NPM1–Mutant E	eGFP–NPM1	5'ATGATCAGTTATTATTTTCTTAAAGAGACTTGGGCAAGGGACTGCCAGAGATCTTGAAT -3'	5'ATTCAAGATCTCTGGCAGTCCCTTGCCCAAGTCTCTTTAAGAAAATAATAACTGATCAT–3'
eGFP–NPM1–Mutant E-C275A	eGFP–NPM1–Mutant E	5'-TTGAATAGCCTCTTGGTCAGTCATCCGGAAAGCATTCTTCACATAATT–3'	5'-AATTATGTGAAGAATGCTTTCCGGATGACTGACCAAGAGGCTATTCAA-3'

Circular Dichroism Spectroscopy

Lyophilized NPM1–C_{52} or NPM1–C_{56} peptides were reconstituted in CD buffer to a final concentration of 32 μM. For control experiments, 5% acetonitrile was added to each peptide solution, then the CD spectrum of each peptide was measured using a Jasco J-710 spectrometer. CD spectra were obtained at 23 °C over a range of 190–260 nm at 0.5 nm intervals; reported spectra represent the averages of 4 individual scans. For samples involving avrainvillamide, a blank spectrum of avrainvillamide in CD buffer (320 μM) containing 5% acetonitrile was obtained; this spectrum was subtracted from all spectra of peptide solutions containing avrainvillamide. Similarly, a blank spectrum of 13079nt in CD buffer (32 μM) containing 5% acetonitrile was obtained and subtracted from all spectra of peptide solutions containing the oligonucleotide.

Electrophoretic Mobility Shift Assay (EMSA)

Note: This series of experiments was conducted by Mariah Hanley.

Preparation of ^{32}P-labeled 13079nt: To a 1.5 mL low-adhesion microcentrifuge tube was added 5 μL of a solution of 13079nt (40 μM), 3 μL kinase buffer, 3 μL T4 polynucleotide kinase, and 12 μL ATP (γ-^{32}P, 1.67 μM, 120 μCi). The mixture was incubated at 37 °C for 60 minutes, and then was heated to 95 °C for 2 minutes. The solution was cooled to 23 °C, then was diluted with 500 μL water and loaded onto a 3K Ambion filter. The mixture was filtered by centrifugation (14 000 × *g*, 23 °C, 15 minutes), then the filter was washed with sequential 500 μL portions of water and a 100 mM solution of KCl in water. The purified oligonucleotide was eluted by inverting the filter and centrifuging (14 000 × *g*, 23 °C, 20 minutes). The DNA solution

was heated to 90 °C for 10 minutes, then was allowed to cool slowly 23 °C and then to 4 °C to induce G-quadruplex formation.

EMSA: For each lane, 9 μL reaction mixtures were prepared containing 25 μM peptide, 2 μL of the DNA solution, and 1 μL of either DMSO or a DMSO solution of avrainvillamide (final concentration = 50 μM), in EMSA buffer. The reaction mixtures were incubated at 37 °C for 60 minutes. Meanwhile, a pre-cast 8% TBE gel was pre-electrophoresed (4 °C, 100 V, 60 minutes). To each EMSA reaction was added 1 μL 50% (v/v) glycerol. Each reaction mixture was loaded onto the gel; the gel was then electrophoresed using TBE running buffer (4 °C, 120 V, 60 minutes). The gel was then wrapped in plastic and exposed to a phosphor image screen. The screen was visualized using a Typhoon Trio Imager (GE Healthcare).

Western Blot Analysis of Levels of Thr^{199}-Phosphorylated NPM1

For each dosing condition, a 25-cm^2 culture flask was charged with a suspension of HCT–116 cells (3.0×10^5 cells/mL, 5 mL) and incubated overnight at 37 °C. The following day, the growth medium was removed and replaced with fresh medium containing DMSO (vehicle control) or DMSO solutions of avrainvillamide (0.5, 1.0, or 4.0 μM). The cells were incubated at 37 °C for the specified time points. Once the appropriate amount of time had elapsed, the culture medium from each flask was transferred to a 15-mL centrifuge tube. The cells were rinsed with 2 mL PBS, which was added to the centrifuge tube. The cells were treated with a solution of trypsin (0.05% (w/v), 1 mL), then the flasks incubated at 37 °C until most of the cells had detached (ca. 5 – 10 minutes). The detached cells were transferred to the centrifuge tube. Each flask was rinsed with two 2 mL portions of PBS to quantitatively transfer the remaining detached

cells to the tube. The cells were pelleted by centrifugation (183 × *g*, 4 °C, 10 minutes) and the supernatant discarded. The cells were resuspended in 1 mL of pre-cooled (4 °C) PBS, transferred to a 1.5-mL centrifuge tube, and centrifuged again (500 × *g*, 4 °C, 3 min). The supernatant was discarded, and the cells were washed with two 500 µL of PBS. The cell pellets were cooled on ice and treated with pre-cooled (4 °C) sucrose-hypotonic. The suspension was incubated at 4 °C for 3 minutes, then the samples were briefly vortexed (ca. 5 seconds) and centrifuged (6800 × *g*, 4 °C, 3 minutes). The supernatants (cytoplasmic lysates) were transferred to fresh 1.5-mL centrifuge tubes. The remaining pellets were washed twice with 500 µL portions of pre-cooled (4 °C) PBS. The washed pellets were treated with 50 µL pre-cooled (4 °C) RIPA buffer for 1 hour a then were clarified by centrifugation (14 100 × *g*, 4 °C, 10 minutes). Insoluble material was removed using a pipette tip, then the resulting nuclear-enriched lysates were transferred to fresh 1.5-mL centrifuge tubes. The total protein concentrations in both the cytoplasmic and the nuclear-enriched lysates were determined using the BCA kit and protocol (all samples and standards were measured in triplicate).

An aliquot of each of the cytoplasmic lysates were normalized by adding sucrose-hypotonic buffer to each sample to provide a 50 µL sample containing 35 µg total protein. The nuclear lysates similarly normalized by the addition of RIPA buffer to each sample to afford 50 µL samples containing 250 µg total protein. Each sample was diluted with 50 µL of Laemmli loading buffer, proteins were denatured by heating to 95 °C for 10 minutes, then the samples were cooled to 23 °C. The samples were loaded onto a pre-cast 4-12% Bis-Tris mini gel and the gel electrophoresed using MOPS running buffer (4 °C; 100 V, 30 minutes, then 150 V, 90 minutes). The proteins in the gel were transferred under wet conditions to a PVDF membrane (4 °C, 100 V, 90 minutes). The membranes were blocked by immersion in bløk-PO reagent (23 °C,

60 minutes). The membrane was washed twice with TBS-T (5 minutes each) then treated with a solution of primary antibody (anti-NPM1 [phospho-thr^{199}], 1 : 2 000 in IB buffer; 4 °C, 16 hours). The membrane was washed twice with TBS-T, then treated with a solution of secondary antibody (anti mouse IgG-poly-HRP conjugate, 1 : 5 000 in IB buffer, 23 °C, 60 minutes). The membrane was washed four times with TBS-T then twice with TBS. The membranes were visualized using Luminata Forte reagent on a Chemi-Imager (Alpha Innotech). Following imaging, the membrane was washed twice with TBS, then immersed in Restore stripping buffer. The membrane was reblocked and reprobed for total NPM1. Finally, as a loading control, the membrane was stripped, reblocked, and reprobed for 14–3–3β.

PP1β Activity Assays

Isolation of thr^{199}-phosphorylated-NPM1–containing immunocomplexes: HCT–116 cells were grown to 85% confluency in a 150 cm^2 flask. The growth medium was replaced with fresh medium containing okadaic acid (50 nM), then the cells incubated for 8 hr at 37 °C prior to harvesting. The cells were then treated with trypsin, harvested, and lysed in RIPA buffer as above, omitting the incubation with sucrose-hypotonic buffer. Thr^{199}-phosphorylated NPM1 was isolated from the cell lysates by immunoprecipitation using Protein G Dynabeads kit and the following protocol. For each immunoprecipitation reaction, a 50 µL aliquot of beads was added to a 1.5 mL microcentrifuge tube. The tubes were placed on a magnet and the supernatant removed. The beads were washed twice with PBS, then were incubated with a solution of the primary antibody (1 : 200) in PBS (4 °C, 2 hours). After 2 hours the tubes were placed on a magnet and the supernatant was removed. The antibody-conjugated beads were treated with an

aliquot of whole-cell lysate containing 1 mg total protein (4 °C, 16 hours). The tubes were placed on a magnet and the supernatants removed. The beads in each tube were washed with four 500 µL portions of wash buffer. The bead-conjugated immunocomplexes were used directly in the PP1β activity assay. For the PP1β activity assay, the immunocomplexes were washed twice with phosphatase reaction buffer (1 mM MnCl2, 50 mM HEPES, 100 mM NaCl, 2 mM DTT, 0.01% Brij 35, pH 7.5) then resuspended in the reaction buffer and divided into 30 µL aliquots. For each reaction, 0.5 U of PP1β was added to the lysates containing acetonitrile (0.08% v/v, vehicle control) or acetonitrile solutions of avrainvillamide, calyculin A (CA), or leptomycin B (LMB), as indicated. The reactions were incubated at 30 °C for 2 hr.

PP1β phosphatase assay employing thr^{199}-phosphorylated NPM1 as the substrate: The bead-conjugated immunocomplexes were washed twice with PA buffer, then resuspended in 300 µL PA buffer. The suspension was divided into 30 µL aliquots. To each aliquot was added either acetonitrile (0.08% v/v, vehicle control) or acetonitrile solutions of avrainvillamide, calyculin A (CA) or leptomycin B (LMB) as indicated. Each aliquot was treated with PP1β (0.5 U), then the reaction mixtures incubated at 30 °C for 2 hours. LDS sample buffer (10 µL) was then added to each reaction and the mixtures heated to 95 °C for 10 minutes. The denatured samples were allowed to cool to 23 °C, then the proteins were electrophoresed, transferred to membranes, and immunoblotted for thr^{199}-phosphorylated NPM1 and total NPM1 as described above.

PP1β phosphatase assay employing 4-nitrophenylphosphate as the substrate: PP1β (0.5 U) was added to 80 µL PA buffer containing acetonitrile (0.08% v/v, vehicle control), avrainvillamide, leptomycin B, or calyculin A, as indicated. The reactions were initiated by the addition of a 4-nitrophenyl phosphate solution (500 mM in water, 20 µL). The reaction mixtures

were incubated at 30 °C for 2 hr, then the reactions stopped by the addition of 100 μL of PS solution. Reaction progress was measured by reading absorbance of the plate at 405 nm on a SpectraMax Plus 384 plate reader. Percent phosphatase inhibition (% PI) values were determined by the equation:

$$\% \text{ PI} = \left[1 - \frac{(\text{S} - \text{X})}{(C - X)}\right] \times 100\%$$

where S is the sample reading at the end of the reaction, C is the reading from a control well at the end of the reaction, and X is the reading from a well that did not receive PP1β in the reaction. All samples were run at in triplicate on each plate; reported values indicate mean ± standard deviation.

Supplementary Information

Appendix I: Supplementary Data

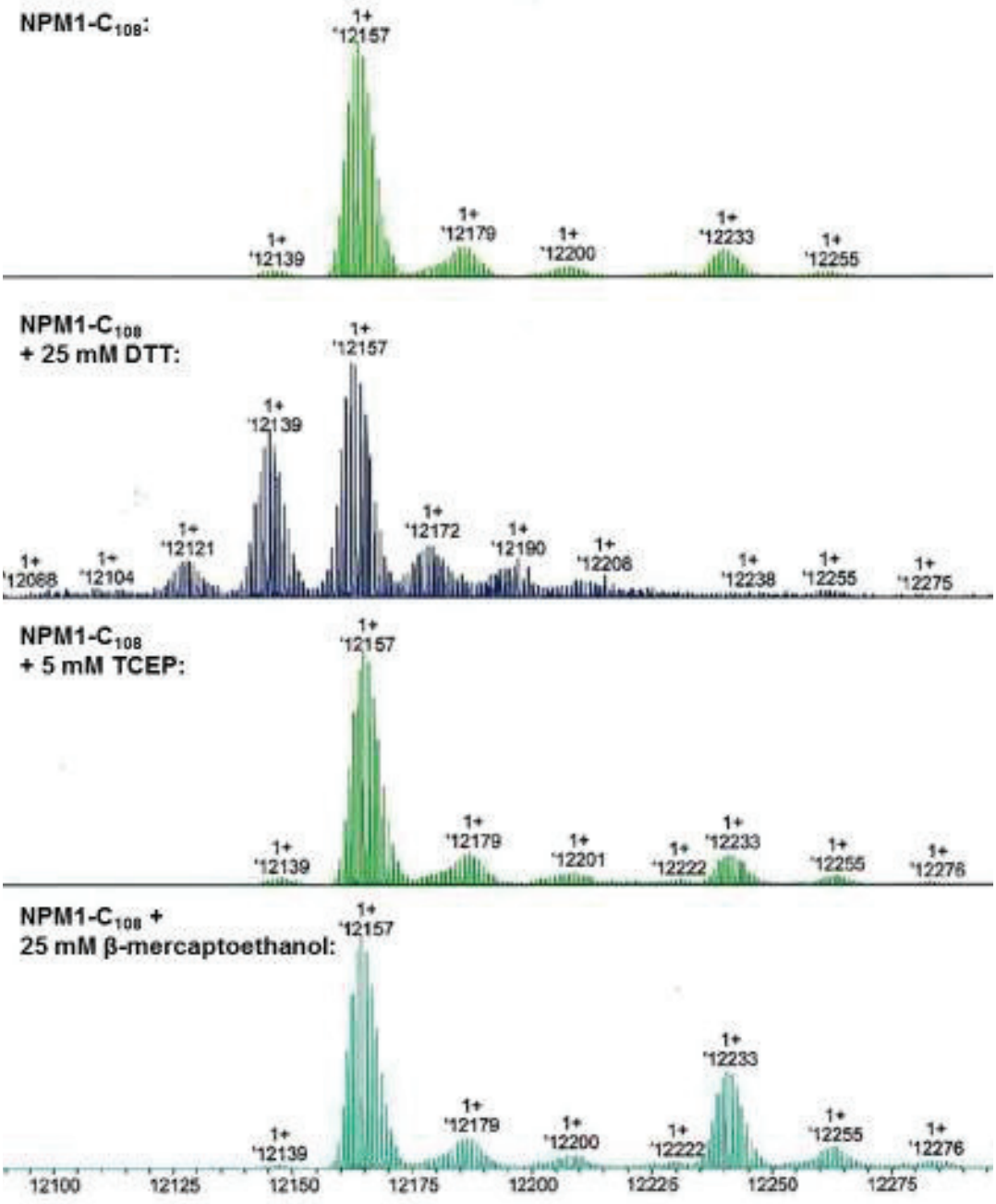

Figure S.1. Identification and attempted reduction of the NPM1–C_{108}-β-mercaptoethanol adduct using standard biocompatible reducing agents.

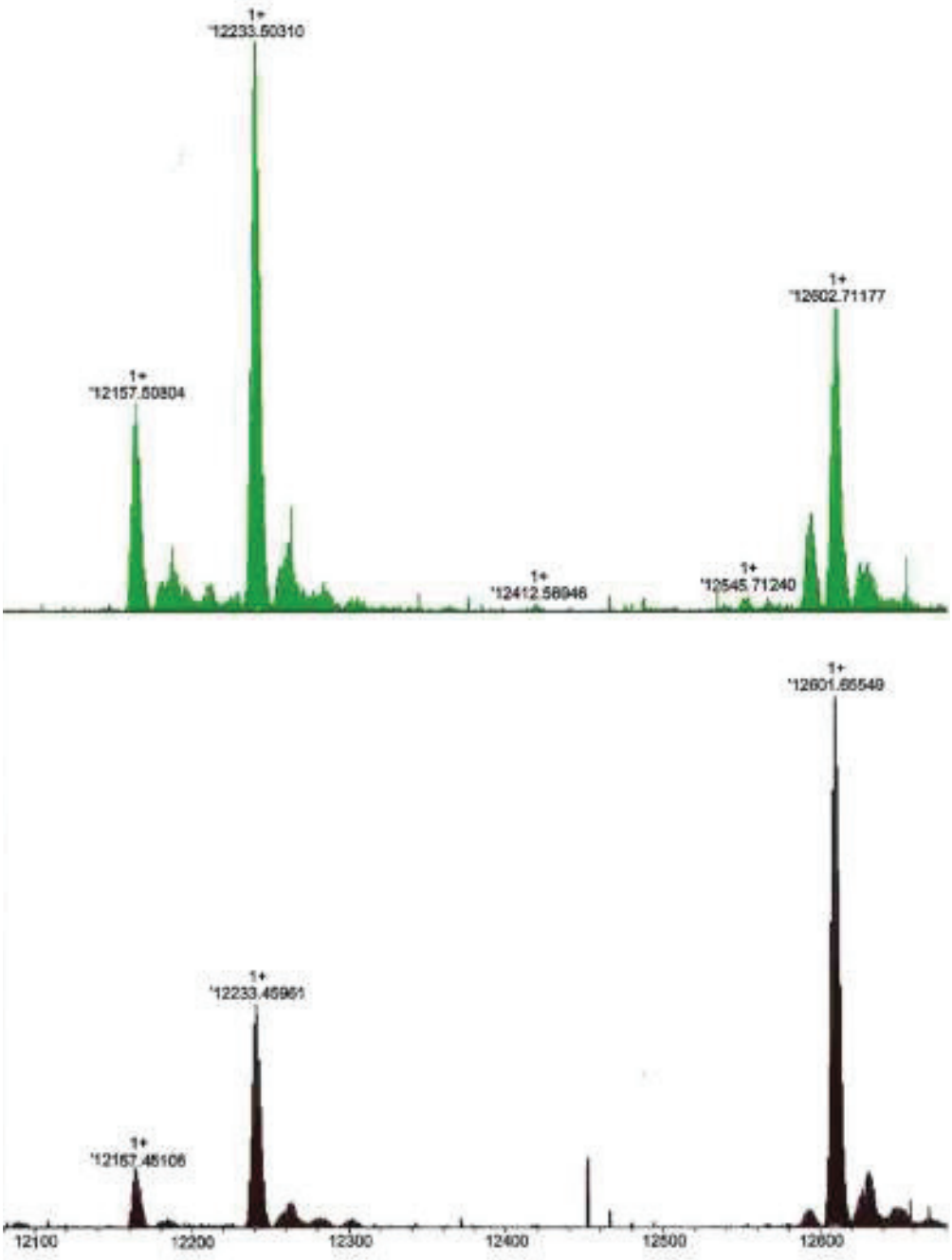

Figure S.2. Mass spectra of NPM1–C_{108} in the presence of either 10 (green trace) or 100 (black trace) equivalents of avrainvillamide, showing the relationship between avrainvillamide concentration and extent of reaction. Both spectra were obtained 4 hours after the addition of avrainvillamide.

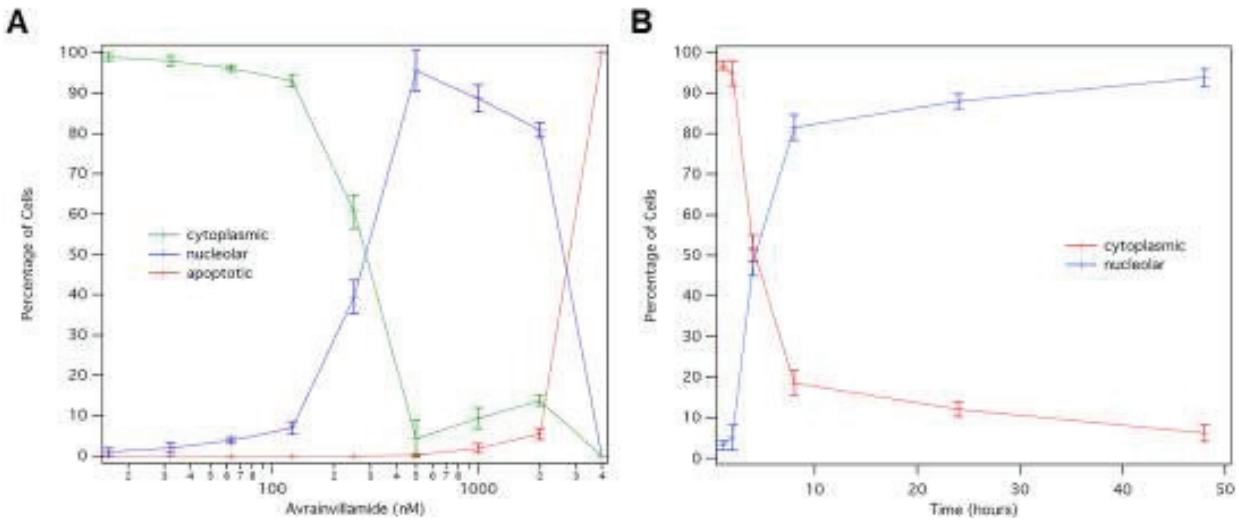

Figure S.3. **A**. The avrainvillamide-induced relocalization of NPM1 and NPMc+ proteins in OCI–AML3 cells as a function of avrainvillamide concentration. Apoptotic cells were defined as those with condensed nuclei and reduced or absent nucleolin immunostaining. **B**. The avrainvillamide-induced (1 μM) localization of NPM1 and NPMc+ proteins in OCI–AML3 cells as a function of time. Apoptotic cells were disregarded in **B**. For both **A** and **B**, a minimum of 150 cells were counted in each of three independent experiments; error bars indicate mean ± standard deviation.

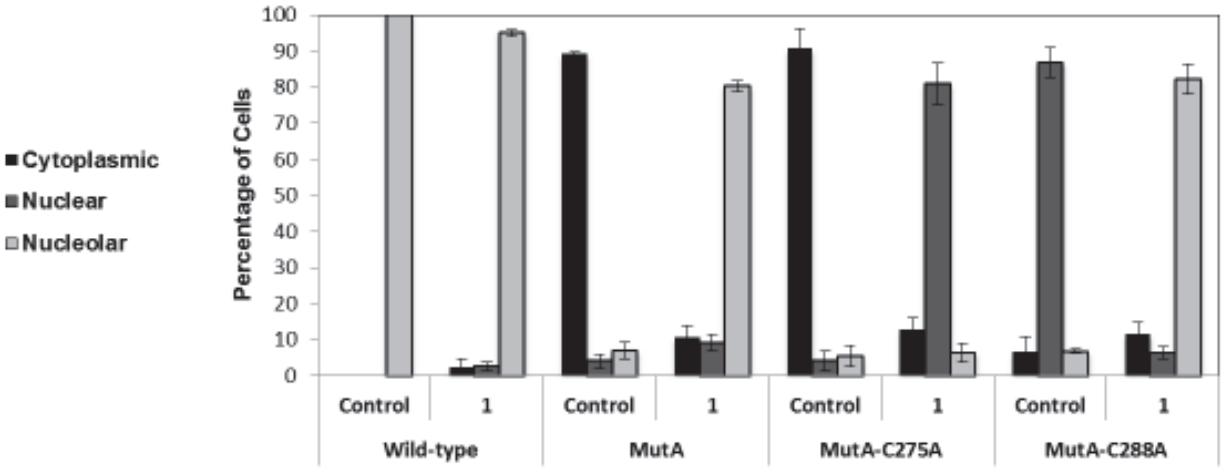

Figure S.4. Quantitation of the effects of avrainvillamide (1 μM, 24 hours) on the subcellular localization of eGFP–NPM1 fusion proteins in HCT–116 cells. A minimum of 150 cells were counted in each of three independent experiments; error bars indicate mean ± standard deviation.

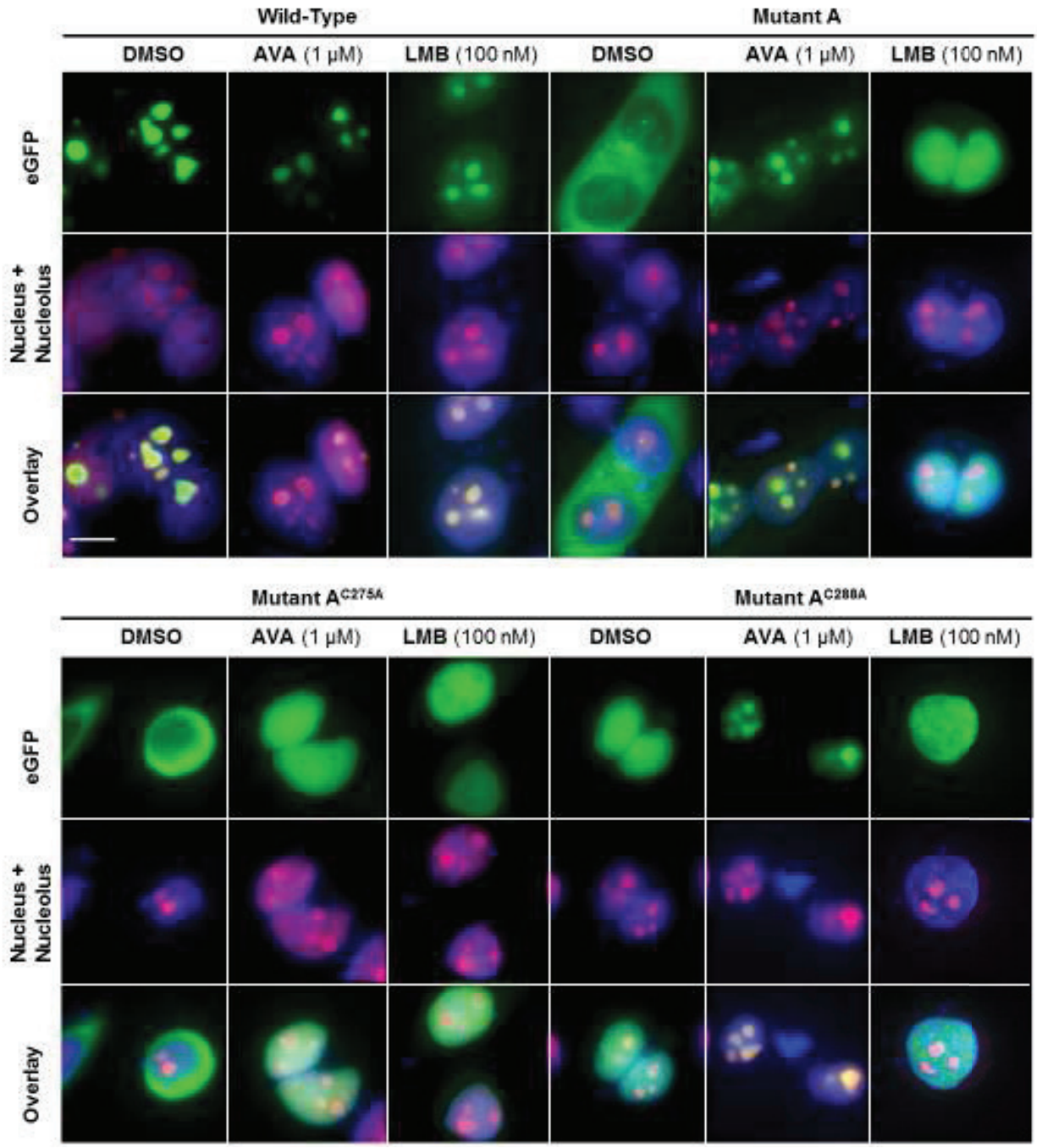

Figure S.5. Representative immunofluorescence microscopy images demonstrating the subcellular localization of eGFP–NPM1 (wild-type) and eGFP–NPM1–Mutant A-derived fusion proteins in HeLa S3 cells following treatment with either DMSO (vehicle control), avrainvillamide (24 hours), or LMB (4 hours). Colors: green, eGFP; red, nucleolin (nucleolar marker); blue (DNA (nuclear marker). Scale bar = 10 μm.

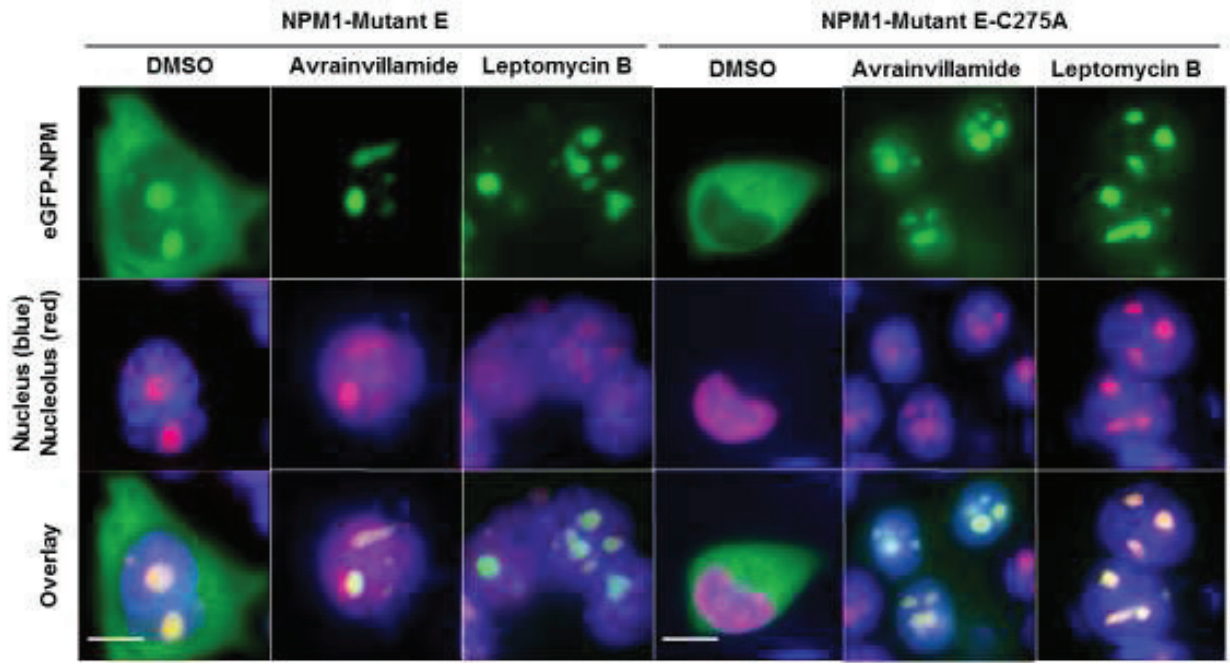

Figure S.6. Representative immunofluorescence microscopy images demonstrating the subcellular localization of the eGFP–NPM-Mutant E and eGFP–NPM1–Mutant E-C275A proteins following treatment with either DMSO (vehicle control), avrainvillamide (1 μM, 24 hr), or leptomycin B (100 nM, 4 hr). Colors: green, eGFP; red, nucleolin (nucleolar marker); blue, DNA (nuclear marker). Scale bars = 10 μm.

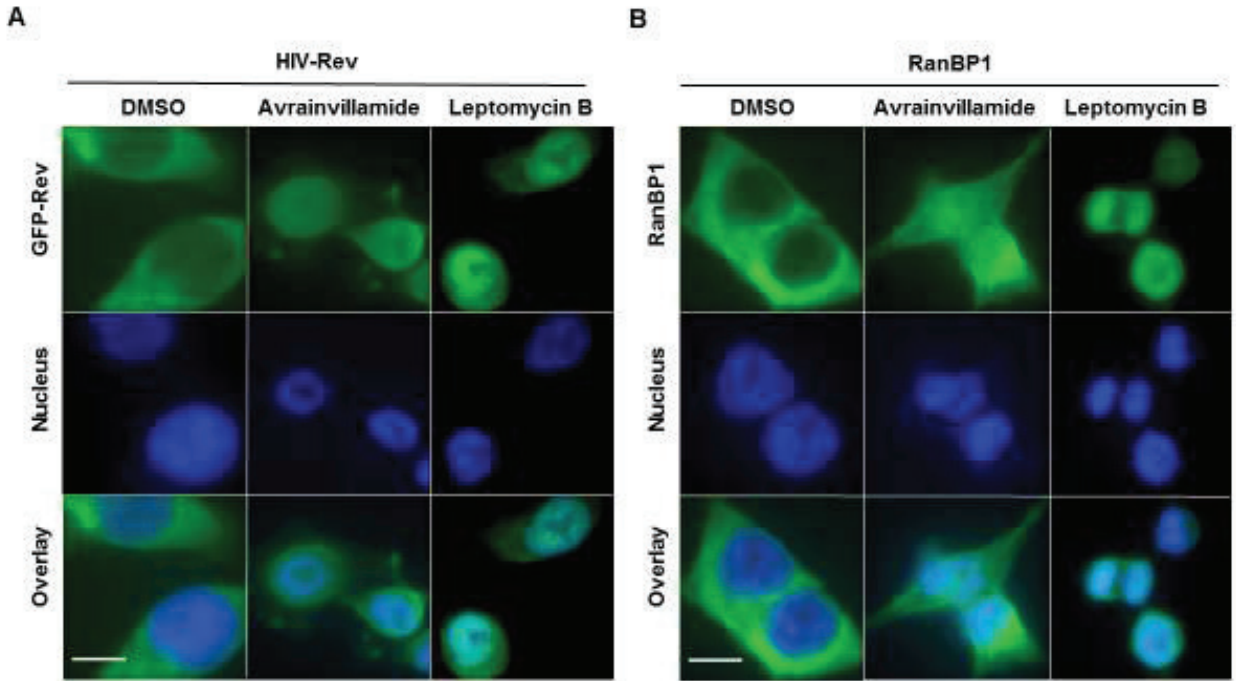

Figure S.7. Representative immunofluorescence microscopy images demonstrating the subcellular localization of (**A**) a GFP–Rev construct and (**B**) RanBP1 in HeLa S3 cells following treatment with either DMSO (vehicle control), avrainvillamide (1 μM, 24 hr), or leptomycin B (100 nM, 4 hr). Colors: green, (**A**) GFP, (**B**) RanBP1; blue, DNA (nuclear marker). Scale bars = 10 μm.

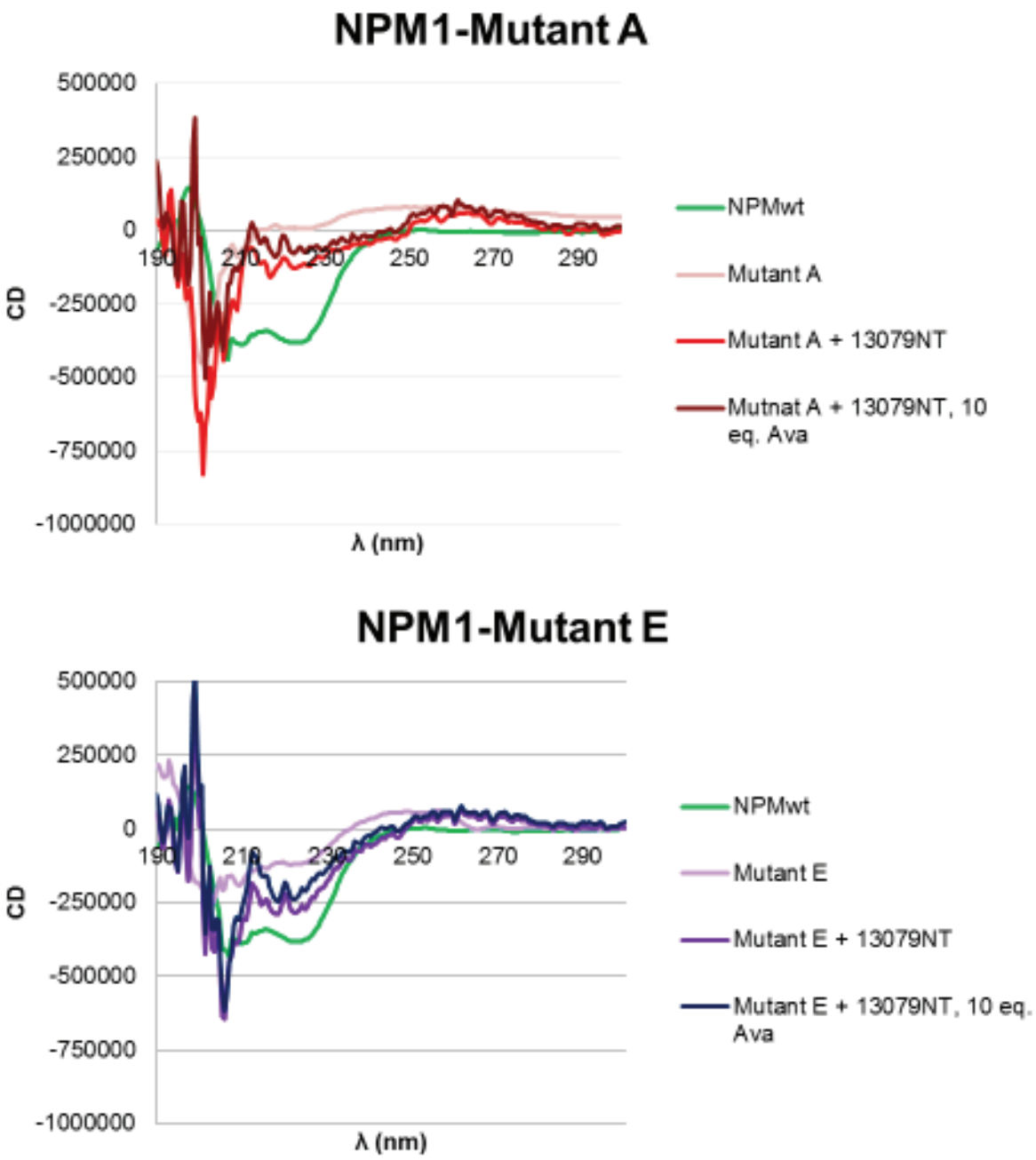

Figure S.8. CD spectra of the C-terminal domains of NPM1–Mutant A (top) and NPM1–Mutant E (bottom) either alone, with 1 eq. of 13079nt, or with both 13079nt and avrainvillamide. The CD spectrum of the C-terminal domain of wild-type NPM1 is overlaid on both spectra for reference.

Appendix II: Supplementary Tables

Table S.1. The subcellular distribution of eGFP–Mutant E and eGFP–Mutant E–C275A proteins in HCT–116 cells following treatment with either DMSO (vehicle control), avrainvillamide (1 μM, 24 hr), or leptomycin B (100 nM, 4 hr). "Cytoplasmic" indicates a fraction of fusion protein is observable in the cytoplasm; note that both constructs always exhibit partial nucleolar localization. "Nucleolar" indicates an exclusively nucleolar localization phenotype. For each dosing condition, a minimum of 150 cells were counted in each of three independent experiments; results indicate the mean ± standard deviation.

	eGFP–NPM1–Mutant E (% of Cells)		**eGFP–NPM1–Mutant E–C275A (% of Cells)**	
	Cytoplasmic	Nucleolar	Cytoplasmic	Nucleolar
DMSO	95.3 ± 2.0	4.7 ± 2.0	94.6 ± 2.1	5.4 ± 2.1
Avrainvillamide	8.3 ± 3.7	91.7 ± 3.7	11.4 ± 4.0	88.6 ± 4.0
LMB	4.8 ± 2.0	95.2 ± 2.0	4.4 ± 1.9	95.6 ± 1.9

Table S.2. The subcellular distribution of GFP–Rev and RanBP1 in HCT–116 cells following treatment with either DMSO (vehicle control), avrainvillamide (1 μM, 24 hr), or leptomycin B (100 nM, 4 hr). "Cytoplasmic" indicates no nuclear retention of the target protein. "Nuclear" indicates altered Crm1-mediated nuclear export, but does not necessarily indicate complete nuclear retention of the target protein. For each dosing condition, a minimum of 150 cells were counted in each of three independent experiments; results indicate the mean ± standard deviation.

	GFP–Rev Localization (% of Cells)		**RanBP1 Localization (% of Cells)**	
	Cytoplasmic	**Nuclear**	**Cytoplasmic**	**Nuclear**
DMSO	94.7 ± 1.2	5.3 ± 1.2	96.4 ± 0.6	3.6 ± 0.6
Avrainvillamide	23.3 ± 3.7	76.7 ± 3.7	15.9 ± 4.9	84.1 ± 4.9
LMB	5.9 ± 1.9	94.1 ± 1.9	7.8 ± 1.5	92.2 ± 1.5

Table S.3. Fraction of HCT–116 cells exhibiting supernumerary centrosomes following treatment with either DMSO (vehicle control), avrainvillamide (1 μM), or leptomycin B (25 nM).[81] For each dosing condition, a minimum of 150 cells were counted in each of three independent experiments; results indicate the mean ± standard deviation.

Dosing Time:	**24 hours**		**48 hours**	
Number of centrosomes (n):	$n \leq 2$	$n > 2$	$n \leq 2$	$n > 2$
DMSO	97.2 ± 1.2	2.8 ± 1.2	96.9 ± 1.5	3.1 ± 1.5
Avrainvillamide	32.9 ± 4.7	67.1 ± 4.7	9.9 ± 5.7	90.1 ± 5.7
LMB	21.7 ± 6.1	78.3 ± 6.1	7.5 ± 5.9	92.5 ± 5.9

[81] A lower concentration of LMB was required in experiment due to the extreme cytotoxicity of 100 nM LMB at longer time points.

Appendix III: Optimized Procedures for the Synthesis of Avrainvillamide

Due to the constant need for material for evaluation in biological assays, the synthesis of avrainvillamide has been conducted several times since the initial report.[4] While many steps were readily scaled up without affecting reaction yields, some steps required further optimization in order to increase material throughput at larger scales. This section thus includes revised procedures for synthetic steps which differ significantly from the original total synthesis.

Materials: Commercial solvents and reagents were used as received with the following exceptions. Dichloromethane, tetrahydrofuran, *n*-hexane, and toluene were purified by the method of Pangborn et al.[82]*tert*-Butylbenzene and trimethylamine were distilled from calcium hydride at atmospheric pressure and were stored under argon. Zinc dust was activated by the method of Knochel and Rao.[83] 2-Propanesulfonyl chloride was distilled from phosphorus pentoxide at approximately 40 Torr (house vacuum) and was stored under argon. 3-Chloro–3–methyl-1-butyne was distilled from calcium chloride at atmospheric pressure and was stored under argon.

General Experimental Procedures: All reactions were performed in single-neck, flame-dried, round-bottom flasks fitted with rubber septa under a positive pressure of argon, unless otherwise noted. When necessary (as noted in text), solutions were deoxygenated by successive freeze-pump-thaw cycles (≥ 5 cycles). Rotary evaporation was performed at approximately 40 Torr

[82] Pangborn, A. B.; Giardello, M. A.; Grubbs, R. H.; Rosen, R. K.; Timmers, F. J. Safe and Convenient Procedure for the Purification of Solvents. *Organometallics*. **1996**, *15*, 1518-1520.

[83] Knochel, P.; Rao, C. J.; Preparation and Reactivity of Functionalized Alkenyl-Zinc, -Copper, and –Chromium Organometallics. *Tetrahedron*. **1993**, *49*, 29-48.

(house vacuum). Flash column chromatography was performed as previously described[84] using silica gel (60 Å grade) purchased from Agela Technologies (Wilmington, Delaware). When indicated, silica gel was deactivated prior to flash column chromatography by treatment with a 20% solution of triethylamine in ethyl acetate.

Note: For clarity, intermediates which have not previously appeared in this text have been assigned numbers, beginning with **26**.

[84] Still, W. C.; Kahn, M.; Mitra, A. Rapid Chromatographic Technique for Preparative Separations With Moderate Resolution. *J. Org. Chem.* **1978**, *43*, 2923-2925.

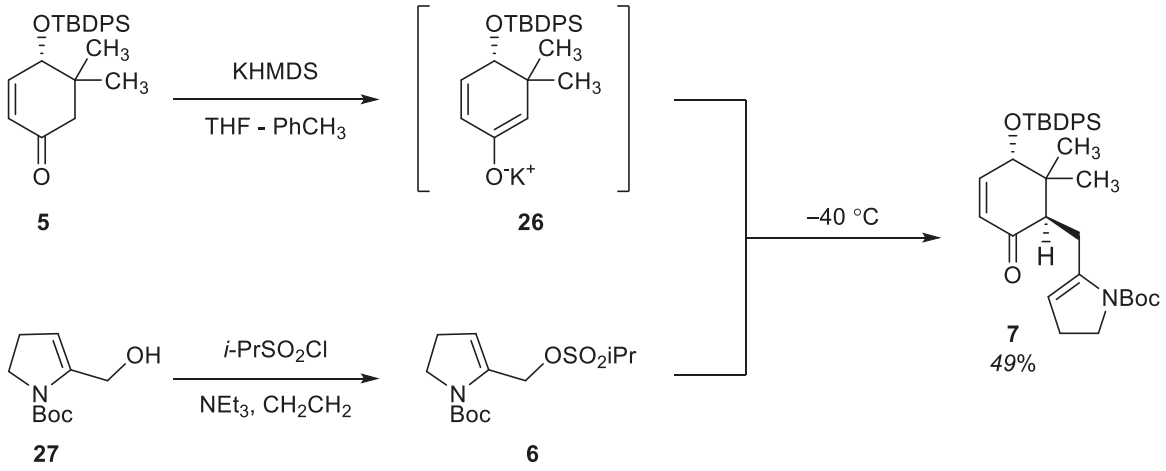

Alkylation of Enone **5** with *iso*-Propylsulfonate **6** (Alkyation Product **7**):

Note: In light of the extreme instability of electrophile **6**, it was found that forming enolate **26** prior to beginning the synthesis of **6** was critical for the success of this reaction. Enone **5** was dried azeotropically from toluene (3 × 8 mL portions) prior to use.

Enolate 26. A solution of potassium hexamethyldisilazide (0.5 M in toluene, 29.0 mL, 14.5 mmol, 1.1 eq.) was added dropwise via syringe to a cold (–78 °C) solution of enone **5** (5.00 g, 13.2 mmol, 1 eq.) in THF (37 mL). The resulting bright yellow solution was maintained at –78 °C while electrophile **6** was synthesized.

Electrophile 6. To a stirring solution of alcohol **27** (4.00 g, 20.1 mmol) in CH_2Cl_2 (48 mL) at 0 °C was added, in sequence, triethylamine (3.07 mL, 22.1 mmol, 1.1 eq. relative to **5**) and 2-propanesulfonylchloride (2.48 mL, 22.1 mmol, 1.1 eq. relative to **5**). The resulting yellow solution was maintained at 0 °C for 20 minutes. *n*-Hexane (50 mL) was then added to the reaction mixture, and the resulting white suspension was allowed to warm to 23 °C over 10 minutes. The suspension was filtered through a 1.5-cm pad of silica gel over a 1.5-cm pad of Celite, eluting with 10% acetone in hexanes (350 mL). The filtrate was concentrated by rotary

evaporation, then the residue obtained was dried azeotropically from benzene (3 × 5 mL portions) to afford crude electrophile **6** as a yellow oil. Crude **6** so obtained was used without further purification.

Alkylation Product 7. Electrophile **6** was dissolved in THF (5 mL). The resulting solution was transferred via cannula to the solution of enolate **26** at –78 °C. The reaction flask was immediately transferred to a –40 °C cooling bath, and the reaction mixture maintained at –40 °C for 36 hr. The reaction mixture was partitioned between ethyl acetate (250 mL) and saturated aqueous sodium bicarbonate solution (125 mL), then the organic layer was washed with a saturated aqueous sodium chloride solution (125 mL). The product solution was dried over $MgSO_4$, the solids filtered, and the filtrate concentrated by rotary evaporation. The residue was purified by flash column chromatography on deactivated silica gel (eluting with 5% ethyl acetate in hexanes initially, grading to 10% ethyl acetate in hexanes; eluent also contained 1% triethylamine) to afford alkylation product **7** as a white foam (3.60 g, 6.4 mmol, 49%). Spectral data matched those previously reported for **7**.

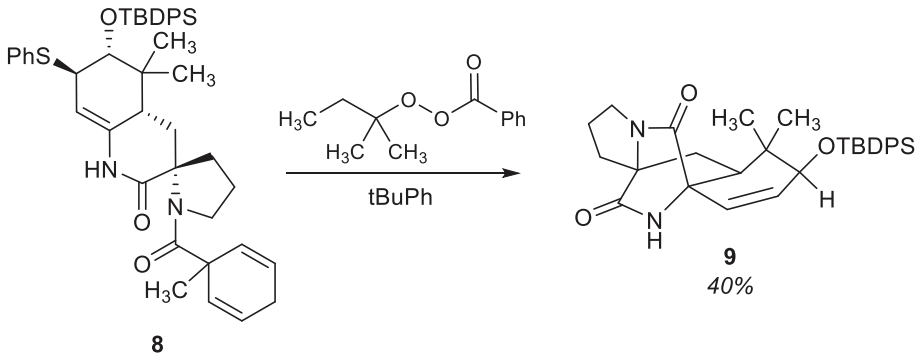

Radical Cyclization of bis-Amide **8** (Diketopiperazine **9**):

Note: *tert*-Butylbenzene was deoxygenated by five successive freeze-pump-thaw cycles immediately prior to use.

Diketopiperazine 9. A solution of *tert*-amylperoxybenzoate (854 µL, 4.2 mmol, 6 eq.) in *tert*-butylbenzene (140 mL) was deoxygenated by one freeze-pump-thaw cycle, then the reaction flask was transferred to an oil bath preheated to 119 °C. In a separate flask, a solution of bis-amide **8** (500 mg, 698 µmol, 1 eq.) in *tert*-butylbenzene (5 mL) was deoxygenated by one freeze-pump-thaw cycle. The solution of **8** was loaded into a syringe and transferred to the solution of *tert*-amylperoxybenzoate over 90 minutes using a syringe pump. After the addition was complete, an additional portion of *tert*-amylperoxybenzoate (284 µL, 1.4 mmol, 2 eq.) was added to the reaction mixture over 20 minutes. The yellow reaction mixture was maintained at 119 °C for 1 hr. The reaction mixture was cooled rapidly to 23 °C by immersing the reaction flask in an ice-water bath. The reaction mixture was loaded directly onto a silica gel column, and diketopiperazine **9** was purified by flash column chromatography (eluting with hexanes first to remove *tert*-butyl benzene, then 25% acetone in hexanes). Diketopiperazine **9** was isolated as an off-white foam (142 mg, 276 µmol, 40%).

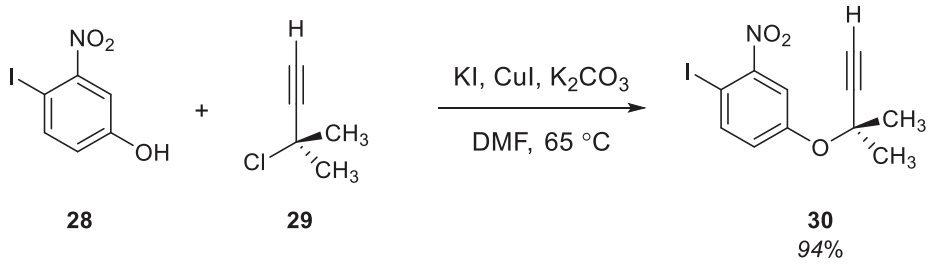

28 **29** **30**

94%

Alkylation of phenol **28** (Propargyl ether **30**):

Copper iodide (28.8 mg, 0.15 mmol, 0.02 eq.), potassium iodide (2.13 g, 12.8 mmol, 1.7 eq.), 3-chloro-3-methyl-1-butyne (**29**, 1.70 mL, 15.1 mmol, 2.0 eq.), and potassium carbonate (2.09 g, 15.1 mmol, 2.0 eq.) were added to a stirring suspension of 4-iodo-3-nitrophenol (**28**, 2.00 g, 7.5 mmol, 1 eq.) in DMF (10 mL) at 23 °C. The reaction flask was transferred to an oil bath preheated to 65 °C, and the reaction mixture was maintained at 65 °C for 2.5 hr. The reaction mixture was allowed to cool to 23 °C, then was partitioned between 200 mL water and 150 mL hexanes. The aqueous layer was extracted with 3 × 150 mL portions of hexanes, then the organic phases were combined and extracted with sequential 150 mL portions of 1 M KOH solution, 1 M HCl solution, water, and saturated aqueous sodium chloride solution. The product solution was dried over Na_2SO_4, the solids filtered, and the filtrate concentrated by rotary evaporation. The crude residue was purified by flash column chromatography on silica gel (eluting with 8% ethyl acetate in hexanes) to afford propargyl ether **30** as a pale yellow oil (2.35 g, 7.1 mmol, 94%).

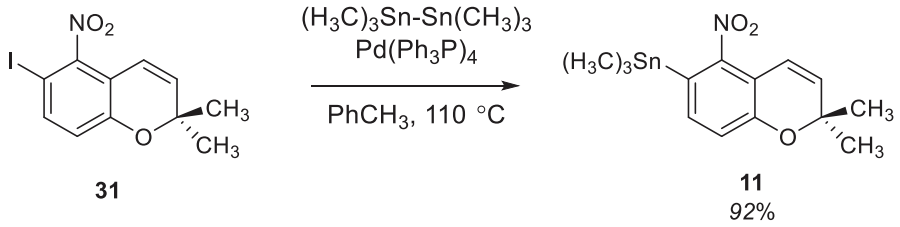

Stannylation of *ortho*-Iodonitroarene **31** (Stannane **11**).

Note: Toluene was deoxygenated by three successive freeze-pump-thaw cycles prior to use.

Stannane 11. Hexamethylditin (10.0 g, 30.5 mmol, 1.1 eq.) and tetrakis(triphenylphosphine)palladium (1.57 g, 1.4 mmol, 0.05 eq.) were added to a solution of iodoarene **31** (9.00 g, 27.2 mmol, 1 eq.) in toluene (272 mL) at 23 °C. The reaction flask was fitted with a reflux condenser and transferred to an oil bath preheated to 120 °C. The bright yellow reaction mixture was maintained at 120 °C for 23 hr, then was allowed to cool to 23 °C. The reaction mixture was diluted with 200 mL pentane, then was filtered through a 2-cm pad of silica gel, eluting with 50% diethyl ether in hexanes (800 mL). The filtrate was concentrated by rotary evaporation and the residue purified by flash column chromatography on silica gel (eluting with 25% CH_2Cl_2 in hexanes), affording stannane **11** as a yellow oil which solidified upon storage at –20 °C.

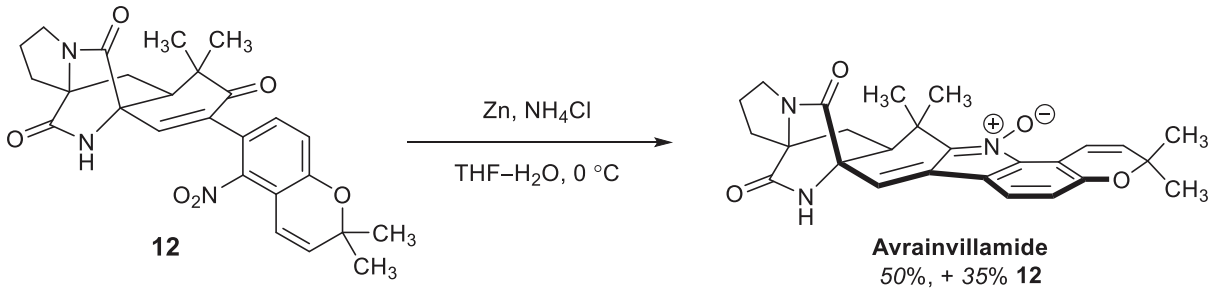

Reductive Cyclization of **12** (Avrainvillamide, **1**):

Note: Zinc dust was activated immediately prior to use. All operations involving the synthesis and purification of avrainvillamide were conducted in the dark to minimize the risk of photochemical rearrangement reactions.

Avrainvillamide. A suspension of zinc dust (1.0 M in THF) was activated according to the procedure of Knochel and Rao,[83] then was allowed to cool to 23 °C. Meanwhile, a saturated aqueous solution of ammonium chloride (6.9 M, 42.1 μL, 13.8 eq.) and water (21.1 μL) were added in sequence to a stirring solution of enone **12** (10.1 mg, 21 μmol, 1 eq.) in THF (1.06 mL) at 0 °C. Three aliquots of the zinc suspension (28.3 μL, 28.3 μmol, 1.7 eq.) were added to the biphasic reaction mixture at 5-minute intervals. Following the final addition, the reaction mixture was allowed to stir at 0 °C for 45 minutes. The reaction mixture was diluted with 20 mL ethyl acetate, then filtered through a 0.2 μM membrane to remove insoluble zinc salts and unreacted zinc dust. The filtrate was washed with saturated aqueous sodium chloride solution (10 mL). The product solution was dried over Na_2SO_4, the solids filtered, and the filtrate concentrated by rotary evaporation. The crude residue was purified by flash column chromatography on silica gel (eluting with 20% ethyl acetate in CH_2Cl_2 initially, grading to 60% ethyl acetate in CH_2Cl_2) to afford avrainvillamide as a bright yellow solid (4.7 mg, 10.6 μmol, 50%). Also afforded unreacted enone **12** as a yellow solid (3.5 mg, 7.3 μmol, 35%).

Appendix IV: Mass Spectra

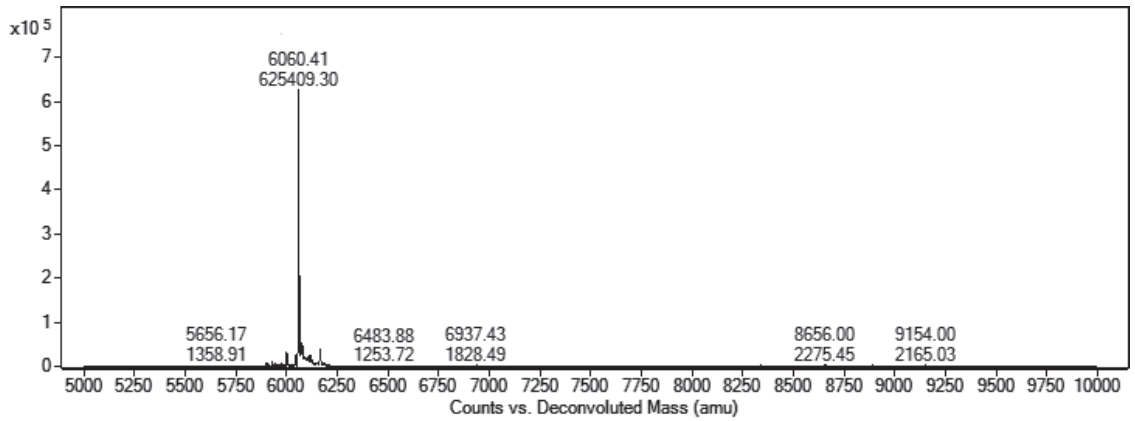

Peptide Sample: NPM1 (wild-type)

Peptide Sequence:

SVEDIKAKMQASIEKGGSLPKVEAKFINYVKNCFRMTDQEAIQDLWQWRKSL

Predicted Molecular Weight: 6060.04

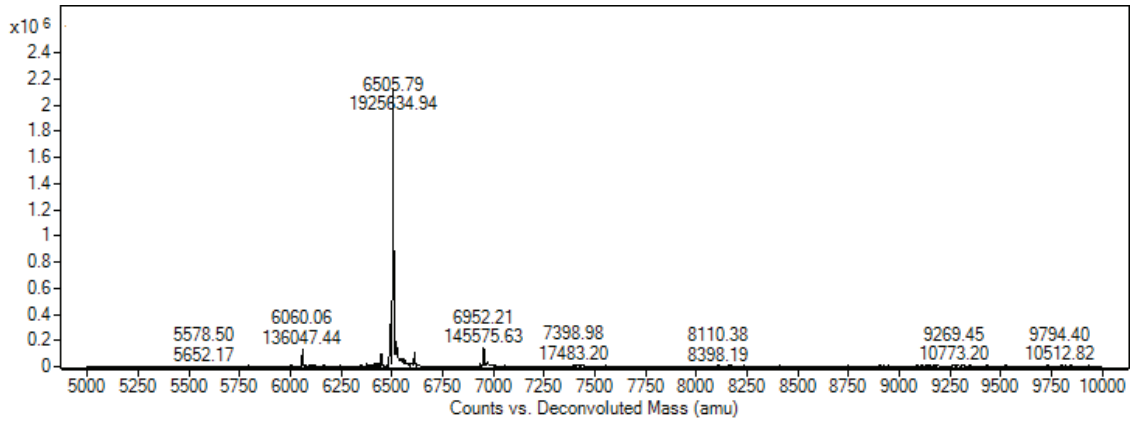

Peptide Sample: NPM1 (wild-type) + 3 eq. avrainvillamide

Predicted Molecular Weight: 6060.04 (peptide), 6505.55 (adduct)

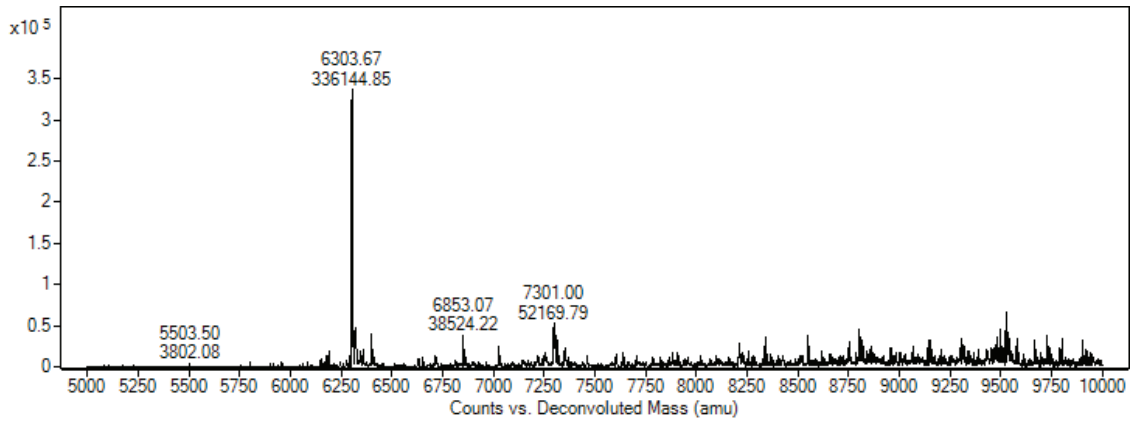

Peptide Sample: NPM1-Mutant A

Peptide Sequence:

SVEDIKAKMQASIEKGGSLPKVEAKFINYVKNCFRMTDQEAIQDLCLAVEEVSLRK

Predicted Molecular Weight: 6303.36

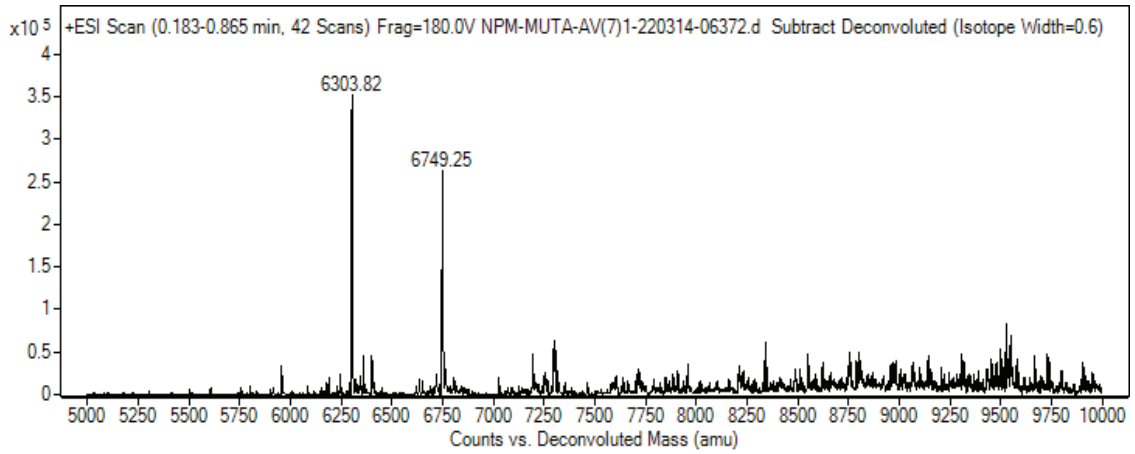

Peptide Sample: NPM1-Mutant A + 3 eq. avrainvillamide

Predicted Molecular Weight: 6303.36 (peptide), 6748.87 (mono-adduct), 7194.38 (bis-adduct)

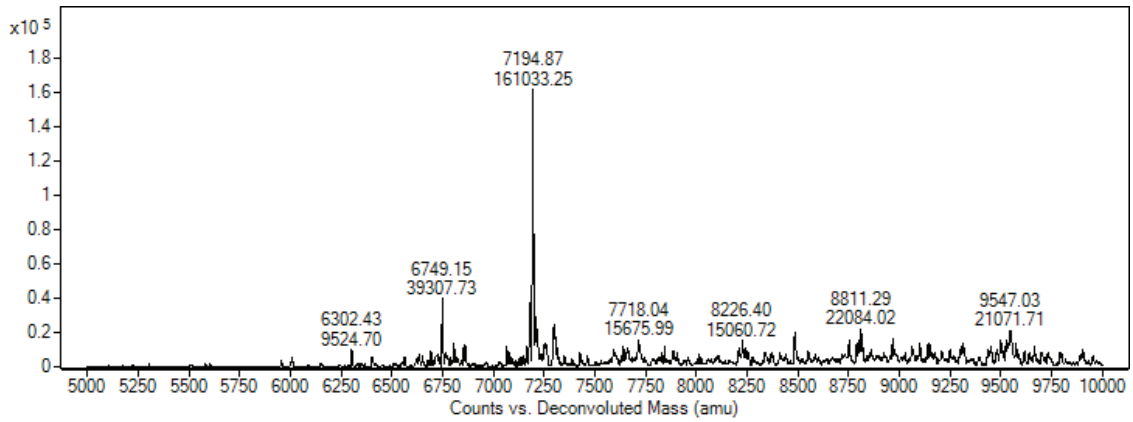

Peptide Sample: NPM1-Mutant A + 10 eq. avrainvillamide

Predicted Molecular Weight: 6303.36 (peptide), 6748.87 (mono-adduct), 7194.38 (bis-adduct)

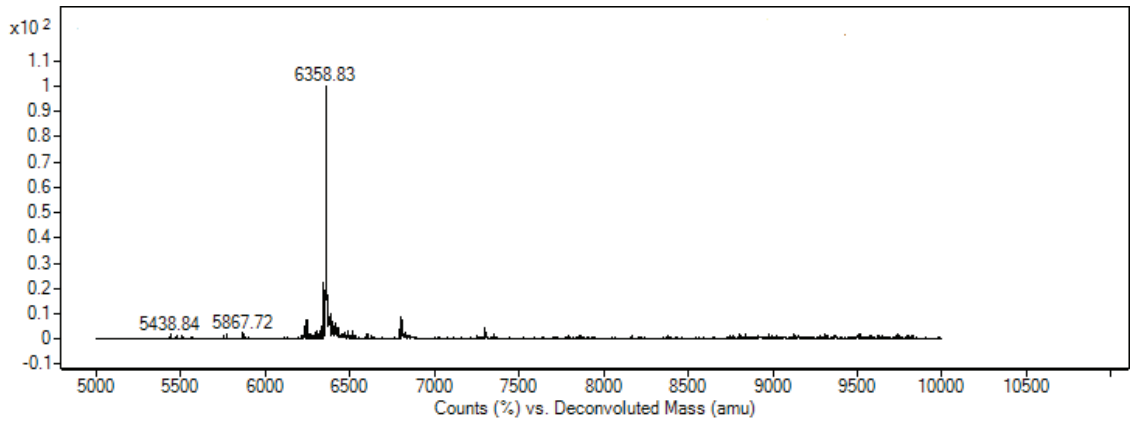

Peptide Sample: NPM1-Mutant A-C275A

Peptide Sequence:

SSVEDIKAKMQASIEKGGSLPKVEAKFINYVKNAFRMTDQEAIQDLCLAVEEVSLRK

Predicted Molecular Weight: 6358.37

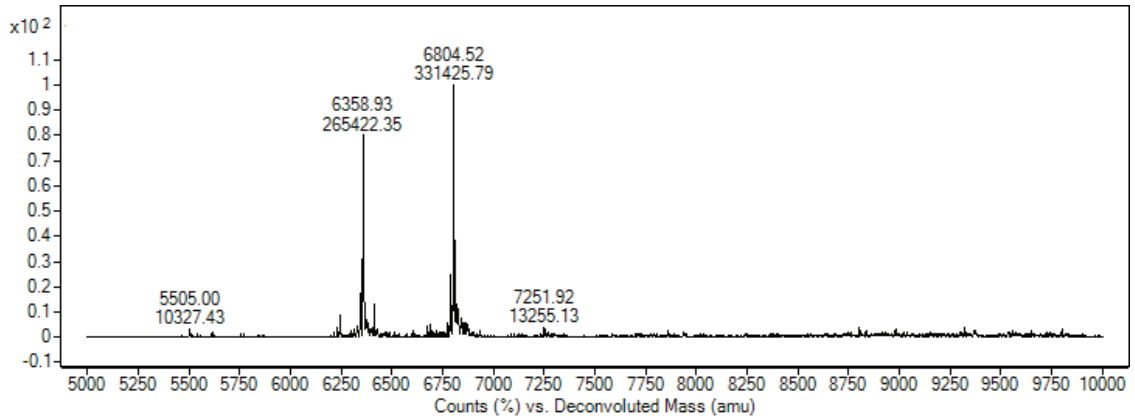

Peptide Sample: NPM1-Mutant A-C275A + 3 eq. avrainvillamide

Predicted Molecular Weight: 6358.37 (peptide), 6803.88 (adduct)

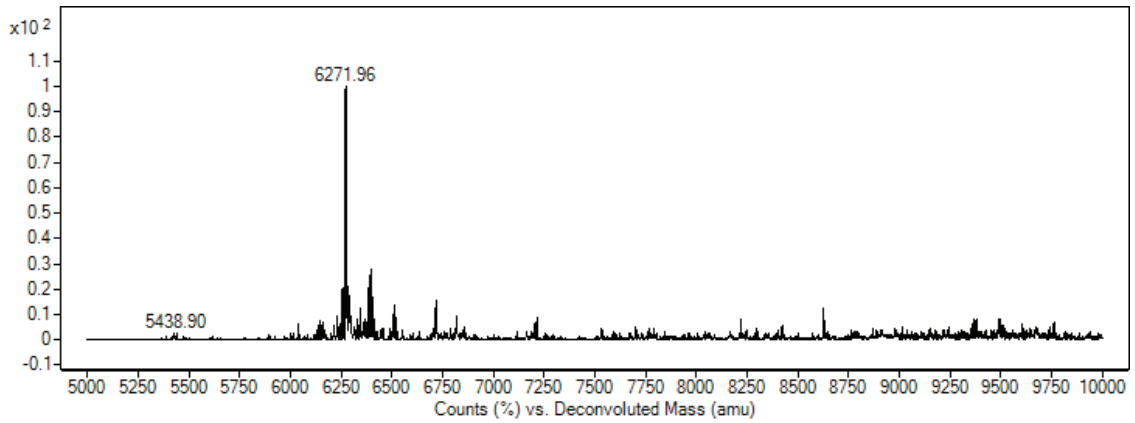

Peptide Sample: NPM1-Mutant A-C288A

Peptide Sequence:

SVEDIKAKMQASIEKGGSLPKVEAKFINYVKNCFRMTDQEAIQDLALAVEEVSLRK

Predicted Molecular Weight: 6271.29

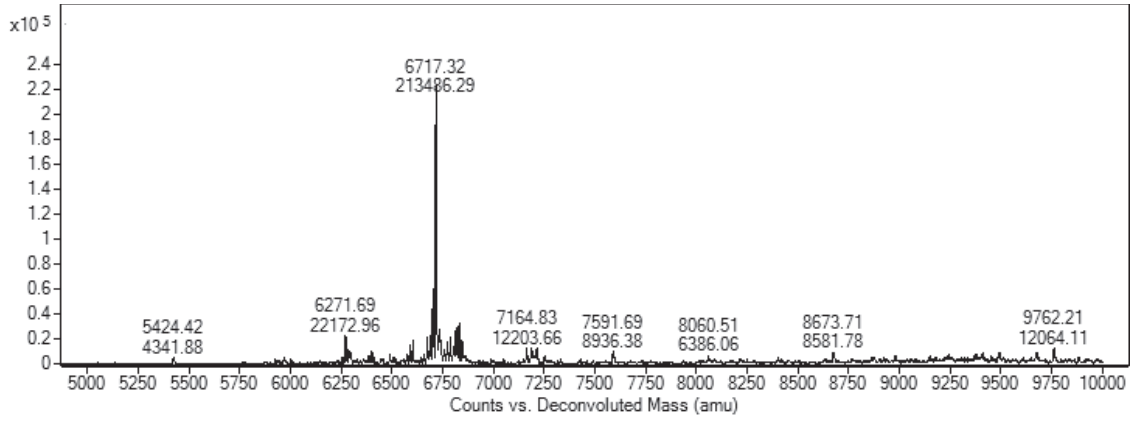

Peptide Sample: NPM1-Mutant A-C288A + 3 eq. avrainvillamide

Predicted Molecular Weight: 6271.29 (peptide), 6716.80 (adduct)

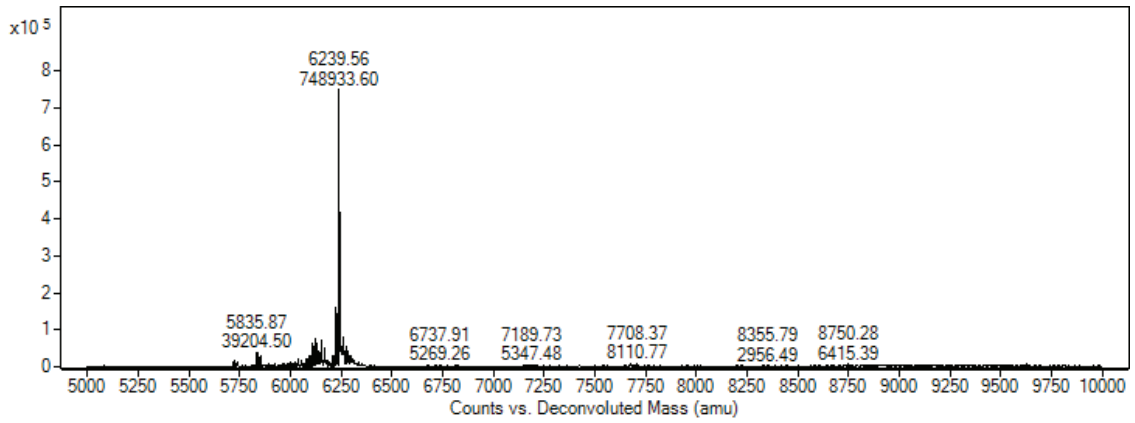

Peptide Sample: NPM1-Mutant A-C275,288A

Peptide Sequence:

SVEDIKAKMQASIEKGGSLPKVEAKFINYVKNAFRMTDQEAIQDLALAVEEVSLRK

Predicted Molecular Weight: 6239.23

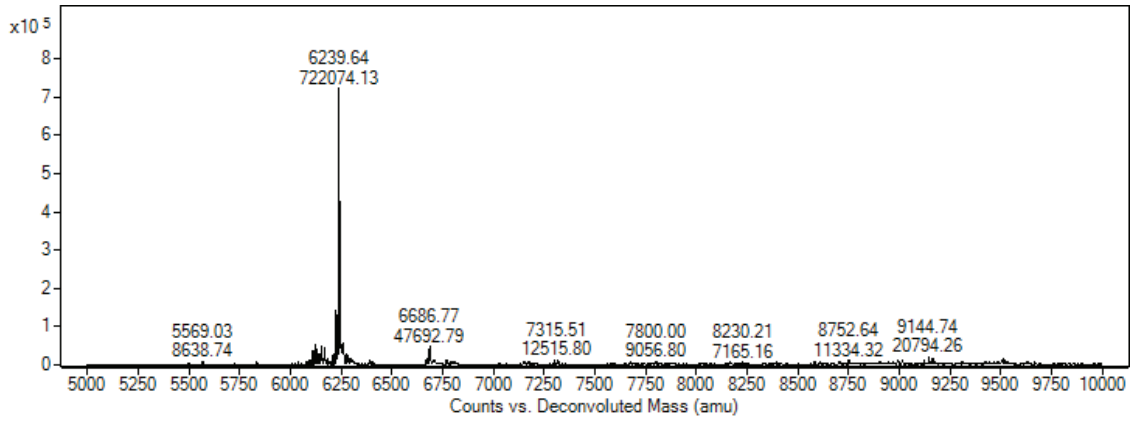

Peptide Sample: NPM1-Mutant A-C275,288A + 3 eq. avrainvillamide

Predicted Molecular Weight: 6239.23 (peptide), 6684.74 (adduct, not observed)

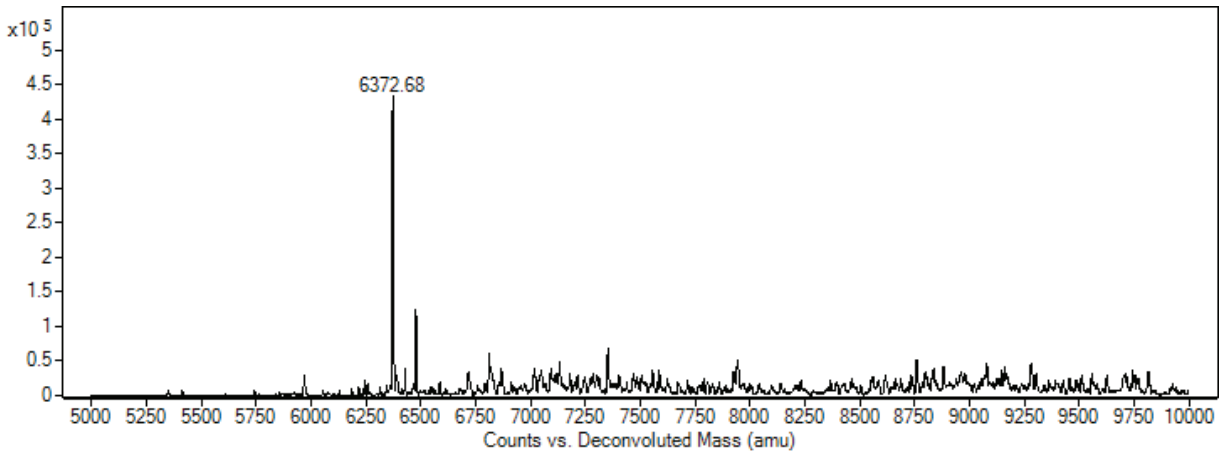

Peptide Sample: NPM1-Mutant E

Peptide Sequence:

SVEDIKAKMQASIEKGGSLPKVEAKFINYVKNCFRMTDQEAIQDLWQSLAQVSLRK

Predicted Molecular Weight: 6372.41

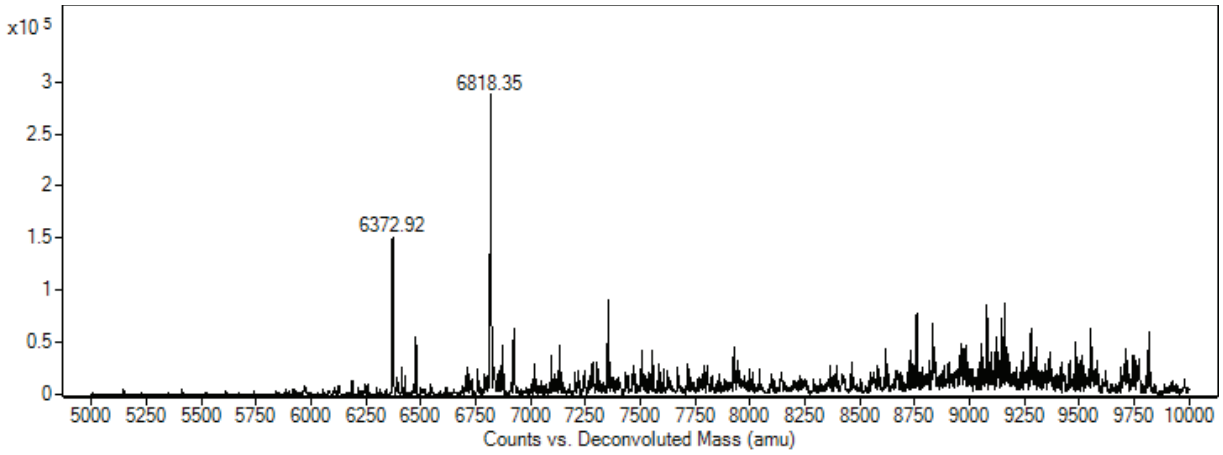

Peptide Sample: NPM1-Mutant E + 3 eq. avrainvillamide

Predicted Molecular Weight: 6372.41 (peptide), 6817.92 (adduct)

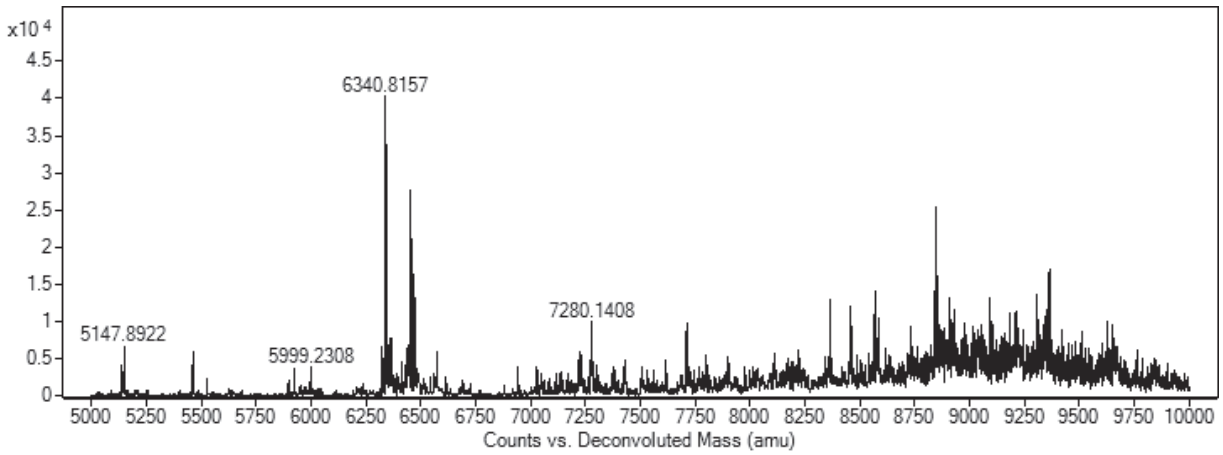

Peptide Sample: NPM1-Mutant E-C275A

Peptide Sequence:

SVEDIKAKMQASIEKGGSLPKVEAKFINYVKNAFRMTDQEAIQDLWQSLAQVSLRK

Predicted Molecular Weight: 6340.34

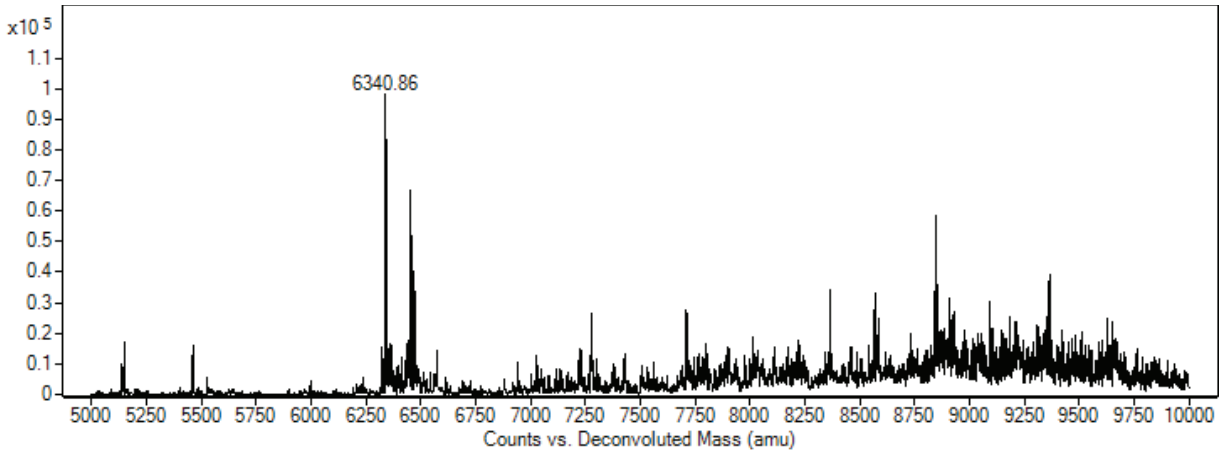

Peptide Sample: NPM1-Mutant E-C275A

Predicted Molecular Weight: 6340.34 (peptide), 6785.85 (adduct, not observed)

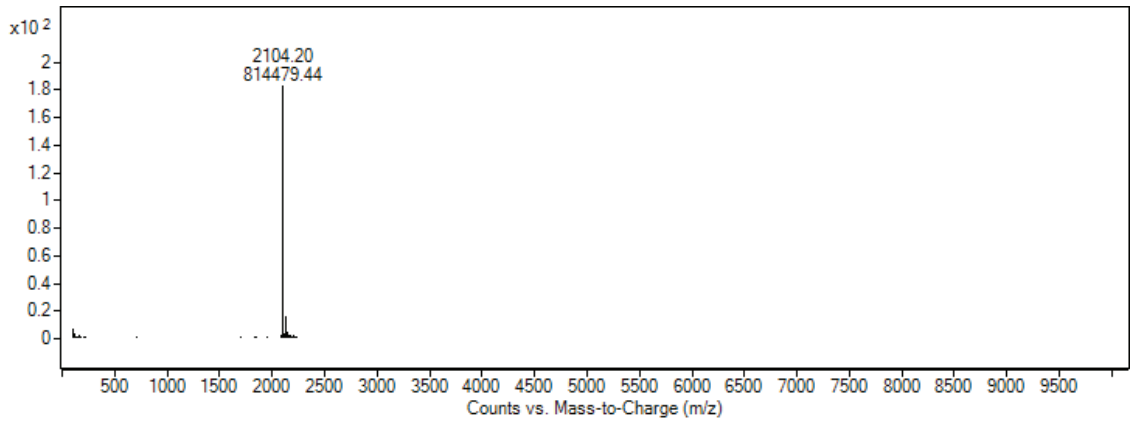

Peptide Sample: CRM1 (513-530)

Peptide Sequence: EKRFLVTVIKDLLGLCEQ

Predicted Molecular Weight: 2104.55

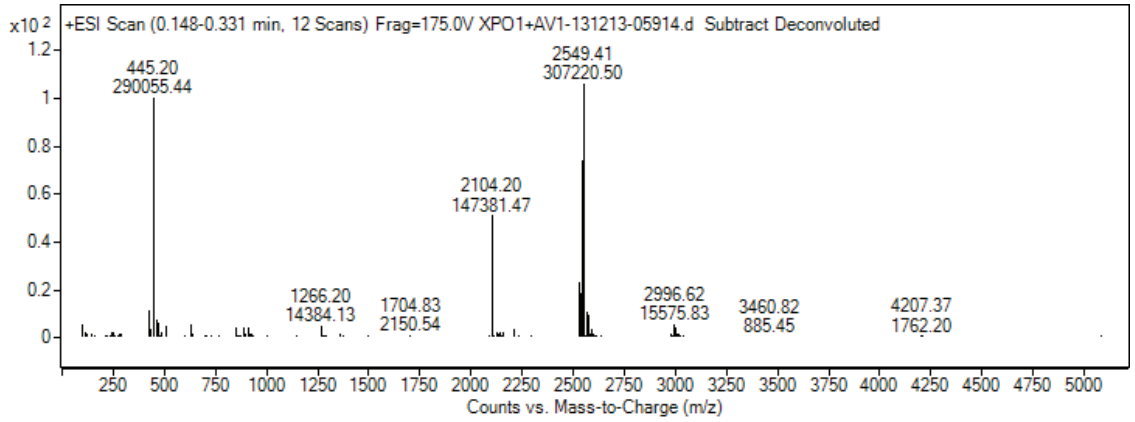

Peptide Sample: CRM1 (513-530) + 3 eq. avrainvillamide

Predicted Molecular Weight: 2104.55 (peptide), 2550.06 (adduct)

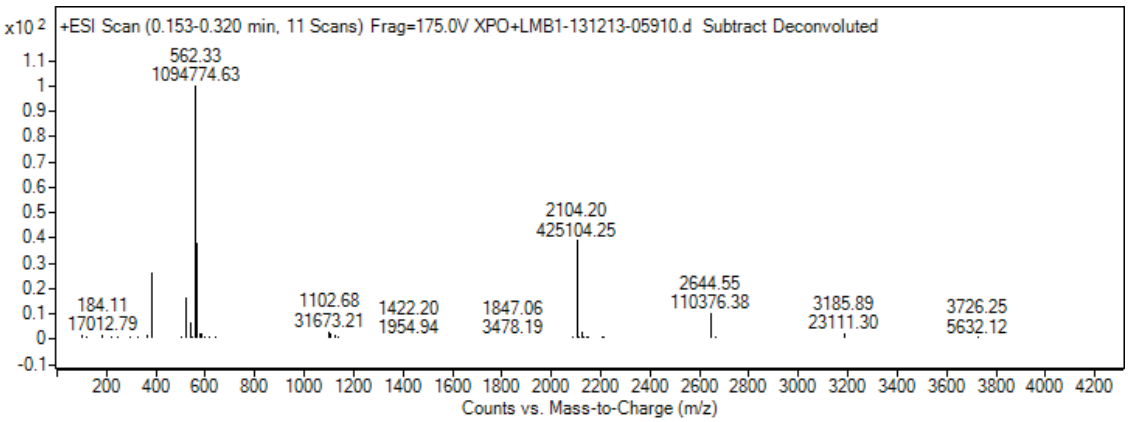

Peptide Sample: CRM1 (513-530) + 3 eq. leptomycin B

Predicted Molecular Weight: 2104.55 (peptide), 2645.28 (adduct)

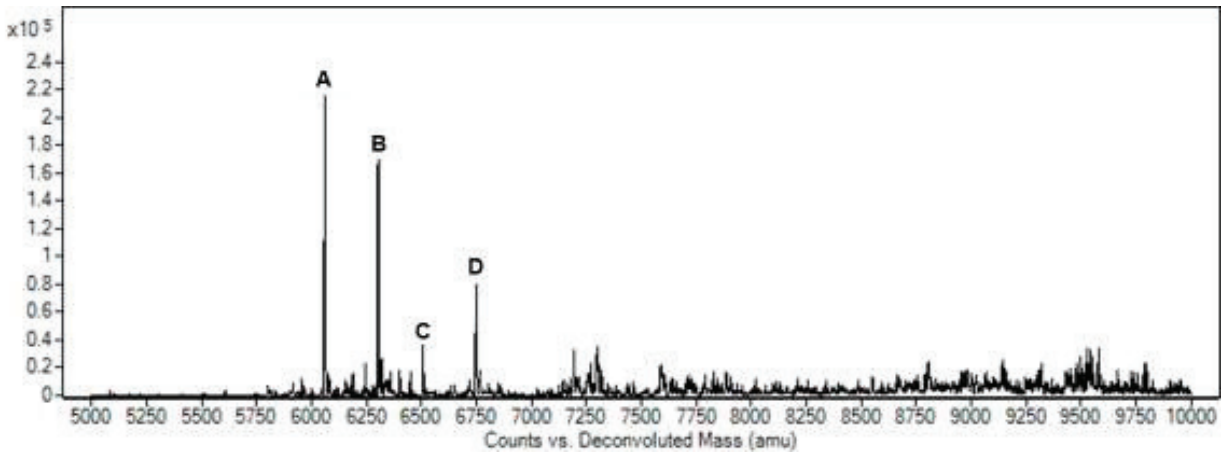

Peptide Sample: NPM1 (wild-type) + NPM1-Mutant A + 0.5 eq. avrainvillamide

A: NPM1 (wild-type)

B: NPM1-Mutant A

C: NPM1 (wild-type)-avrainvillamide adduct

D: NPM1-Mutant A-avrainvillamide adduct

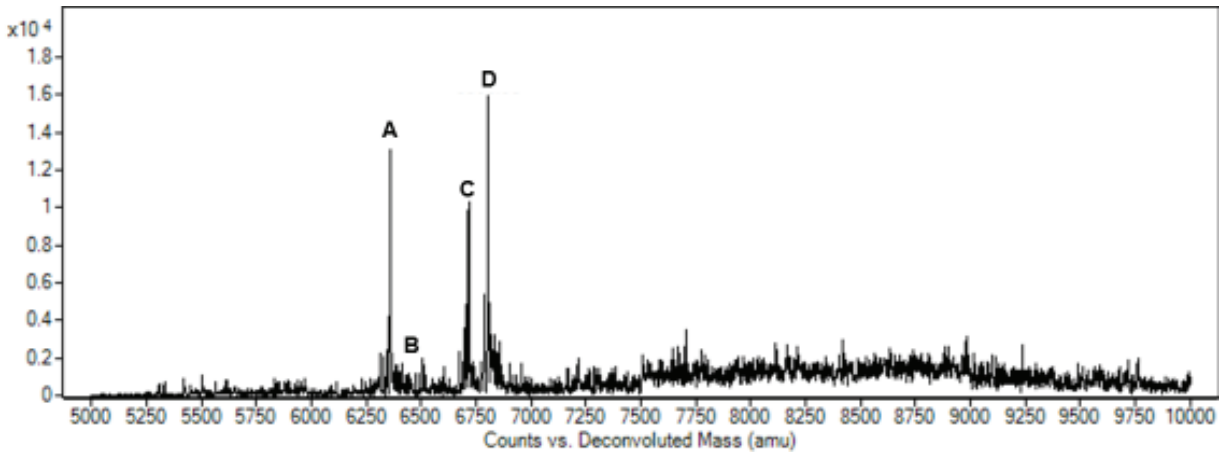

Peptide Sample: NPM1-Mutant A-C275A + NPM1-Mutant A-C288A + 0.5 eq. avrainvillamide

A: NPM1-Mutant A-C275A

B: NPM1-Mutant A-C288A

C: NPM1-Mutant A-C275A-avrainvillamide adduct

D: NPM1-Mutant A-C288A-avrainvillamide adduct